UNIVERSITY OF JOHANNESBURG

How to cite this thesis

UNIVERSITY OF JOHANNESBURG

SYNTHESIS OF ZINC PHTHALOCYANINE-GOLD NANOPARTICLES CONJUGATED COMPOUNDS AND DETERMINATION OF PHOTODYNAMIC EFFECTS IN A BREAST CANCER CELL LINE

AN *IN VITRO* STUDY

A thesis submitted to the Faculty of Health Sciences, University of Johannesburg, in fulfillment of the requirements for the degree of Doctorate Technology, Biomedical Technology

By

Ivan Sosthene Mfouo-Tynga

(Student number: 200504361)

Supervisor:

Prof Heidi Abrahamse   Date:

Co-supervisor:

Dr Nicolette Nadene Houreld   Date:

DECLARATION

I, Ivan S. Mfouo Tynga, declare that this thesis is my own, unaided work. It is being submitted for the Degree of Doctorate of Technology, Biomedical Technology, at the University of Johannesburg. This work has not been submitted before for any degree or examination in any other institution.

_____   _____

Ivan S. Mfouo-Tynga   Date

EXECUTIVE SUMMARY

Cancer is a disease that occurs following mutations in the genes, which control cell growth. These mutations are caused by different causes and viral infections are among those. Cancer cells can conquer other cells and tissues causing changes to their deoxyribonucleic acids (DNA). Cancer appears almost incurable once it has started to metastasize and invade other body organs. At that stage, any therapeutic intervention was believed to cause more harm than curative effects (Gallucci, 1985; Kardinal and Yarbro, 1979). Late diagnosis and treatment reduces the possibility of an effective cure (He *et al.*, 2007). The development of a malignant tumour from cells in the breast is known as breast cancer. Breast cancer is generally initiated in the stromal cells, which are fibrous and fatty tissues, or in the glandular cells; which produce breast milk (American Cancer Society, 2014). Breast cancer is the leading cancer among women and cause of cancer death worldwide (Ferlay *et al.*, 2008). It is a heterogeneous disease with several markers, which are essential for diagnosis and include the estrogen receptors (ER), progesterone receptors (PR) and human epidermal growth factor receptor 2 (HER-2) (Mosoyan *et al.*, 2013; Yang *et al.*, 2013).

Like all cancer, breast cancer can be cured if diagnosed at an early stage. Treatment of cancer has evolved from palliative therapies to conventional therapies, which consist of surgery, hormonal therapy, radiation therapy, immunotherapy, chemotherapy, and adjuvant therapy. (Gallucci, 1985; Kardinal and Yarbro, 1979). Photodynamic therapy (PDT) has become popular as an alternative cancer treatment modality. PDT depends on molecular oxygen and photodynamic action for effective cancer destruction (Von Tappeiner and Jesionek, 1903; Von Tappeiner and Joblauer, 1904). Today, PDT is designated as a chronological and minimally invasive cancer therapy with numerous benefits over conventional treatments. The initial step of this therapy consists of the administration of drugs to patients,

commonly known as photosensitizers (PSs); which refers to the light sensitivity features of these compounds. Photosensitizers are formulated in a specific manner that confers them to a limited biodistribution, low dark toxicity (inactive state) and affinity to highly proliferating cells such as cancer cells (Brown *et al.*, 2004; Castano *et al.*, 2004; Peng *et al.*, 2009, Agostini *et al.*, 2011). The third generation PSs have minimal accumulation in normal tissue and maintain a high tumour binding specificity (Konan *et al.,* 2002; Hudson *et al.,* 2005; Staneloudi *et al.,* 2007). Furthermore, Staneloudi *et al.* (2007) found that PSs conjugated to biomolecules such as single-chain monoclonal antibody fragment, are also more effectively cleared from the circulation than first and second generation PSs.

The engineering of small particles led to nanotechnology, an interdisciplinary field that enables exceptional interactions with molecules both on the surface of and inside cells (Wei, 2012; Cai and Chen, 2007). In nanomedicine, nanoparticles (NPs) are applied to medicine and can be simultaneously used as medical imaging agents, therapeutic agents, diagnostic agents, active implant agents or drug delivery agents (Selim and Hendi, 2012). Nanoparticles have attracted attention because of the surface to mass ratio, the quantum properties, and the capability of NPs to absorb and carry others (Buzea *et al.*, 2007; Chaturvedi *et al.,* 2012; Lubick and Betts, 2008). Drug delivery NPs are commonly used in nanomedicine and offer additional advantages such as improving drug therapeutic effect and pharmacological properties. They do so by enhancing the solubility of poorly water soluble drugs, altering pharmacokinetics, improving bioavailability, improving specificity toward targeted cells and extending drug half-life (Bednarski *et al.*, 2015). In this study, we aimed to conjugate NPs to a second generation PS and determine the photo-induced cell damage of the multiple particles delivery complex (MPDC) in breast cancer cells.

A dose response study was performed on a commercially available breast cancer cell line (MCF-7), cultured as monolayer, treated with two gold NPs (AuNPs and AuDENPs) and irradiated to evaluate the light-induced cell damage and identify the NPs, to be conjugated to a sulfonated Zinc Phthalocyanine (ZnPcS$_{mix}$). Two concentrations of NPs were used (1 and 3 mM) and laser irradiation was done using a 532 nm diode laser at fluences of 5, 10 and 15 J/cm^2 before assessing cell viability (trypan blue exclusion assay), proliferation (Adenosine triphosphate (ATP) luminescence assay) and cytotoxicity (lactate dehydrogenase (LDH) membrane integrity assay). Conjugated compounds or MPDC were synthesized and characterized by ultraviolet visible (UV-Vis) and Fourier transform infrared (FTIR or IR) spectroscopies, transmission electron microscopy (TEM) and Zeta potential analysis for absorption peak, FTIR spectral shift and identification of new functional groups, shape and size, and surface charge and size distribution, respectively.

In order to determine the optimal concentration of conjugate to be used for the cell damage study, a second dose response was conducted using 5 concentrations (0.1, 0.3, 0.5, 0.7 and 0.9 µM) of conjugate and one laser fluences (10 J/cm^2) before assessing cell viability, proliferation and cytotoxicity. Thereafter, the ultimate study was conducted using 0.3 µM ZnPcS$_{mix}$-AuDENPs (MPDC) and 10 J/cm^2 laser fluence using a 680 nm diode laser. Cell damage was assessed by inverted light microscopy for cell morphology; fluorescent microscopy for subcellular localization; Apoptox-Glo triple assay for all cell viability, caspase activity and identification of cytodamage markers; flow cytometric analysis for both cell death pathways and mitochondrial membrane potential, enzyme linked immunosorbent assay (ELISA) for cytochrome C release and real-time reverse transcriptase polymerase chain reaction (RT-PCR) array for gene expression following MPDC-mediated PDT.

The first dose response revealed that gold encapsulated dendrimers (AuDENPs) were the most suitable NPs for photo-induced cytodamage and were used for conjugation to a second generation PS (ZnPcS$_{mix}$). Results showed that AuNPs induced a significant increase in cytodamage in a light-dependent (irradiated AuNPs) and light-independent manner (unirradiated AuNPs). AuDENPs were better photo-destructive agents and induced significant cytodamage only with the irradiated AuDENPs.

Characterization analysis revealed that MPDC had an absorption peak at 674 nm, and FTIR spectra peak shifts at 3126.12 and 1636.56 when compared to those of AuDENPs (3341.86 and 1640.23, respectively) and at 3126.12, 1636.56, 1400.42 and 501.19 when compared to those of ZnPcS$_{mix}$ (3529.39, 1638.50, 1400.46 and 638.35, respectively). New functional groups were identified in MPDC and confirmed successful conjugation. MPDC had a spherical shape and a size of less than 5 nm in diameter. The zeta potential revealed a surface charge of +36 mV. The size distribution analysis indicated than more than 95% of MPDC has an average diameter of 5 nm (approximately) and no further purification procedure was required. MPDC had good physical and photosensitizing properties, which had therapeutic importance as 674 nm is in the near infrared region of the spectrum (therapeutic window).

The photosensitizing abilities of the conjugate were tested in the second dose response, which showed a decreased cell viability around 50% when MCF-7 cells were treated with 0.3 µM MPDC and a laser fluence of 10 J/cm^2. These parameters were used to conduct the cell damage experiment. Subcellular localization of any PS has a critical importance for the induction of cytodamage. MPDC localized in mitochondria and lysosomes, which are the preferred subcellular localization sites for PSs. The laser activated MPDC in PDT treated cells caused significant change in cell morphology and the appearance of apoptotic-like morphological features. Increase in cytotoxicity, caspase activity, cell depolarization and

level of cytochrome C release was identified with PDT-treated cells. Finally, the primary response of PDT on the expression of genes involved in cell death pathways was investigated. Four genes were affected and the upregulation of BAX, BCL-2, CASP2 and ULK-1 genes subsequent to PDT was observed.

This study showed that the therapeutic efficiency of NPs and second generation PSs can be improved by combination of these two agents. MPDC demonstrated effective photo-damaging capability with relatively low concentration when compared to $ZnPcS_{mix}$ or AuDENPs mediated-PDT. Even at the low dose used during the cell damage study, the MCF-7 cells were still sensitive to the treatment. The induction of mitochondrial dependent (intrinsic) apoptosis is likely to be the main mode of cell death. Evidence of induction of autophagy (seen by the upregulation of the ULK-1 gene) and probable formation of autophagosomes may indicate the means of killing the cancer cells more effectively. The gene expression profile confirmed that the cell destruction is due to PDT and eliminated the suspicion of an accidental cell death scenario, which mostly occurs during necrotic responses. Future work should be conducted on both monolayer and multicellular tumour spheroid MCF-7 cells and further combination of the $ZnPcS_{mix}$-AuDENPs compound to antibodies that are specific to breast cancer.

DEDICATION

In memory of my late father, Tynga Sidoine (1953-2005),
I dedicate this work to my mother, Monique and my wife, Desy.

William Shakespeare said, "Some are born great, some achieve
greatness, and some have greatness thrust upon them".
However, I do have none of those but Christ within me,
therefore greatness is my portion and I am on my way to see
glorious days.

To God all-Mighty be all the glory.

ACKNOWLEDGEMENTS

7. I would like to thank my friend Edwin and Mulisa for their help with the synthesis of the Gold encapsulated dendrimers.

8. I consider and thank Bishop Djuma Aime, Pastor Marie-Louise, Pastor Delphin, Pastor Nadine, Pastor Franck, Pastor Micky and Pastor Monique, all for their prayers and spiritual efforts during the course of this study as I acknowledge that invisible or spiritual forces also determine our daily life.

9. A special thank to all my family members, who took their time to think, enquire, and support me with encouraging messages, it really did make a difference and touched me in a very unique way.

10. My cousin, Dr Voua Otomo Patricks for enduring similar challenges during his studies, for his sympathy, understanding and support in difficult times.

11. I thank God for providing and giving the ability in the midst of difficulties to start a family. And to my wife you are my divine mine, I love you dearly and want to thank you for venturing and embarking on this journey with me, you made it all the more pleasant.

12. A humongous love and thank you to my older sister Synthia, for her constant support and wonderful laughter. You are forever supportive and you will never know how much we value your presence in our lives. I would like to extend my gratitude to your husband Jean Medard, my niece Daltia and nephew Diel-Ephraim for their friendship and equally constant care. Your visit came at the right time; one of the opaquest hour, when all my motivation and strength were gone. You gave me strength to believe, to persevere and to finish this race.

Now to Him who is able to keep me from falling, and to Him who is able to do immeasurably more than all I ask or imagine, according to His power that is at work within me, to Him be glory throughout all generations, for ever and ever.

OUTCOMES OF THE STUDY

The research outcomes of the study were presented at the following conferences and workshops:

- The 8th African Laser Centre Student Workshop, Stellenbosch, South, 02-06 December 2015 (Oral Presentation).
- SPIE Conference, Munich, Germany, 21-25 June 2015 (Oral Presentation).
- The 60th Annual South African Institute of Physics (SAIP) Conference, Nelson Mandela Bay, Port Elizabeth, South Africa, 30 June to 03 July 2015 (Oral Presentation).
- World Association of Laser Therapy Biennial Congress, Washington, DC, USA, 9-12 September 2014 (Poster Presentation)
- The 3rd International conference and Exhibition on Clinical and Cellular Immunology Summit, Baltimore, USA, 29 September-01 October 2014, (Oral Presentation).

The following publications were produced:

- Ivan Mfouo-Tynga, Nicolette Nadene Houreld and Heidi Abrahamse (2016). Evaluation of cell damage induced by irradiated Zinc-Phthalocyanine-gold dendrimeric nanoparticles in a breast cancer cell line. *Submitted to Scientific Reports.*
- Ivan Mfouo-Tynga, Nicolette Nadene Houreld and Heidi Abrahamse (2016). Synthesis and Characterization of Zinc Phthalocyanine-Gold Dendrimeric Nanoparticles and its Application in Breast Cancer Therapy. *Submitted to the Journal of Biomaterials.*
- Ivan Mfouo-Tynga and Heidi Abrahamse (2015). Cell Death Pathways and Phthalocyanine as an Effective Agent for Photodynamic Cancer Therapy. *International Journal of Molecular Science* **16**:10228-10241.
- Ahmed El-Husseiny, Ivan Mfouo-Tynga, Mohammed Abdel-Harrith and Heidi Abrahamse (2015). Comparative study between the photodynamic ability of gold and silver nanoparticles in mediating cell

death in breast and lung cancer cell lines. *Journal of Photochemistry and Photobiology B: Biology* **153**:65-75.

- Ivan Mfouo Tynga, Nicolette Nadene Houreld and Heidi Abrahamse (2015). Photodynamic Effects of Gold Nanoparticles in a Breast Cancer Cell Line (MCF-7) in Vitro. In: Lilge L.D. and Sroka R. (eds) Progress in Biomedical Optics and Imaging - Proceedings of SPIE, Volume 9542, 954204. doi: 10.1117/12.2184043 SPIE 9542, Medical Laser Applications and Laser-Tissue Interactions VII, 954204 (July 15, 2015); doi:10.1117/12.2184043, Published.

- Ivan Mfouo-Tynga, Ahmed Hussein, Mohamed Abdel-Harith and Heidi Abrahamse (2014). Photodynamic ability of silver nanoparticles in inducing cytotoxic effects in breast and lung cancer cell lines. *International Journal of Nanomedicine* **9**:3771–3780.

- Ivan Mfouo-Tynga, Nicolette Nadene Houreld and Heidi Abrahamse (2014). Induced Cell Death Pathway Post Photodynamic Therapy Using a Metallophthalocyanine Photosensitizer in Breast Cancer Cells. *Photomedicine and Laser Surgery* **32(4)**:205-211.

TABLE OF CONTENTS

CHAPTER ONE

INTRODUCTION

CHAPTER TWO

LITERATURE REVIEW

CHAPTER THREE

METHODOLOGY

CHAPTER FOUR

RESULTS

CHAPTER FIVE

DISCUSSION AND CONCLUSION

REFERENCES

LIST OF APPENDICES

LIST OF FIGURES

mechanisms: direct tumor cell killing, vascular destruction and immune system activation. (Anaphase-promoting complexes, APCs; hypoxia-inducing factors, HIF; vascular endothelial growth factor, VEGF; cyclooxygenase-2) (http://www.hindawi.com/journals/ijp/2012/637429/fig5/).

Conjugate mediated PDT induced changes in gene expression and BAX, BCL-2, CASP-2 and ULK-1 genes were significantly up-regulated as represented in the volcano plot. In the volcano plot, the horizontal line designates the target threshold (p=0.05) and vertical lines, the fold change (central) and target fold change threshold (peripheral) in gene expression.

Figure 34   The primary response of conjugate-mediated PDT on the expression of genes involved in cell death pathways was the up-regulation of Ulk-1, Bax, Casp-2 and Bcl-2 genes. The Ulk-1 protein protonates and activates the FIP200. Ulk is part of a protein complex containing Atg13, Atg10 and FIP200 (autophagosome), which drives the subsequent cellular damage and death. The Bax protein directly affects the mitochondria while the Cas-2 protein is activated by reactive oxygen species (ROS) and then Casp-2 transforms a mitochondrial damaging protein into its truncated and activated form (tBid). The p53-induced death domain associated protein (PIDD) can also convert pro-Casp-2 into the active Casp-2. Apoptogenic proteins (such as Cytochrome C) released from mitochondria participate in the assemblage of the apoptosome, activation of other effectors (Casp-3/6/7) and cell death. Mitochondrial damage and depolarization induce change in cellular ATP levels, activation of the 5' adenosine monophosphate activated protein kinase (AMPK) and AMPK-induced cell death. This cell death response stimulates Bcl-2 protein to prevent further cell damage.   97

LIST OF TABLES

when compared to the respective population type of the untreated control cells.

Table 12	Percentage of various cell populations after flow cytometric analysis. The lowest percentage of cell death (apoptotic and necrotic) and highest percentage of normal population were obtained with untreated cells. These apoptotic populations significantly increased (around 63%, cumulated percentage) in Actinomycin D-treated and the highest percentage of necrotic population (42%) was seen with Hydrogen peroxide (H_2O_2)-treated cells. Experiments were repeated four times (n=4) and significant differences were indicated as * ($p<0.05$), ** ($p<0.01$) and *** ($p<0.001$) were noted when compared to the respective population type of the untreated control cells.	82
Table 13	Percentage of various cell populations after flow cytometric analysis. The lowest percentage of cell death (apoptotic and necrotic) were obtained with untreated and $ZnPcS_{mix}$ controls. These apoptotic populations significantly increased (around 65%) in Actinomycin D- and PDT-treated cells. Experiments were repeated four times (n=4) and significant differences ($p<0.05$), ($p<0.01$**) and ($p<0.001$***) were noted when compared to the respective population type of the untreated control cells.	83

UNIVERSITY
OF
JOHANNESBURG

LIST OF ABBREVIATIONS

AFF-R	Alanylalanyl-phenylalanyl-rhodamine
AIDS	Acquired immune deficiency syndrome
AIF	Apoptosis inducing factor
AMPK	5' adenosine monophosphate activated protein kinase
APCs	Anaphase promoting complex
ARC	Apoptosis repressor with caspase recruitment domain
ATG	Autophagy
ATP	Adenosine triphosphate
AuDENP/s	Gold encapsulated dendrimers
AuNP/s	Gold nanoparticles
BAX-2	Bcl-2-associated X protein
BCL-2	B cell lymphoma-2
Ca^{2+}	Calcium ion
CASP-2	Caspase-2
CD	Complex death domain
cDNA	Complementary Deoxyribonucleic acids
CO_2	Carbon dioxide
COX-2	Cyclooxygenase-2
C_t	Threshold cycle
DAPI	4',6-diamidino-2-phenylindole
DEFCAP	Death effector filament forming ced-4-like apoptosis protein
DMEM	Dulbecco's Modified Eagle's Medium
DNA	Deoxyribonucleic acid
EDTA	Ethylene diamine tetra acetic acid

ELISA	Enzyme linked immunosorbent assay
E_m	Emission
EPR	Enhanced permeability retention
ER	Estrogen receptor
ER	Endoplasmic reticulum
E_x	Excitation
FITC	Fluorescein isothiocyanate
FTIR	Fourier Transform Infrared
G	Generation
G-C	Guanine-cytosine
gDNA	Genomic Deoxyribonucleic acid
GF-AFC	Glycyphenylalanyl-aminofluorocoumarin
h	Hour
H_2O_2	Hydrogen peroxide
Hb	Hemoglobin
HbO_2	oxyhemoglobin
HBSS	Hank's balanced salt solution
HER-2	Human epidermal growth factor receptor 2
HIF	Hypoxia inducing factor
HIV	Human immune deficiency virus
HPV	Human papilloma virus
IAP	Inhibitor of apoptosis protein
IP3	Inositol 1,4,5-triphosphate
IR	Infrared
ISC	Inter-system crossing
JC-1	J-aggregate forming cationic dye
LDH	Lactate dehydrogenase

LEDs	Light emitting diodes
MCF	Michigan Cancer Foundation
mPC	Metal Phthalocyanine
MPDC	Multiple particles delivery complex
mTOR	Mammalian target of rapamycin
NAD^+	Nicotinamide adenine dinucleotide ion
NADP	Nicotinamide adenine dinucleotide phosphate
NAPH	Nicotinamide adenine dinucleotide phosphate hydrogen
NIR	Near infrared
NO	Nitric oxide
Nox	Nicotinamide adenine dinucleotide phosphate oxidase
NPs	Nanoparticles
O_2	Molecular oxygen
PI3K	Phosphatidylinositide 3 kinase
PAR	Poly ADP (Adenosine Diphosphate)-Ribose
PARB	Poly ADP (Adenosine Diphosphate)-Ribose binding site
PARP	Poly ADP (Adenosine Diphosphate)-Ribose Polymerase
PBS	Phosphate buffered saline
PC	Phthalocyanine
PCR	Polymerase chain reaction
PDT	Photodynamic therapy
PET	Positionemission tomography
PI	Propidium Iodide

PIDD	p53-induced death domain associated protein
PR	Progesterone receptor
PS	Photosensitizer
RAIDD	Receptor interacting protein-associated ich-1/ced-3-homologue protein with a death domain
RIP	Receptor interacting protein
RLU	Relative light unit
RNA	Ribonucleic acid
ROS	Reactive oxygen species
RT	Reverse transcriptase
S	Singlet state
T	Triplet state
TB	Tuberculosis
TEM	Transmission Electron Microscopy
TMB	Tetramethyl-benzidine
TNFR-1	Tumor necrosis factor receptor-1
ULK	Unc-51-like kinase
US-FDA	United States Food and drug administration
UV-Vis	Ultra-violet visible
VEGF	Vascular endothelial growth factor
ZnPcS$_{mix}$	Mix Zinc Phthalocyanine

LIST OF SYMBOLS

A	Absorbance
α	Alpha
cm^2	Centimetre/s squared
$^{\circ}C$	Degrees centigrades
r^2	Radius squared
eV	Electron Volts
Ex	Excitation
Em	Emission
g	Gram/s
h	Hour/s
OH^-	Hydroxyl
J	Joule/s
J/cm^2	Joules per centimetre/s squared
κ	Kappa
L	Litre/s
<	Less than
>	Greater than
μg	Microgram/s
μM	Micromole/s
μm	Micrometre/s
μl	Microlitre/s
μs	Microsecond
min	Minute/s
mg	Milligram/s
mW	Milliwatts
mW/cm^2	Milliwatt/s per centimetre squared
nm	Nanometre/s
nM	Nanomolar/s
ns	Nanosecond/s

n	Number of samples
O_2	Oxygen
%	Percent
pg	Picogram/s
rpm	Revolutions per minute
$^1O_2$	Singlet Oxygen
$^3O_2$	Triplet Oxygen
W	Watt/s
λ	Wavelength
$\Pi(d)^2$	Pi multiplied by diameter squared

CHAPTER ONE

INTRODUCTION

1.1   Background

Cancer refers to a group of diseases that are characterized by unregulated cell proliferation throughout the body. Cancer is predicted to cause more damage and its incidence is thought to increase by more than 80% by the year 2030, especially in developing regions. Breast, colorectal and lung cancers are the most diagnosed, and their incidences are related to extended lifespan and increased cancer related risk factors such as smoking, unhealthy diet and obesity (Centre for Disease Control and Prevention, 2015; National Cancer Institute, 2015).

Photodynamic therapy (PDT) is a minimally invasive therapeutic approach that targets and destroys cancers. This approach combines light, oxygen and photochemical agents known as photosensitizers (PSs). Each PS is activated by light irradiation at a precise wavelength, which matches the absorption properties of the PS. Light activated PSs interact with molecular oxygen leading to the generation of reactive oxygen species (ROS) such as singlet oxygen, hydroxyl radicals, superoxide anions and hydrogen peroxide. Generated ROS is cytotoxic and causes sequential cell damage and eradication of cancer cells. Photosensitizers have a special affinity for cancer cells and, hence, reduce the toxic effects to adjacent healthy cells. PSs have attracted the interest of researchers as seen with the development of first, second and now third generation PSs (Agostinis *et al.*, 2011; Calzavara-Pinton *et al.*, 2007).

Abraxane, a nanoparticles-albumin-paclitaxel conjugate, has been approved by the United States Food and Drug Administration (US-FDA) for breast and lung cancer treatment, and marked the entry of nanotechnology

in cancer therapy (Gradisha *et al.*, 2005; Casaluce *et al.*, 2012). Nanoparticles (NPs) have the ability to passively accumulate in tumours, a mechanism known as the enhanced permeability and retention (EPR) effect. Once inside a cell, NPs damage the vasculatures of tumour cells (Torchilin, 2011; Maeda *et al.*, 2006; Matsumura and Maeda, 1986).

1.2   Problem Statement

In Africa, it has been recognized that malaria, tuberculosis (TB), human immune deficiency and acquired immune deficiency syndrome (HIV/AIDS) are major heath-threatening conditions. Currently, cancer has emerged as a major health problem in developing continents as the condition causes more deaths than malaria, TB and HIV/AIDS, taken together. It is now the most common condition on the continent, with 16 million new cases diagnosed annually (World Health Organization, 2008). It was estimated that South Africa could see an increase in incidence up to 78% in cancer cases by 2030. Breast cancer is the most common occurring cancer in South African women, and increased incidence is seen each year (Benn, 2009; Herbst, 2015).

Target therapy is a new treatment approach that aims to increase the therapeutic efficacy by using conjugated compounds rather than one therapeutic agent. In order to realize selective delivery, certain receptors on the tumour cell surface have been identified as potential targets, and NPs have the ability to recognize and bind to these receptors. NPs can be conjugated to chemotherapeutic agents and deliver them into tumour cells after uptake and internalization by receptor-mediated endocytosis (Aslain *et al.*, 2013; Torchilin, 2005).

In this study we intended on improving photo-induced cell damage in breast cancer cells by combining NPs to a second generation PS, sulfonated Zinc-Phthalocyanines (ZnPcS$_{mix}$), which previously showed effective light-

induced cytodamage in various cancer cell lines. Using gold nanoparticles (AuNPs), we wanted to determine the effects of AuNPs alone, irradiated AuNPs, and AuNPs combined to $ZnPcS_{mix}$ before and after irradiation. We also wanted to determine the role of AuNPs at the centre of a dendrimeric-PS hybrid, and how it would affect the therapeutic efficacy *in vitro* using a MCF-7 breast cancer cell line.

1.3   Objectives of the Study

This objectives of the study were as follow:

- to compare the light-induced effects of two gold structured nanoparticles in a breast cancer cell line,
- to combine the most suitable gold structured nanoparticle to sulfonated Zinc-Phthalocyanine ($ZnPcS_{mix}$),
- to characterise the combined compounds also known as multiple particles delivery complex (MPDC),
- to determine the treatment parameters that leads to an approximately 50% decrease in cell damage,
- to determine the subcellular localization of MPDC,
- to identify the photo-induced mechanisms of cell damage subsequent to MPDC-mediated PDT,
- to elucidate the expression profile of genes involved in cell death pathways.

CHAPTER TWO

LITERATURE REVIEW

2.1   Cancer

Vertebrate organisms consist of organ systems composed of several functioning organs. Organs are made of tissues that are in turn made up of numerous cells; the basic units of life. An individual consists of trillions of living cells and regulatory mechanisms for proper control of cellular events and activities, including cell growth, division and death (Cavalier-Smith, 1987; Pepper and Herron, 2008; Folse and Roughgarden, 2010). However, when these mechanisms fail to regulate cellular activities, the cells begin to grow out of control and become cancerous.

Cancer arises following cell malignant transformations, which render cells self-sufficient and insensitive to regulate growth signals, and are able to sustain angiogenesis and evade apoptosis, as well as to replicate perpetually and invade neighboring cells and tissues. These transformations are triggered by mutations that occur from exposure to harmful chemicals, radiation, ultraviolet (UV) light, and genetic replication inaccuracies. These mutagens alter the genetic material by altering the structure and sequence of nucleotide bases. Errors occurring during cellular replication, as well as in protein synthesis, are the principal consequences and influence cell growth, division and aging (Jumaa *et al.*, 2005; Hanahan and Wienberg, 2000; Fadeel and Orrenius, 2005).

Subsequent to deoxyribonucleic acid (DNA) damage, normal cells activate repair or death mechanisms to deal with the damage. While in cancer cells, such damage remains unrepaired and stimulates further cell replication and transformation. Such genetic modification can be acquired from parents (inherited mutations), malfunctioning metabolism (hormones, immune

conditions) or inappropriate genetic replication. Additionally, external stimuli such as cigarette smoke or sun exposure, and infections may cause tumour formation through genetic damage and modification.

All these effectors may lead to cancer formation and may act together. After exposure to cancer-inducing factors, an extended time lapse is usually observed before symptoms become detectable in the form of a tumour. A tumour is a swelling or abnormal mass of tissue that may be solid or not. A tumour can be considered as pre-malignant or non-cancerous, also known as benign, as they do not spread to other body parts (American Cancer Society, 2014). Like leukemia, certain cancers do not form tumours, they are usually comprised of blood or blood-forming particles and move into other tissues where they mature. Though cancer may metastasize, they are named based on their site of origin and differ in their manifestations and required specific therapeutic approaches. As a consequence of the uncontrolled spread of cancer cells, death of the entire organ and the organism is usually the ultimate outcome (Bonnet *et al.*, 2004; American Cancer Society, 2014). Many cancers as seen today could have been prevented, especially those caused by the heavy consumption of cigarette and alcohol. In 2014, more than 31% of estimated cancer deaths was due to tobacco use, and a similar proportion of cancer occurring in economically developed countries was associated with poor eating habits and lifestyles (American Cancer Society, 2014).

2.1.1 Burden of cancer

An approximated 12 million new cancer cases occurred annually worldwide, with the majority located in developing regions. Cancers affecting the lungs, female breasts, bowel and prostate glands are diagnosed more frequently with lung cancer representing one tenth of all occurring cancers in men (Figure 1). In 2012, a global estimation of 8.2 million lives were lost due to cancer, and 60% of those were from developing regions. Lung, liver,

stomach and bowel cancers are the most deadly forms of cancers and account for 50% of all cancer deaths worldwide. The most diagnosed and also most damaging is lung cancer, which causes a fifth of cancer-related deaths (Cancer Research UK, 2014).
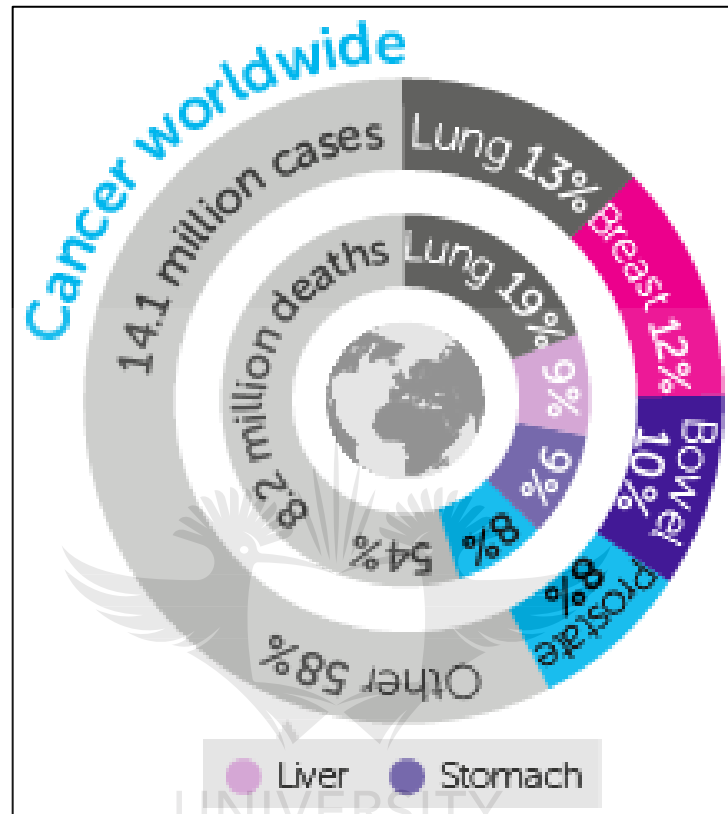
Figure 1: Global Cancer burden. An estimated 14.1 million cases were reported with lung (13%), breast (12%), bowel (10%) and prostate (8%) been the most diagnosed cancers. Meanwhile, deaths due to cancer totaled 8.2 million with lung (19%), liver (9%), stomach (9%) and prostate (8%) being the most common (Cancer Research UK, 2014).

2.1.2 Cancer stages

From the time of exposure, to cancer inducible factors, to death, the cancer cell evolves from its most undamaged form to its most devastating state, and is known as the cancer stage. Staging is a comprehensible approach to identify the tumour size, location, proliferating rate and metastasizing ability. It provides health professionals with further information on the physiological status of neighboring organs and predictions on the type of

treatment and its efficacy, risk of recurrence and prognosis of the cancer (American Society of Clinical Oncology, ASCO, 2015).

Most cancers have five stages. The first or stage 0, is characterized by a cluster of cells that have become tumourous and start to proliferate. At this stage the tumour is still small and highly treatable through standard surgical removal. In stage 1, tumour cells are localized and diffuse through the basement membrane where they start to invade nearby tissue. It is called the early cancer stage or localized stage as growing cancer cells remain in a lump partly in neighboring tissue, and begin to threaten life. The following stage (stage 2) or regional spread occurs as a result of lymph vessel invasion by the ever proliferating cancer cells, which also get into the lymph nodes (immune system). At this stage the tumour is large in size, grown in depth and has spread within the overall area. In stage 3, the cancer formation is iniated and stage 4 is the most severe, includes metastasis to distant lymph nodes, into the blood stream where cancer cells invade complete capillaries and further to any body parts. They form new colonies in other organs and it is called advanced or metastatic stage (Cancer Institute NSW, 2014).

2.1.3 Cancer in Africa

Since 2008 no comprehensive cancer study has been done involving the entire African continent. Cancer has been identified as a strengthening public health concern in Africa. It is anticipated that 1.28 million new cancer cases and 970 000 cancer deaths will occur annually by 2030, which will result from a decrease in the burden of communicable diseases, adoption of new dietary and lifestyle behaviors, and prolonged life. The lack of awareness of current and future cancer burdens coupled with present and prominent public health issues, including HIV/AIDS, malaria, TB, and perinatal complications lead to relatively little attention and allocation of

resources to fight cancer (Ferlay *et al.*, 2008; World Health Organization, 2008).

Africa has a unique and mosaic demography with respect to nationalities, beliefs, languages, dialectics, culture, and economic status. Together these demographic factors may effect the incidence and outcomes of cancer. Also, whites of European provenance, represent a substantial percentage of inhabitants, as much as 9% in South Africa (CIA, 2010; Statistics South Africa, 2012). Cancer in Africa shows remarkable discrepancies that are dependent on demographic factors, which determine the type of cancer, stage of diagnosis, survival, and incidence as well as death rates. These differences highlight various risk factors, detection practices (diagnostic and screening), recognition of early signs and symptoms and availability of treatment (Jemal *et al.*, 2010; Kavanos, 2006; Curados *et al.*, 2007).

Major cancers in men

Kaposi sarcoma had the leading incidence as well as leading number of cancer deaths in Eastern Africa. When compared to the male population in Northern Africa, these rates appeared to be 20 times less and coincided with a lower incidence of disease caused by the human herpes virus (Ferlay *et al.*, 2008; Ziegler *et al.*, 2003). Esophageal cancer was ranked as the second most occurring and deadliest cancer in Eastern African men. These figures were seven times higher than the rest of the continent, with the exception of the southern part of Africa, which was 30% more (Ocama *et al.*, 2008; Schneider *et al.*, 2007). Esophageal cancer is not fully understood, but the major risk factors include poor diet, and consumption of both tobacco and alcohol. A synergic relationship was established between smoking and alcohol as people who smoke and drink heavily had a 30-fold increased risk (American Cancer Society, 2014).

Liver cancer is the most common cancer and leading cause of cancer-related death in Middle and Western African men. Chronic infection with hepatitis B virus in sub-Saharan Africa and hepatitis C virus in Northern Africa are the main source of the cancer on the continent and worldwide (Blumberg, 1984; Franceschi and Raza, 2009; American Cancer Society, 2014). Lung cancer was the most diagnosed and largest cause of cancer deaths among Northern African men in 2008. This incidence rate appeared to have doubled in the southern part of the continent, where the tobacco epidemic and smoking are more prominent. In Southern African men, smoking may contribute to 65% of lung cancer and similar trends are seen in western countries (Reddy *et al.*, 1996; Shafey *et al.*, 2009; Sitas *et al.*, 2004).

In contrast to lung cancer, bladder cancer incidence and mortality rates among Southern African men are half of those seen in Northern African men, especially in Egyptian men, who have the highest incidence of bladder cancer in the world (Parkin, 2008). Infection with the *Schistosoma hematobium* parasite may account for the prediposed individuals more than 40% incidence of bladder cancer on the continent (Mostafa *et al.*, 1999; Parkin, 2006). Among Southern African men, prostate cancer was the most diagnosed with an incidence rate that doubles that of the second highest regional rate in Western Africa and almost seven times higher than the lowest regional rate in Northern Africa. This elevated rate was due more to increased diagnosis than to occurrence (Parkin *et al.*, 2008).

Major cancers in women

Cervical cancer represented more than 25% of all cancer occurring among Eastern African women in 2008, and was also the leading cause of death due to cancer. Eastern Africa had the highest cervical cancer rate worldwide. This could have been attributed to the lack of preventive measures and the high prevalence of human papilloma virus (HPV) infection

(Ferlay *et al.*, 2008; American Cancer Society, 2011). In contrast to cervical cancer in Eastern African women, breast cancer was the commonest cancer and leading cancer-related death among women in Southern and Northern Africa for the same period of time. With the high prevalence of white populations, which are prone to a high prevalence of reproductive risk factors for breast cancer (early menarche, late pregnancy and obesity), this makes the southern part of African the region with the highest incidence rate for breast cancer (Parkin *et al.*, 2010; Vorobiof *et al.*, 2011).

In contrast to male cancers, cervical cancer in Eastern African women and breast cancer in both Southern and Northern African women were the most commonly occurring cancer among women, with a similar frequency to the rest of the continent. However, a shift from previous decades had been and continues to be seen in which breast cancer is taking over cervical cancer, and becoming more and more prominent in Africa due to the adoption of the kind of lifestyle associated with developed countries (Mackay *et al.*, 2006).

2.2 Breast Cancer

Breast cancer is the development and proliferation of abnormal cells within the breasts. It usually begins in the inner lining of the lactiferous milk ducts or the lining of the lobules and is known as ductal carcinoma and lobular carcinoma, respectively (Figure 2). The majority of breast cancer occurs in females due to the physiological function of the female breasts to produce milk (Birkenfeld and Kase, 1994).

Breast cancer is the leading cancer among women and cause of cancer death worldwide (Ferlay *et al.*, 2008). The condition has several markers and is known as a heterogeneous disease. The estrogen receptors (ER), progesterone receptors (PR) and human epidermal growth factor receptor 2 (HER-2) are essential for diagnosis and selection of suitable therapies. Additionally, most breast cancer tumours express alpha estrogen receptor

(αER), which is of particular importance in cancer therapy (Mosoyan *et al.*, 2013; Yang *et al.*, 2013).
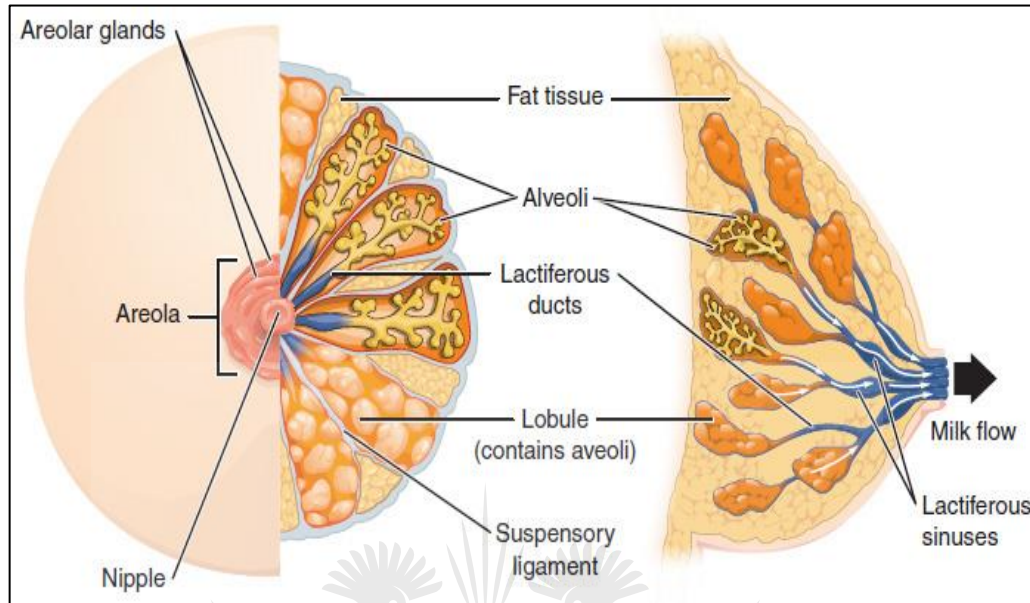
Figure 2: Anatomy of the breast. During lactation, milk moves from the alveoli through the lactiferous ducts to the nipple (http://cnx.org/contents/9cccba49-6490-4e5b-a366-9991b7dbc56c@4).

2.2.1 Risk factors

It appears that breast cancer is more common among elderly women in developed countries, who have prolonged lives as compared to their counterparts in developing countries. The risk of breast cancer increases with age; the older a woman is, the higher her risk of the disease. A woman in her 60s is 100 times more likely to develop this cancer than a 20 year old female (Institute of Medicine, 2012).

The risk seems to be proportional to the hormonal activity in the breasts. A mother who breast-feed decreases her lifetime risk of contracting breast cancer. Women who have breast-feed by the age of 20 years further decrease their lifetime risk of this cancer. The risk increases slightly with late pregnancy and doubles in women who have their first child at an age older than 30 years, and triples in women who never give birth. Both pregnancy

and breast-feeding play a preventive role in breast cancer (Collaborative Group on Hormonal Factors in Breast Cancer, 1997; Newcomb *et al.*, 1994). Additionally, increased blood levels of estrogen increases the risk of breast cancer, while increased blood levels of progesterone is associated with a decreased risk of the same cancer in premenopausal women (Yager and Davidson, 2006).

Experts argue that lifestyles and diet of women in rich and poor countries are the major differential factors. With the globalization and adoption of developed countries lifestyle, this discriminatory aspect of the disease seems to fade away in poor countries, which currently showed increased breast cancer incidence and higher mortality rate (Mackay *et al.*, 2006; Parkin *et al.*, 2010; Vorobiof *et al.*, 2011). In the United Kingdom, alcohol consumption accounts for 6% of breast cancer in women. Alcoholic beverages can be classified as a carcinogen as it can lead to breast cancer development in women in a dose-dependent manner. As a woman's consumption of alcohol increases, so does her risk of breast cancer (Allen *et al.*, 2009). Low fat intake has been found to have a slight decrease on breast cancer risk and recurrence in premenopausal women (Chlebowskin *et al.*, 2009; Hunter *et al.*, 1996; Prentice *et al.*, 2006). However, a high intake of dietary fat was found to play a minor role in the development of breast cancer and should be avoided (Pala *et al.*, 2001; Sonestedt *et al.*, 2008).

A British Broadcasting Corporation news report announced that gaining excess weight post menopause increases the risk of developing cancer, particularly breast cancer. A 10 kg gain resulted in an increase in 18%, while an increase of 25 kg in women older than 25 years led to a 45% increased risk of breast cancer (British Broadcasting Corporation, 2006). Several other studies have supported the finding that obesity was associated with increased risk of breast cancer as obese women are likely to develop larger tumours, and experience poor breast cancer prognosis with a 30%

increased risk of mortality (Ligibel, 2011; Protani *et al.*, 2010; Kroember *et al.*, 2005; Caan *et al.*, 2006; Holmes *et al.*, 2005). Women with a close relative with breast or ovarian cancer has a risk of developing these cancers. Generally, breast cancer is not inherited and hereditary breast cancer accounts for only 5% of all breast cancer. A woman with a mutation in breast cancer genes (BRCA1 and BRCA2) has a 60 to 80% risk of developing breast and/or ovarian cancers (Malone *et al.*, 1998).

2.3   Cancer Treatments

2.3.1 Conventional modalities

Breast cancer, like any other cancer, can be cured if diagnosed at an early stage, late diagnosis and treatment reduces the possibility of an effective cure (He *et al.*, 2007). Many conventional means of dealing with cancer exist and consist of surgery, hormonal therapy, radiation therapy, immunotherapy, chemotherapy, and adjuvant therapy. Ancient practices declared cancer incurable once it had started to metastasize and invade other body organs. At that stage, any therapeutic intervention was believed to cause more harm than curative effects. The first recorded evidence of breast cancer dates from Ancient Egypt around 1500 BC; while no effective treatment were available, palliative treatments were well-known as the only treatment option (Gallucci, 1985; Kardinal and Yarbro, 1979).

Primitive surgery, with multiple complications, was then developed and emerged as a treatment option due to the fact that cancer essentially forms a tumour including benign tumours, which are localized and do not spread to other body parts. Following the discovery of anesthesia in 1846 key ongoing improvements in general surgery as well as in cancer surgery advanced, and that stage of development was known as the century of the surgeon. Cancer surgeries or cancer operations are medical procedures that remove the entire tumour and surrounding lymph nodes (Figure 3) (American Cancer Society, 2014; Sudhakar, 2009).
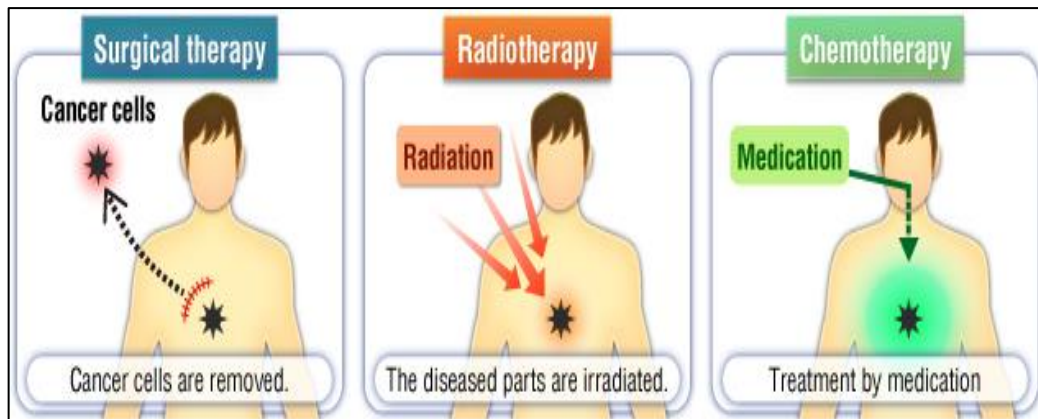
Figure 3: Conventional therapy modalities. Cancer cells are removed through surgery, destroyed by radiation or through an administered drug (http://www.hirt-japan.info/en/what/difference.html).

In the late 1970s, ultrasound (sonography), computed tomography (CT scans), magnetic resonance imaging (MRI scans) and positron emission tomography (PET scans) were fully developed and commonly used in surgery. In the 21st century, methods such as miniature video cameras and endoscopy are being utilized to remove organs through tube, and less invasive methods including cryosurgery (liquid nitrogen spray) are being used to destroy tumours. Currently, a device that is able to generate an intense beam of electromagnetic radiation is being used for drilling and cutting purposes in surgery (Sudhakar, 2009). Despite its efficacy in removing neoplastic tissues, surgery is limited to certain cancer stages and is a very risky procedure as wound-associated problems, extreme bleeding and increased patient morbidity are often observed (Steele *et al.*, 2006; El-Tamer *et al.*, 2007; Vitug and Newman, 2007; Hogan and Joyce , 2012).

The usage of x-rays, gamma rays, and charged particles in cancer therapy is known as a radiation therapy. It is a common therapeutic procedure in the United States and approximately half of all cancer patients would receive this therapy. These high-energy radiation particles are directed to the cancer site and destruction occurs through nucleic material damage (Figure 3). Cell damage beyond repair leads to obstruction in cell division, cell

degradation and elimination through the bodie's natural defense mechanisms. Systemic radiation is commonly used to deliver radioactive agents, which travel through the bloodstream to the cancer cells. Both external beam radiation and internal radiation approaches can be utilized to deliver radioactive material to neoplastic sites (Veldeman *et al.*, 2008; Noda *et al.*, 2009).

In cases of curative intent, radiation therapy is mostly used in combination with other conventional therapeutic modalities. Radiation therapy is usually offered as a treatment plan, which starts with simulation. The therapy targets both cancer and normal cells, yielding numerous side effects. Potential damage to normal cells is taken into consideration during the planning phase, and the tolerated dose of radiation by normal cells is determined in the targeted location prior to treatment. Many observed palliative effects are often associated with this therapy in some parts of the body, including the brain, spine, bones and esophagus (Kavanagh and Timmerman, 2006; Brada *et al.*, 2007; Patel and Arthur, 2006; Lam *et al.*, 2007).

Chemotherapy is one of the most commonly used cancer therapeutic approaches along with surgery and radiation therapy, and have been used separately or in combination to maximize the therapeutic effect in the past decades. The discovery of nitrogen mustard as a potent anti-proliferating agent for lymphoma, led to the development and use of numerous chemotherapeutic drugs in research for better therapeutic approaches for various cancer types (Sudahkar, 2009). Chemotherapy uses medicines or drugs to cure cancer (Figure 3). Compared to surgery or radiation, chemotherapy is not a targeted therapy and has the ability to kill cancer throughout the body. The main propose is to cure cancer by preventing cancer cells from metastasizing, preventing tumour growth, destroying cancer cells throughout the body, and relieving the symptoms associated with cancer. Several chemotherapeutic drugs can be used simultaneously

and is known as combination chemotherapy, where each drug has a different mechanism of action. This can enhance treatment efficiency and reduce the possibility of cancer cells developing drug resistance (von Minckwitz *et al.*, 2012; Barker *et al.*, 2009).

Drug parameters such as type, dosage, delivery strategy, administration frequency and duration of the treatment vary according to the cancer type and stage, and have to be determined prior to commencement of treatment for optimal effect (Zirakzadeh *et al.*, 2013; Gralow *et al.*, 2008). Due to the fact that chemotherapy is a fairly generalized therapy as it affects most of the body parts, the manifestation of numerous side effects are mostly seen after chemotherapy interventions. In order to alleviate these side effects, current research aims to develop new approaches for drug combination, liposomal and monoclonal antibody therapy to target cancer cells, chemo-protective agents to normal cells, hematopoietic stem cell transplantation and chemotherapeutic agents to overcome drug resistance (Kadakia *et al.*, 2012; Sak, 2012; Albain *et al.*, 2009).

2.3.2 Photodynamic therapy (PDT)

An alternative cancer modality, PDT has become popular over the years with its discovery dating back to the early 20th century. It was accidentally revealed that certain fluorescent dyes identified as acridine orange localized in *Paramecium* spp. Protozoa and had the ability to destroy their hosts after extreme sunlight exposure of those microorganisms (Raab, 1900; Oleinick and Evan, 1998). It was also elucidated that the destruction seen required the involvement of molecular oxygen leading to the recognition of photodynamic action (Von Tappeiner and Jesionek, 1903; Von Tappeiner and Joblauer, 1904). Today, PDT is known as a promising anticancer treatment that uses distinctive drugs, along with light at a precise wavelength to complement the absorption properties of the drugs to kill various neoplastic cells. Photoradiation therapy, phototherapy or

photochemotherapy are other types of PDT (Mroz *et al.*, 2011; Manifold and Anderson, 2011; Juzenas and Juzieniene, 2010; Huang, 2005).

Photodynamic therapy continues to gain interest in biomedical research and application, where it is extensively used in both experimental and clinical settings to successfully treat various cancers. Photodynamic therapy produces toxic oxygen species that kill cells and these species are commonly known as ROS such as singlet oxygen, superoxide, and hydroxyl radicals. Some of the drugs used in PDT have been approved by the US-FDA, and this treatment is being used for several conditions including bladder conditions, cancer affecting the skin and gastrointestinal system, non-cancerous skin conditions and retinal conditions (Hamblin and Mroz, 2008; Ortel *et al.*, 2009).

Photodynamic therapy is a chronological process with numerous benefits over conventional treatments; it is designated as a minimally invasive and targeted therapy. In the clinical setting, the initial step of this therapy consists of the administration of drugs to patients through a predetermined topical, oral or intravenous route. The drugs are commonly known as photosensitizers (PSs), which refers to the light sensitivity characteristic of these compounds. Photosensitizers are formulated in a specific manner that confers on them a limited biodistribution, to have an affinity to highly proliferating cells such as cancer cells, as will as low dark toxicity (inactive state) (Brown *et al.*, 2004; Castano *et al.*, 2004; Peng *et al.*, 2009, Agostini *et al.*, 2011). Time lapse, or drug to light interval, is observed for proper localization of a PS into cancer cells. The duration of this interval can vary and depends on the PS. Following this, the second step in this process is the light-dependent activation of the PS. The core of the mechanism of action is coupled with the interaction with molecular oxygen.

Parameters in photodynamic reactions (light, PS, Oxygen)

Sunlight as the source of irradiation should be avoided as it has diverse wavelengths and intensities, leading to inappropriate PS activation or non-activation and unintended outcomes (Allison *et al*., 2004; Mang, 2004). Light sources can vary, and for effective PDT, a specific wavelength of light that matches the absorbance properties of the PS and proper light fluence are required. The choice of both PS and light wavelength are determined by the tumour location. Tissues have several chromophores and absorb light in the form of photons. The lower light wavelengths are ideal for superficial irradiation. Melanocytes in the skin, and both hemoglobin (Hb) and oxyhemoglobin (HbO_2) in red blood cells are able to absorb light in the red region of the spectrum. Human tissues contain a high concentration of water molecules, which absorb longer light wavelengths in the near-infrared spectrum (NIR), offering better tissue penetration *in vivo* (Mang, 2004; Allison *et al.,* 2004; Brancaleon and Moseley, 2002; Sibata *et al*., 2001).

Photosensitizers are activated at different wavelengths, light is absorbed maximally in the range of 650 to 1 350 nm. This is also known as the optical window or therapeutic window and is preferred with a tissue penetration that can reach up to 1 cm (Figure 4). Any photon in the therapeutic window possesses enough energy to penetrate tissues and activate PSs (Plaetzer *et al*., 2009; Zhu and Finlay, 2008). At wavelengths less than 600 nm, more photons are absorbed by systematic chromophores and yield minimal activation of PSs (Agostini *et al*., 2011). The importance of the light in PDT and the accessibility of light to tumour cells has attracted the attention of engineers to develop light devices suitable for PDT applications.
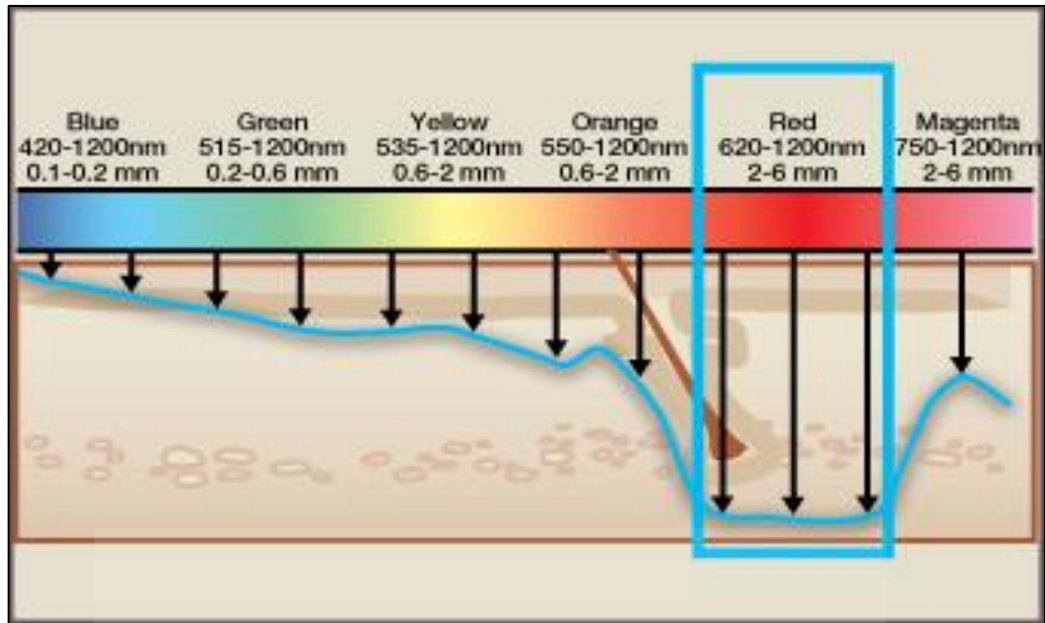
Figure 4: Light penetration into tissue is a function of the wavelength. Shorter wavelengths have minimal penetration and are absorbed by the majority of systematic chromophores, while at longer wavelengths in the red to near infrared region the penetration is deeper (http://www.ilightpro.com/What-is-IPL/Benefits-of-IPL.aspx).

Today, several reliable light devices exist to deliver light to the region of treatment and are commercially available. They include various lasers, light emitting diodes (LEDs), and fiber optic cables. With current technology, light can be effectively introduced to almost any part of the body. Light applicators can be designed and used for complicated and high risk anatomical structures (Mang, 2004; Brancaleon and Moseley, 2002; Nyst *et al.*, 2007; Weersink *et al.*, 2005; Samkoe *et al.*, 2007; Drobizhev *et al.*, 2006; Juzieniene *et al.*, 2004).

The availability of molecular oxygen in the treatment body area during light irradiation is a determining factor for effective treatment. Without substantial molecular oxygen, PDT will yield no therapeutic effect and possibly lead to tumour resistance to PDT. Thus, the level of molecular oxygen has to be evaluated during PDT (Huang *et al.*, 2003; Chen *et al.*, 2002; Vakrat-Haglili *et al.*, 2005). The presence of oxygen in the tumour can be assessed using several methods including fluorescence quenching-based optical probes,

19

PET, magnetic resonance spectroscopy, non-invasive phosphorescence and real time imaging techniques (Vaupel and Mayer, 2007; Hutchingson *et al.*, 2004; Woodhaus *et al.*, 2007; Vaupel *et al.*, 2007). Oxygen depletion during the photodynamic reaction can be compensated through fractionating into regulated light and dark periods or decreasing the fluence rate. The efficacy of PDT in hypoxic and cancer cells can be improved by increasing the level of oxygen by hyperoxygenation, thus making cells more susceptible to PDT. The level of oxygen is directly proportional to the efficacy of PDT (Huang *et al.*, 2005).

In photodynamic reactions, PSs are the central and most important elements, they are naturally occurring or synthetic agents that are able to absorb photons. Their interactions with molecular structures and ability to transfer energy are critical for the induction of cytodamage (Allison *et al.*, 2004; Nastri *et al.*, 2010; Denis and Hamblin, 2013). Photosynthesis is a fundamental and indispensable biological process on earth as it makes energy available for metabolism. Like PSs, many have been able to transfer energy and have critical roles in photosynthetic reactions. However, PSs suitable for PDT have characteristic structures that allow them to successfully undergo photodynamic reactions, known as type I reaction and type II reaction.

Certain dyes, such as porphyrins (Figure 5) and chlorophyll derivatives from plants and microorganisms have been reported to possess structures for PDT applications. Most PSs have heterocyclic ring structures identical to chlorophyll and hematoporphyrin structures (Allison *et al.*, 2004). Several compounds have been identified and characterized but only a few have entered the clinical trial stage and received approval worldwide (Allison and Sibata, 2010; Huang *et al.*, 2008). Photosensitizers generally adhere to the following criteria: they are commercially available, stable with simple chemical formulation and low dark toxicity, hydrophilic (specially for intravenous application) for adequate systemic application with multiple

administration routes, preferentially accumulates in tumour cells, is rapidly cleared from the body and normal cells, specifically light activated, and able to generate photodynamic reactions with strong photocytotoxicity and with pain free-therapy (Allison and Moghissi, 2013; Denis and Hamblin, 2013). Since the discovery of PDT, the development of PSs has grown and attracted the attention of many scientists.
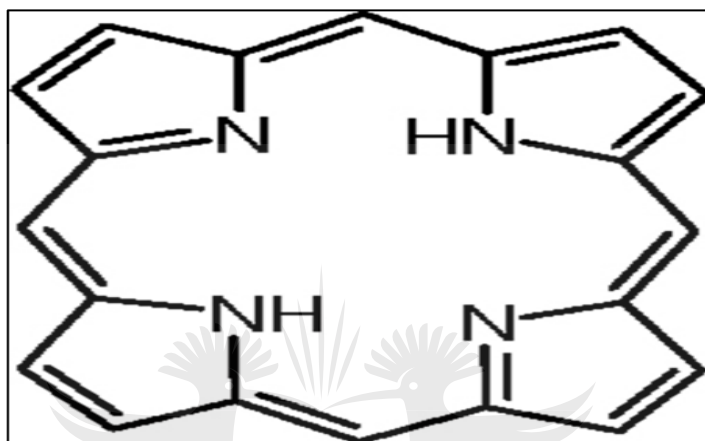
Figure 5: Porphyrin structure (Chemistry About, 2009).

First generation PSs included hematoporphyrins and porphyrin and their derivatives, and were developed between the 1970s and 1980s. Photofrin became the first approved PS for clinical trials. Later, PSs belonging to this primary generation were subjected to criticism for their extended retention in the body, subsequent poor clearance, poorly defined and unstable chemical structures, and their limitation to superficial conditions as their poor absorption properties prevented light penetration, allowing only a maximum light penetration depth of 5 mm (Allen *et al.*, 2001; Huang *et al.*, 2008). These drawbacks then led to the development of second generation PSs such as Foscan, Verteporfrin, Laserphyrin, Visudyne and Phthalocyanine. Due to their good optical, photophysical and photochemical characteristics, they have been intensively used in preclinical and clinical trials for photodynamic applications in various solid tumours (Allen *et al.*, 2001; Loewen *et al.*, 2006; Jankun *et al.*, 2004; Du *et al.*, 2006).

Despite good reports, second generation PSs are currently being improved and conjugated to molecules such as antibodies, liposomes and others to form third generation PSs for target PDT applications. The conjugation is thought to confer specific affinity to cellular markers, which may or may not be tumour-associated markers. Conjugation may or may not affect internalization processes, but improved internalization of PSs leads to enhanced cytodamage in PDT (Huang *et al.*, 2008). The availability of multiple PSs with different structures and functional properties makes PDT an extremely versatile and equally, an exciting approach to treat cancer. The advanced understanding of molecular pathways helps to design improved treatment regimens. As most cancers are treated with combination therapies, PDT is integrated into rationally designed combined regimens that exploit molecular responses to PDT for improved efficacy.

2.3.3 Photodynamic mechanisms of action

Photodynamic actions use and depend upon the combination of PSs, light and molecular oxygen to cause cancer destruction through programmed or non-programmed cell death pathways (Mroz *et al.*, 2011; Oleinick *et al.*, 2002, Mfouo-Tynga and Abrahamse, 2014). In practice, PDT is a sequential process and involves the diagnosis, administration of PSs, light activation of PSs and tumour destruction (Figure 6) (Regehly, 2008; Majumdar *et al.*, 2014).

Upon light activation of PSs, the induction and the rest of the photodynamic reactions depend solely on specific sets of PS characteristics, known as photophysical and photochemical properties (Figure 7). The photophysical properties allow the light activated PSs to change states. Prior to activation, PSs are in a stable ground singlet state. Subsequent to light irradiation, photon energy is absorbed by PS, which is excited single electrons in the uppermost occupied orbit are brought to the lowermost unoccupied orbit, taking the PS to an excited singlet state (Foote, 1991).
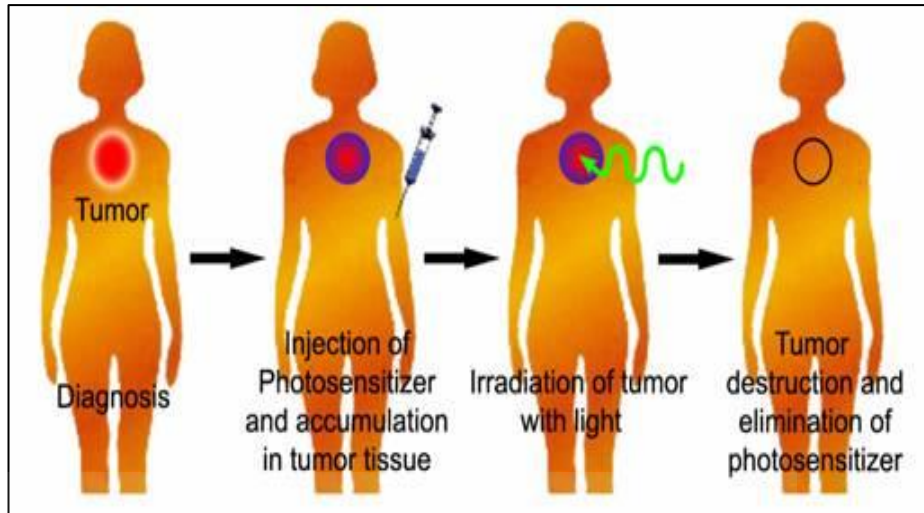
Figure 6: Mechanism of action in photodynamic cancer therapy. Following diagnosis, a photosensizer is administrated and preferentially accumulates in neoplastic cells. Light activation leads to the destruction of cancerous cells and tissues (Regehly, 2008).
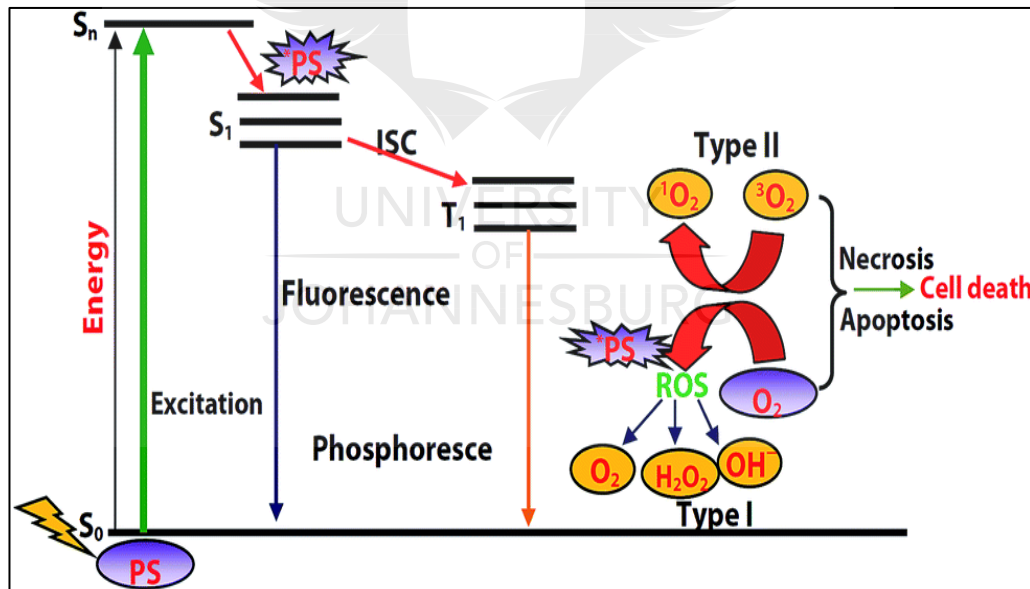
Figure 7: Modified Jablonski energy level diagram for photodynamic therapy (PDT). This treatment requires three elements: a photosensitizer (PS), light, and molecular oxygen (O_2). S_0, S_1 and S_n indicate ground or zero, first and n order of the singlet electronic state of PS, respectively. T_1 represents the triplet state of the excited PS. The molecule undergoes intersystem crossing (ISC) and triplet state PS interacts with O_2, generating different ROS, which cause cytotoxicity and subsequent cell death (Majumdar *et al.,* 2014).

Many physical pathways may be involved during intersystem crossing, converting the excited singlet state PS to the long-lived and excited triplet state PS. The triplet state has the ability to undergo photochemical processes and interact with triplet state molecules such as molecular oxygen, through type I or type II reactions (Figure 8). In a type I reaction, electrons are transferred from the excited triplet state PS to molecular oxygen forming a superoxide anion, which can later form hydrogen peroxide. In the presence of a suitable reducing agent, hydrogen peroxide can form hydroxyl radicals and hydroxide ions. In a type II reaction, electrons are transferred from the excited triplet state PS to molecular oxygen forming an excited state singlet oxygen. Both type I and type II reactions generate ROS, which are responsible for the cytodamage observed during PDT and type II reactions occur more frequently in photodynamic reactions (Foote, 1991).
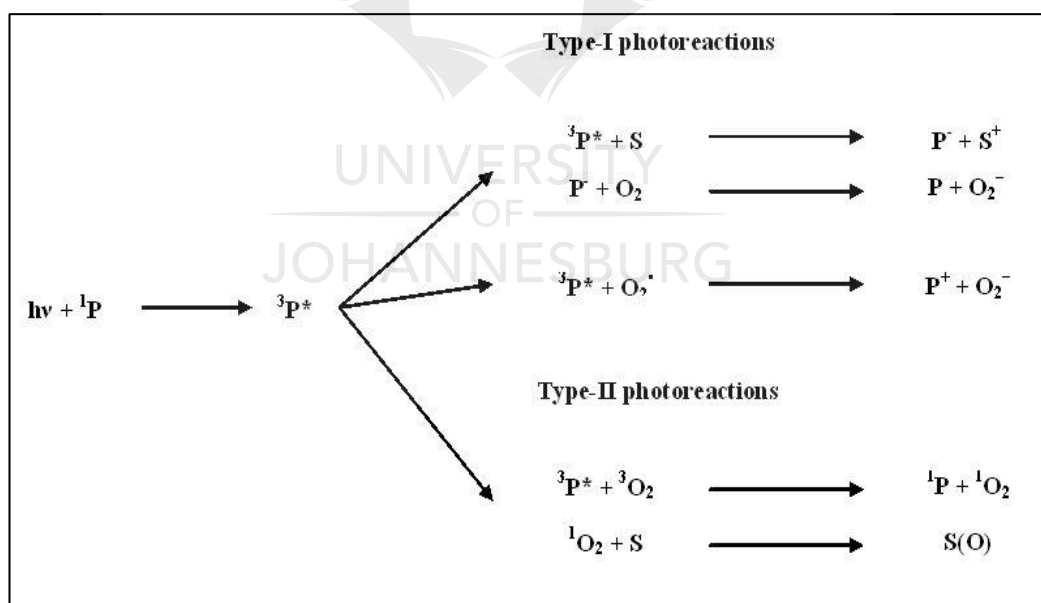
Figure 8: Type I and type II photoreactions, where ^1P is the PS in the singlet ground state, $^3P^*$ is PS in the triplet excited state, S is a substrate molecule, P^- is reduced PS, S^+ is an oxidized substrate molecule, O_2 is molecular oxygen (triplet ground state), O_2^- is the superoxide anion, $^3O_2$ is triplet ground-state oxygen, $^1O_2$ is singlet excited state oxygen, and S (O) is an oxygen adduct of a substrate.

2.4 Phthalocyanine

2.4.1 Phthalocyanine family of photosensitizer

Effective PSs tend to have a high affinity for excitation by apposite photons and a low energy difference between the uppermost occupied molecular orbit and lowermost unoccupied molecular orbit. This contributes to their thus their seen deep color (Denis and Hamblin, 2013). Phthalocyanine (PC) is a deep blue dye and belong to the family of second generation macrocyclic structured PSs, which are porphyrin derivatives. They are synthesized through various routes but the most common method of synthesis consists of producing the tetrabenzoporphyrazin from o-cyanobemzamide and phtalimide (Figure 9). With their porphyrin-like structures, PC derivatives have the ability to transfer electrons and accommodate more than 60 different elemental ions. They are multi-functional and have been extensively used (Swavey and Tran, 2013).
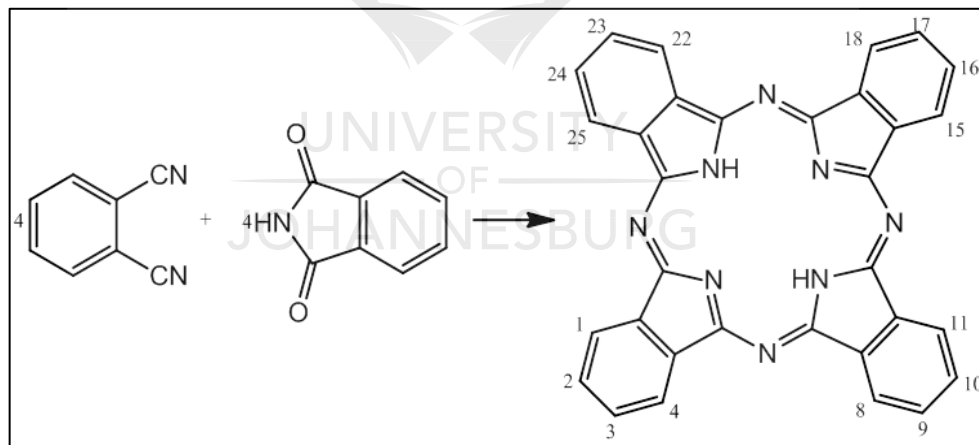
Figure 9: Synthesis of phthalocyanine (Swavey and Tran, 2013).

An important subgroup of this family is the metal-containing PC (mPC, one or two metal ions). They show enhanced electron transfer abilities and are used for various applications in different fields including molecular electronics, optoelectronics, and photonics (de la Torre *et al.*, 2004; Cid *et al.*, 2007; Campidelli *et al.*, 2008). Moreover, they have the merit and

potential to be a good candidate PS for PDT as they display strong light absorption capability in the NIR region of the spectrum, which offers greater light penetration into tissues and adequate generation of singlet oxygen (Dougherty *et al.*, 1993; Moan, 1990; Cook *et al.*, 1995). The unsubstituted mPC shows low solubility in organic solvents, and the introduction of proper substituents such as sulfonated groups increases their solubility (Chaidogiannos *et al.*, 2009; Iannuzzi *et al.*, 2014).

2.4.2 Cell death mechanisms

Cell death has been classified as programmed and non-programmed cell death responses, which follow into apoptotic, autophagy and necrotic pathways and cell senescence (Kroemer *et al.*, 2009). Cell death is continually under investigation and understood as the incapacity of cells to maintain essential biological functions. However, this biological process appears to be indispensable for both proper development and homeostasis in mammalian individuals (Engelberg-Kulka *et al.*, 2006). Damaged and superfluous cells become harmful by obstructing normal physiological performances and need to be removed through cell damaging mechanisms such as cell death. Features of cell death are indicated in Table 1 (Schultz and Harrington, 2003; Yuan and Kroemer, 2010).

Apoptosis is a regulated and chronological cell death mechanism that eradicates old cells and superfluous cells without the release of harmful substances. Cellular morphology, enzymatic activity, functional and immunological features reveals the type of cell death response and can be categorized as programmed, physiological, survival, accidental or pathological responses (Table 1) (Kroemer *et al.*, 2009). Nuclear and membrane damage usually characterize apoptosis, which is also known as a programmed cell death response (Erental *et al.*, 2012). Apoptosis is initiated by specific cellular signals that have the ability to stimulate the cascade pathways and ultimately deliver a suicidal response. Activation of

caspases; cysteine aspartyl proteases are the hallmark of apoptosis as these proteases induce and regulate apoptotic-related events and subsequent nuclear and polypeptide degradation. Caspases can stimulate other effectors to destroy cellular contents (Patel *et al.*, 2012; Peracchio *et al.*, 2012).

Table 1: Distinctive characteristics of cell death pathways. Different cell death pathways can be classified according to morphological appearance (apoptotic, autophagic, necrotic), enzymological criteria or regulators (distinctive classes of proteases, such as caspases, calpains and kinases) and functional aspects (programmed or accidental, physiological or pathological).

DISTINCTIVE FEATURES	CELL DEATH PATHWAYS		
	Apoptosis	Autophagy	Necrosis
MORPHOLOGY	Shrinkage; Blebbing; Chromatin Condensation; DNA Degradation; Nuclear Fragmentation, Apoptotic Bodies	Decreased Cell Size; Double Membrane Vesicles; Organelle Degradation	Cell Swelling; Loss of Membrane Integrity; Organelle Swelling; No DNA Laddering
REGULATORS	Death Receptors; Bcl-2 Family; Beclin 1; Caspases; IAPs; Adaptor Proteins; Kinases; Phosphatases; Calcium Ions, Calpains; BCNI1	mTOr; PI3 Kinase; ATG Family; UPR Stress Sensors; Beclin 1; Kinase (JNK); Bcl-2 Family; IP3 Receptor	Calcium Ions; Ion Channels; Metabolic Failure; PARB, Calcium Regulated Proteins; RIP Kinase; Death Receptors; Ceramides
STIMULI	ROS; DNA Damage; Death Receptors Ligands; Developmental Programs; Organelle Stress; Anti-Cancer Drugs; ER Calcium Release	Nutrient Starvation; Protein Aggregation; ER Stress; Calcium Overload; Developmental Programs; Hypoxia; Ischemia; Damaged Organelles; Proteasome Impairment	Bacterial Toxins; Metabolic poisons; Ischemia; Stroke; Calcium Overload
RESPONSE	Programmed, physiological	Survival, accidental, physiological	Accidental, pathological

Abbreviations: ATG, autophagy; Bcl-2, B-cell lymphoma 2; IAPs, inhibitor of apoptosis proteins; IP3 receptor, Inositol 1,4,5-trisphosphate (IP3) receptors ER, Endoplasmic reticulum; mTOR, (mammalian) target of rapamycin; PAR, poly(ADP-ribose); NO, Nitrite oxide; PARB, PAR-binding site; PI3 kinase, phosphatidylinositide 3-kinases; UPR, Unfolded Protein Response; ROS, reactive oxygen species; RIP1: a specific kinase that is recruited to the death-inducing signaling complex;

Furthermore, the inhibition of pro-survival proteins activity and apoptosis are enhanced by the binding members of the B-cell lymphoma 2 (Bcl-2) family. Cells that are undergoing apoptosis round up and stop communicating with adjacent cells, their plasma membrane start to bleb and phosphatidyl serine translocates to the outer membrane layer. Further cellular alterations include cross-linkage, protein polymerization, chromatin condensation, nuclear fragmentation (into 185 nucleotides only) by cation dependent endonucleases, cell fragmentation, and apoptotic bodies' appearance and removal. Apoptotic responses are further subdivided into the intrinsic and extrinsic pathways (Yuan and Kroemer, 2010; Erental *et al*., 2012; Kim *et al*., 2012; Kang *et al*., 2011).

A permeable mitochondrial membrane coupled with the release of some apoptogenic proteins such as cytochrome C and coenzyme Q are among the characteristic features of the intrinsic pathway, while death receptor activation mediated by tumor necrosis factor receptor-1 (TNFR-1) or Fas/CD95 protein from the plasma membrane is one of the main initial events during the extrinsic pathway. Proteins such as beclin-1 prevent the caspase-dependent cell death response and show anti-apoptotic potential and activity (Yuan and Kroemer, 2010; Erental *et al.,* 2012; Kim *et al*., 2012; Kang *et al*., 2011).

Photodynamic therapy using silicon phthalocyanine as PS caused cytodamage in malignant T-lymphocytes. These specific PCs were effective in destroying Bcl-2 proteins, inducing cytodamage and promoting apoptotic-like events (Lam *et al*., 2010). In a similar experiment and upon irradiation, a mPC in breast cancer cells led to the occurrence of apoptotic signs such as the predominance of apoptotic cells, nuclear fragmentation, oligonucleosomal degradation, and a marked increased level of Bcl-2, DNA fragmentation factor alpha-1 and caspase 2 (Mfouo-Tynga *et al*., 2014). Where mitochondria are the preferred site of subcellular location PSs are prone to affect Bcl-2 protein and eventually induce apoptotic responses

(Mroz *et al.*, 2011). Another criterion for the induction of the apoptotic pathway is the increased level and transfer of calcium ions (Ca^{2+}) from the endoplasmic reticulum (ER) to the mitochondria. A non-nuclear and Ca^{2+}-dependent apoptotic response was established by the overload of Ca^{2+} in the mitochondria and was seen as the cause of subsequent cytodamage (Giorgi *et al.*, 2015a). Photodynamic therapy that leads to increased levels of intracellular Ca^{2+} have the ability to cause cell death, which appears to be p53-dependent (Giorgi *et al.*, 2015b).

Autophagy is an essential but not yet fully understood cell death process and is classified as programmed cell death (Nikoletopoulou *et al.*, 2013). However, it is recognized primarily as a survival mechanism, triggered by a sub-lethal dose of stress (Jain *et al.*, 2013). Moreover, this cell death mode was shown to induce the immune response and to play a crucial role in PDT-mediated damage, especially in apoptosis resistant cells (Michaud *et al.*, 2011). In the absence of autophagy actions, cancer cells had acquired and shown resistance to treatment and increased cell survival after therapy (Di *et al.*, 2013). Decreased cell size, the appearance of double membrane vesicles, and organelle alterations are among the most common observed events during an autophagic response (Table 1).

Two ubiquitin-dependent mechanisms and 30 autophagic proteins (Atg) are essential for autophagic responses. The Atg 7 protein plays a crucial role and is able to activate other Atg proteins, autophagosomal assemblage and molecular degradation (Xie *et al.*, 2007). In the case of caspase inhibition, another mechanism is triggered leading to catalase degradation and ROS accumulation and events are related to autophagy (Yu *et al.*, 2006). The formation of an autophagosome wherein degradation takes place is a distinctive mark of autophagy (Mizushima and Klionsky, 2007). Appropriation, transportation to lysosomes, degradation and recycling of residues make up the sequential steps of autophagy (Patel *et al.*, 2012; Peracchio *et al.*, 2012).

Photodynamic therapy-mediated cell death can be achieved through the apoptotic pathway but it has also been associated with the induction of autophagy in various cells. Photodynamic therapy-induced autophagy has been identified as being a survival mechanism by preventing cell death. However, in apoptotic-deficient cells, a successful PC-mediated PDT may be induced cell death through activation of autophagic events. It has been recognized that both apoptosis and autophagy are required for optimal cell death responses where inhibiting autophagy has led to the development of MCF-7 cells resistant to PC-mediated PDT and an enhanced MCF-7 cell survival rate (Xue *et al.*, 2010; Garg *et al.*, 2015). Beclin-1 and mammalian target of rapamycin (mTOR) proteins are prone to trigger an autophagy response, and their functions can be altered by PSs that localize in the ER (Mroz *et al.*, 2011).

Cell death manifestation and inactivation of programmed cell death signals in an accidental event refers to a non-programmed cell death response, also known as necrosis. This is characterized by an inflammatory response where various traumatic situations, toxins and infections are required stimuli for proper necrotic cell death responses (Table 1) (Lemaster, 2005; Kroemer *et al.*, 2009). Inactivation of caspases, enhancement of both signal transduction and catabolic activities have been shown to lead to a necrotic response involving death domain and toll-like receptors. The receptor interacting protein-1 (RIP-1) plays a critical role in the execution of necrotic events. This is a serine/threonine kinase that regulates death receptor signaling and necroptosis, a non-caspase dependent and necrotic-like responses (Cho *et al.*, 2011).

Evidence of both apoptosis and necrosis induction was reported after leukemia cells were treated with dimethytetrahydroxeliandrone-mediated and Hypericin-mediated PDT. At high doses, necrosis was identified in 75% of oral cancer patients who were treated with aminolevulinic acid in PDT

(Lavie *et al.*, 1999; Grant *et al.*, 1993). There appear to be no research reports on the induction of necrosis following PC-mediated PDT.

2.4.3 ROS and mPC-mediated PDT

The term ROS is a collective acronym to designate chemically active and reactive oxygen metabolites. According to their generating sources, they can be subdivided into endogenous and exogenous ROS. Exogenous ROS can be generated from tobacco, pollutants, xenobiotics and radiation while endogenous ROS production is cell type-dependent and major sources include mitochondria, peroxisomes, the ER and Nox (**N**ADPH and **ox**idase) complexes. However, the main sources of ROS in living cells are Nox complexes, 5-lipoxygenase and mitochondria (Nova and Parola, 2008; Turrens, 2003).

During immune responses, the Nox family of nicotinamide adenine dinucleotide phosphate hydrogen (NADPH) oxidases located on cell membranes are essential in innate immunity to produce ROS, metabolic by-products and precursors of oxidants (Rada and Leto, 2008; Arwert *et al.*, 2012). Reactive oxygen species have several roles in different locations and in the mitochondria; they facilitate the action of Tumour necrosis factor alpha (TNF-α) by stabilizing hypoxia-inducing factor-1 (HIF-1) that regulates both immune responses and activates TNF-α (Jung *et al.*, 2008; Serra *et al.*, 2008). The absence of oxidases results in increased vulnerability of patients diagnosed with microbial infection as ROS are able to neutralize and confine bacteria into neutrophil phagosomes. Both Nox family proteins and ROS are critical for an immune reaction and bacterial eradication (Brown *et al.*, 2004).

Growth factors and cytokines are able to stimulate and induce both the Nox complexes and 5-lipoxygenase, which is a complex functional oxidase implicated in the generation of leukotrienes from arachidonic acid. The action of cytokines cause membrane disturbances and the generation of ROS (Dröge, 2002; Soberman, 2003; Chiarugi and Cirri, 2003; D'Autrèaux

and Toledano, 2007). Mitochondria are the cells' power house and are able to utilize high energy intermediates to produce energy in the form of adenosine triphosphate (ATP) through the electron transport chain across the inner mitochondrial membrane. At complex I and complex III of the chain of the electrons are transformed into ROS, which is generally converted by mitochondrial superoxide dismutase into a more harmless form that can cross the mitochondrial membranes and reach the cytoplasm (Cadenas and Davies, 2000). Damaged mitochondria may lead to the induction of cell death in a caspase-dependent or caspase-independent manner and such induction depends entirely on ROS (Green and Kroemer, 2004). The loss of mitochondrial membrane integrity is related to the dissipation of the mitochondrial inner transmembrane potential, causing permeabilization of the outer mitochondrial membrane, release of apoptogenic proteins (cytochrome C, Smac, Diablo and AIF) and finally resulting in apoptosis (Tynga and Abrahamse, 2012; Nova and Parola, 2008).

Photodynamic therapy-mediated cell death mechanisms may include the manifestations of tumouricidal effects, microvascular damage, and local inflammatory reactions, all dependent upon the selection, concentration and ability of the PS to interact with molecular oxygen and generate ROS (Figure 10) (Firdous et $al.$, 2012; Brackett and Gollnick, 2011). Photodynamic reactions might cause an acute inflammatory response and both increased levels of inflammatory cytokines and leukocytes in treated tumour sites (Guillaud et $al.$, 1998; Allen et $al.$, 2001). The development of acute stress responses is characterized by an alteration in Ca^{2+} levels, lipid metabolism, and the production of cytokine and stress mediators (Mroz et $al.$, 2011). In several photodynamic reactions, molecular oxygen acts as the main stimulus and is generated from mitochondria that activate the formation of RIP-3 complex (Coupiene et $al.$, 2011a; Coupienne et $al.$, 2011b).
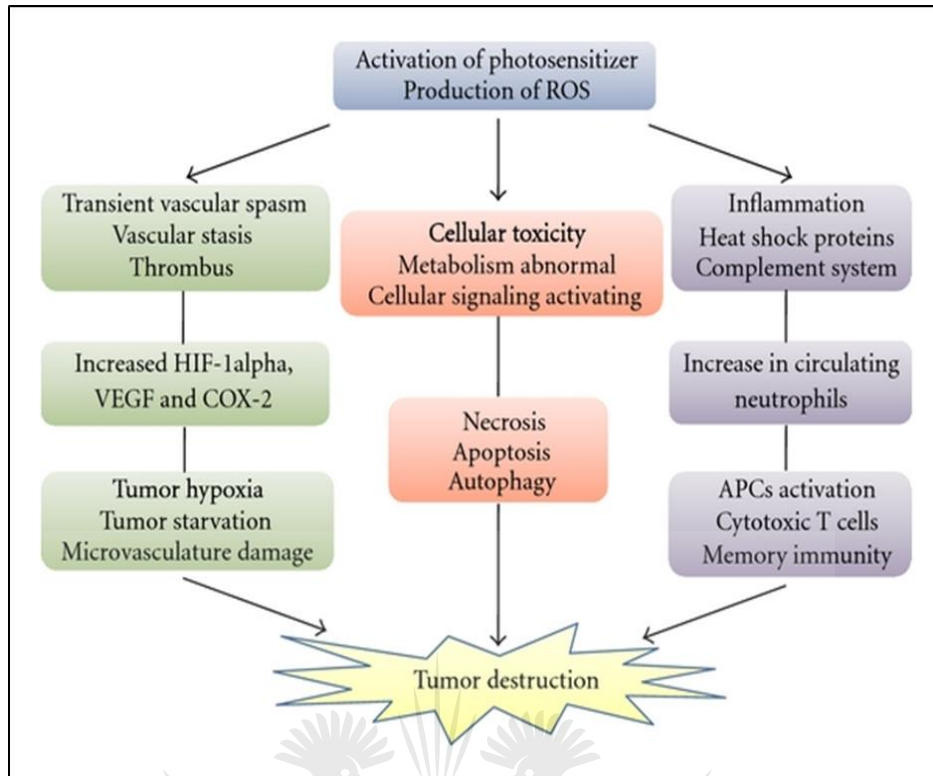
Figure 10: Pathways of PDT-induced tumor cell death or destruction. The antitumour effects of PDT include three main mechanisms: direct tumor cell killing, vascular destruction and immune system activation. (Anaphase-promoting complexes, APCs; hypoxia-inducing factors, HIF; vascular endothelial growth factor, VEGF; cyclooxygenase-2, COX-2) (http://www.hindawi.com/journals/ijp/2012/637429/fig5/).

After their accidental discovery, the red-light-absorbing mPC have been subjected to numerous experiments and utilized as chemical sensors, semiconductors, non-linear optics and PSs. In PDT, they have been shown to increase cell death in a caspase-dependent manner as well as autophagy. Thus, they have been recognized as effective inducers of photodamage in various tumour cells, their preferred accumulation sites (Kadish *et al.*, 2003; Pinzon *et al.*, 2008; Cid *et al.*, 2007; Barret *et al.*, 1934). Apoptotic and necrotic events are frequently identified *in vitro*, the promotion of cell death through translocation of activated p38 to mitochondria, phosphorylation of BCL-2 and/or BCL-X2, through facilitation of cytochrome C release from mitochondria, caspase-mediated PARP cleavage and inhibition of the P13/Akt/mTor pathway (Whitacre *et al.*, 2000; Velloso *et al.*, 2012).

A mixed sulfonated mPC with Zinc ($ZnPcS_{mix}$) at the centre of the macrocyclic structure has been reported to enter neoplastic cells and localize in organelles such as the mitochondria, lysosomes and Golgi apparatus. After activation with a 680 nm diode laser, the $ZnPcS_{mix}$-mediated PDT yielded good photodynamic and damaging effects in lung, colon and breast cancer cell lines (Manoto *et al.*, 2012; Mfouo-Tynga *et al.*, 2012). The effects in A549 cell lines included modified cell morphology, decreased viability and increased cytotoxicity. The increased level of ROS was an indication of its production in both monolayer as well as multicellular spheroid models (Manoto *et al.*, 2011; Manoto *et al.*, 2013). A study of cell death mechanisms following $ZnPcS_{mix}$-mediated PDT pointed out the abundance of apoptotic cells, nuclear degradation and up-regulation of Bcl-2, DNA fragmentation factor alpha, and caspase-2 genes, which all pointed to the involvement in apoptotic cascade events (Mfouo-Tynga *et al.*, 2014). When using sulfonated aluminium PC ($AlPcS_{mix}$) and sulfonated germanium PC ($GePcS_{mix}$) as a mPC in malignant cells, photo-activated forms yielded cytotoxic effects in a dose dependent manner with a predominance of apoptotic cells (Abrahamse *et al.*, 2006). In a different study, the photodynamic outcomes of sulfonated mPC (SnPC, SiPC and GePC) were compared to sulfonated PC in esophageal cancer cell lines. Results revealed improved induction of apoptosis and necrosis with the mPC compared with the unmetallated PC (Setsanyana-Mokhosi *et al.*, 2006).

2.5 Nanotechnology and Cancer Therapy

Nanotechnology is an interdisciplinary field and the engineering of small particles, which measure approximately 1/1 000 the width of a single human hair, can offer exceptional interactions with molecules both on the surface of, and inside, cells (Wei, 2012; Cai and Chen, 2007). Four generations of nanomaterials have been defined by the Centre for Responsible Nanotechnology. These include passive nanostructures (1st generation), which are task-specific structures; active nanostructures (2nd generation),

which are multitask-specific structures such as actuators, drug delivery devices, and sensors; nanosystems (3rd generation), which are multi-interacting compounds; and finally integrated nanosystems (4th generation), which consist of several incorporated systems (Figure 11).
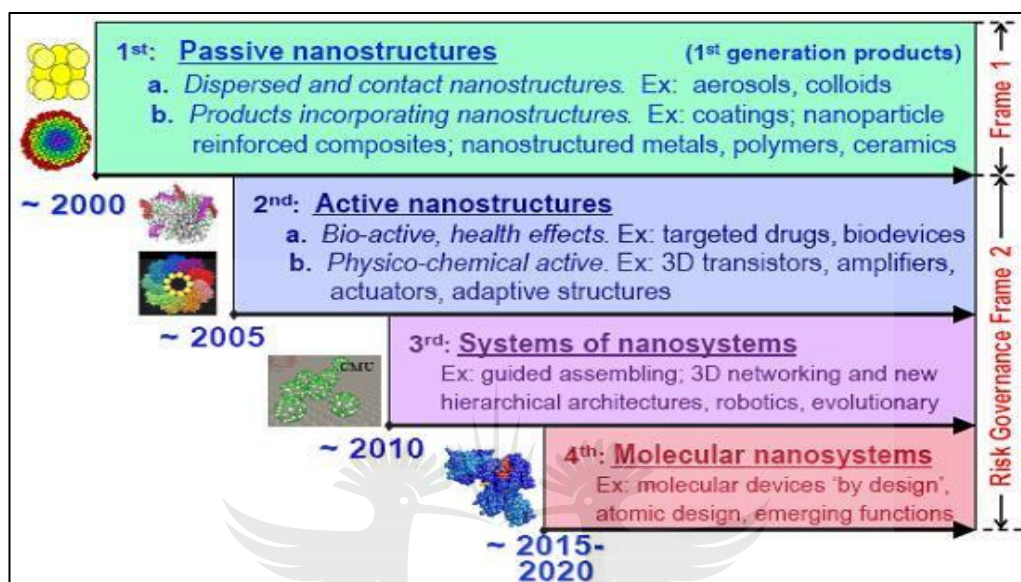
Figure 11: Generations of nanostructures. Passive nanostructures made up the first generation and consist of dispersed, contact and products incorporating nanostructures. The second generation nanostructures are active with distinctive biological and physico-chemical characteristics. Nanosystems form the third generation while the fourth generation, or molecular nanosystems, are integrated nanosystems (Center for Responsible Nanotechnology, 2002).

2.5.1 Nanoscale material properties

The interest of nanoparticles in research continues to escalade and grow in popularity due to their wide possible application ranging from medicine, industry and manufacturing. The relationship between properties and nanoscales is dependent on a number of aspects of nanoscale and larger scale. The most attractive characteristics of nanoparticles compared to larger particles are the high surface area to volume ratio and their quantum effects that may increase the reactivity and electrical strength of nanoparticles (Buzea *et al.*, 2007). Size plays a more pronounced role, the smaller the size the greater the proportion of atoms at the periphery compared to the core. It has been established that a 30 nm-sized particle is likely to have 5% of its atoms at the surface, while 10 and 3 nm-sized

particles would have 20% and 50% of its atoms at the surface, respectively (Chaturvedi *et al.*, 2012). It has been proposed that nanoparticles have better surface area per unit mass and a nanoparticle of any given mass material will likely be more reactant than the same mass of material consisting of larger particles (most catalytic chemical reactions happen at the surfaces) (Taniguchi, 1974; Lubick and Betts, 2008; Edelstein and Cammarata, 1998).

In addition to size, the shape and morphological sub-structure of materials are crucial criteria. Morphological structures depend on conditions such as aerosol- (mostly solid or liquid phase in air); a suspension- (mostly solid in liquids); or an emulsion- (two liquid phases). Modification of properties depends on the presence of and kind of chemical agents. Indirectly, such agents may bring stability against aggregation by maintaining charge and altering the outermost layer of the particle (Liufu *et al.*, 2004). Light-mediated conductance of electrons at polar interfaces of nanoparticles is known as surface plasmon resonance. When the conductive nanoparticles are smaller than the incident wavelength, a localized surface plasmon resonance is generated, and such subwavelength scale nanostructures are polaritonic or plasmonic in nature. Surface plasmon resonance is widely used for measuring absorption of metal nanoparticles such as AuNPs and AgNPs. Surface plasmon resonance is directly dependent on the composition, size, geometry, dielectric environment and separation distance of nanoparticles (Zeng *et al.*, 2014; Lis and Cecchet, 2014; Spring *et al.*, 2014; Link and El-sayed, 2000; Guang Xiang *et al.*, 2010).

2.5.2 Impact of nanoparticles in medical research

Nanoparticles continue to attract attention and the increasing enthusiasm that nanotechnology, as applied to medicine, has already brought significant benefits in the diagnosis and treatments of several diseases (Selim and Hendi, 2012). This attraction is mainly as a result of the surface to mass

ratio, the quantum properties, and the capability of NPs to absorb and carry other compounds (Buzea *et al.*, 2007; Chaturvedi *et al.*, 2012; Lubick and Betts, 2008). Nanoparticles have been engineered in order to achieve multifunctional applicability as they can be simultaneously used as medical imaging agents, therapeutic agents, diagnostic agents, active implant agents or drug delivery agents. Drug delivery NPs are the most commonly used in nanomedicine (Figure 12) and offer additional advantages such as improving drug therapeutic effect and pharmacological properties. They do so by enhancing the solubility of poorly water-soluble drugs, altering pharmacokinetics, improving bioavailability, specificity toward targeted cells and drug half-life by decreasing immunogenicity and drug metabolism, which release more controllable therapeutic compounds. Some NPs appear as promising agents in the fight against chronical diseases (Bednarski *et al.*, 2015).
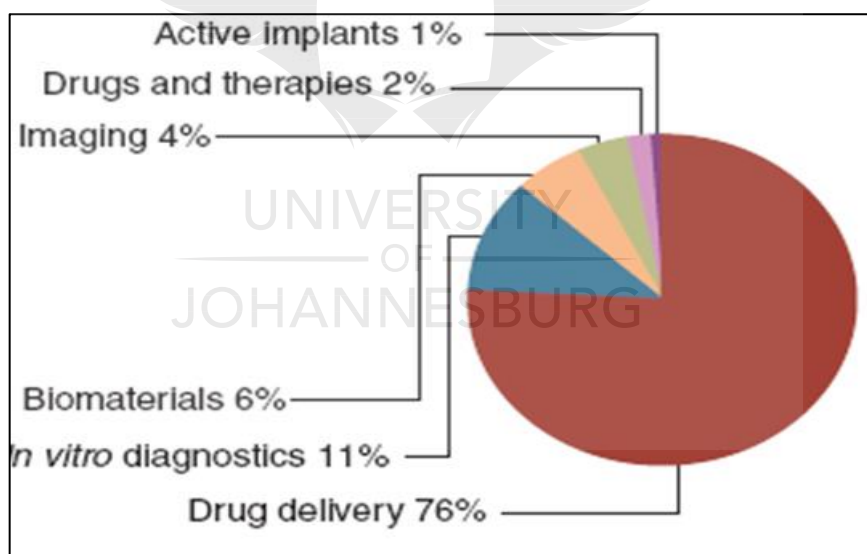
Figure 12: Multifunctionality of nanoparticles and percentage of application. Drug delivery and diagnostics are the most common applications of nanoparticles (Wagner et *al.*, 2006).

The initial purposes when manufacturing NPs-based drug delivery are: more specific drug targeting and delivery, a decrease in toxicity and maintenance of therapeutic effects, greater safety and biocompatibility, and faster development of safer new medicines. Additionally, other factors to be

considered should include: drug incorporation and release, formulation stability and shelf life, biocompatibility, biodistribution, targeting and functionality (De jong and Borm, 2008).

2.5.3 Major nanoprobes

In previous decades, many nanomaterials have been developed for medical applications to interact with biomolecules both on the surfaces as well as inside the cells. This appeared as a revolution in the medical field and quantum dots, carbon nanotubes, paramagnetic NPs, liposomes, gold NPs, and other have been studied for biomedical applications in cancer as indicated in Figure 13 (Cai *et al.*, 2008).
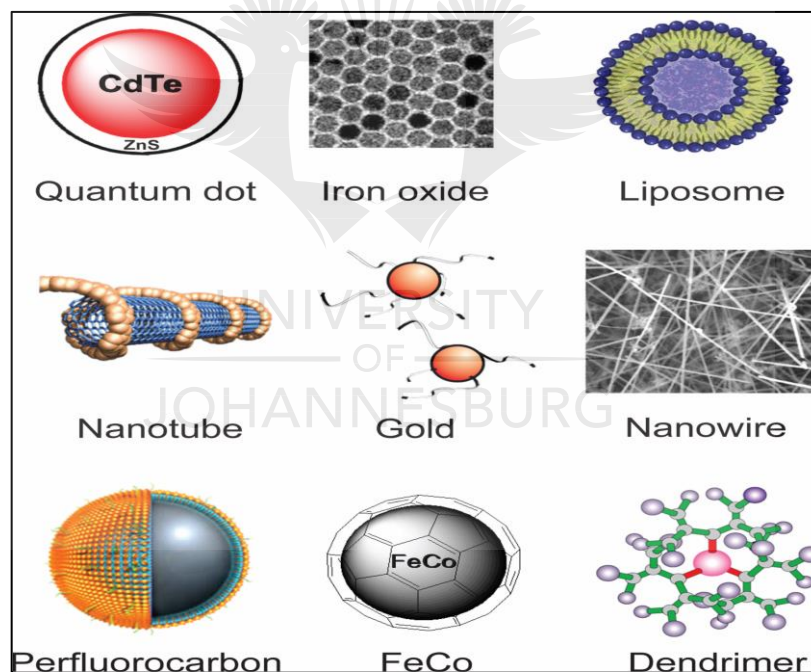
Figure 13: Many nanoparticles have been investigated for biomedical and cancer applications (Cai *et al.*, 2008).

Quantum dots are semiconductor nanomaterials that possess specific and size-dependent conductive features. The properties of quantum dots are being used in diagnosis and treatment both *in vitro* and *in vivo*. These allow for conjugation with biomolecules such as antibodies and peptides or small molecules, where they act as probes to target cancerous structures with

strong affinity to reveal cancer subcellular sites and tumor environment (Bentelila *et al.*, 2009; Hilderbrand *et al.*, 2010; Wang and Chen, 2010). The determination of the dominant and compensation mechanisms of tumour distribution remains a major challenge in clinical setting (Sanz-Moreno and Marshall, 2010).

Carbon nanotubes are good electrical and heat conductors with a large surface area. They are made up of graphene sheets, which consist of a single carbon atomic layer in a honeycomb framework. These tubes possess properties that allow them to release heat after irradiation and their chemistry favors functionalization (Gannon *et al.*, 2007). Despite the lack of cytotoxicity, nanotubes can accumulate inside cellular structures and are one of the most potent nanomaterials with the ability to identify cancer cells and deliver drugs to these cells. They possess unique physicochemical properties and are used in cancer diagnosis and treatment (Gannon *et al.*, 2007; Shun-Ron *et al.*, 2010). They have been experimented on in several cancer treatment modalities and biomedicine areas. To overcome these challenges, conjugation with polymers to functionalize the surfaces of carbon nanotubes and render them better anticancer drug delivery systems are being developed (Adeli *et al.*, 2013).

A liposome is a spherical structured vesicle comprising of at least one lipid bilayer and may contain surface ligands for used in drug delivery (Torchilin, 2006). The spherical lipid bilayers, constituents of liposomes, can be synthesized from phospholipids and cholesterol, and encapsulate various biomolecules for diverse applications (Rooijen and Nieuwmejen, 1980). Liposomes form part of a class of delivery systems that consists of microparticles, polymeric micelles, dendrimers and many more (Rai *et al.*, 2008). They were first discovered by Bangham and then become knwon as controlled and targeted drug delivery systems (Bangham *et al.*, 1965). Several inappropriate applications using liposomes led to inadequate treatment outcomes, suboptimal cancer detection and ineffective monitoring

in cancer treatment (Zhou *et al.*, 2012). In gene therapy, noninvasive imaging approaches combined with liposomal nanoparticles have led to own understanding of delivery and monitoring of the efficiency of the treatment over an extended period (Zhou *et al.*, 2012). Reformulated, improved liposomes showed success and reintroduced liposomes into the cancer field as vesicles for targeted drug delivery (Banerjee, 2001).

Dendrimers are repeatedly branched organic molecules and are symmetrically arranged around the core (Figure 14). They are synthesized in a series of reactions, starting with a dendron containing a single chemical group called the focal point. The categories are determined by generation, which is the number of repeated branching cycles that are achieved during the synthesis (Figure 15). Every revolutionary cycle leads to the generation of a dendrimer that is twice as big as the previous one. The higher the generation, the more exposed functional groups there are on the periphery and the more possible conjugation can take place (Horiba, 2015; Annam Pharm, 2013).
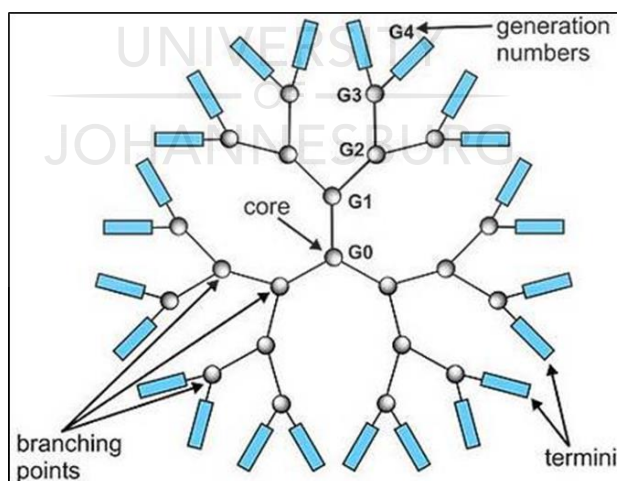
Figure 14: General structure of a dendrimer. A dendrimer has a core and several branching points. The number of termini is determined by the number of generation (http://www.horiba.com/scientific/products/particlecharacterization/applications/pharmaceuticals/dendrimers/).
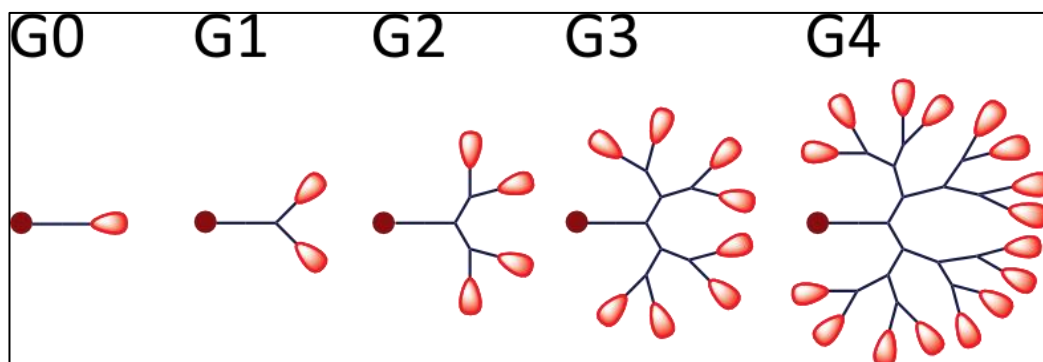
Figure 15: Synthesis of polybranched dendrimers. Dendrimers are synthesized in a series of reactions, with the first reaction (G0), having 1 protected site and 1 unprotected site in a relatively standard conjugation. However, using G0's product, G1 can be synthesized having 1 protected and 2 unprotected sites. By similar methods, G2 offers a 1:4 ratio of reaction sites, G3 offers a 1:8 ratio, and G4 offers 1:16. (http://www.annampharma.com/dendrimers.html, Annam Pharma, 2013).

Dendrimers are interesting and well defined nanostructures, which bear a resemblance to biomolecules with high functionality, adaptability in drug delivery and multi-branched architectures. They are specially structured and different from other polymers by having internal cavities, a small nanoscopic size, a high ratio of surface groups to molecular volume, a narrow polydispersity index and several conjugation sites at the periphery (Kesharwani *et al.*, 2014). Dendrimers have been explored in a variety of applications and one of the most successful applications is drug delivery. Their terminal functionalities create an important platform for conjugation of the drug and targeting moieties. Dendrimers have been entrapped and/or conjugated to hydrophilic and hydrophobic entities by host-guest interactions and covalent bonding, respectively. Additionally, the peripheral functional groups can be employed to alter the properties of dendrimers, enhancing their adaptability (Madaan *et al.*, 2014; Kesharwani *et al.*, 2014).

2.5.4 Gold Nanomedicine and cancer therapy

Gold metals occur in nature in non-oxidized form (Au) and have two main oxidative states: the aurous (Au^{+1}) and auric (Au^{+3}) forms. Nanoparticles made of gold are one of the most well known nanoparticles. Due to their biocompatibility, AuNPs have grown in popularity and been intensively used

in medical applications. They are promising agents for cancer treatment as they have an affinity to amine and thiol groups, enabling them to be conjugated (Nel *et al.*, 2006; Shukla *et al.*, 2005).

The small size of nanoparticles such as AuNPs permits them, like PSs, preferentially accumulate in tumour cells by enhanced permeability and retention effect (Figure 16). They can be used in target therapy and bind to proteins or drugs to recognize specific overexpressed cell surface receptors on cancer cells. They are radiosensitive and when irradiated at specific wavelengths, they resonate and produce heat that can be essential for tumour-selective photothermal therapy. Toxicity studies showed contradictory results, so that while some studies showed that AuNPs have no cellular toxicity, others demonstrated ROS production, mitochondrial damage, cytokine release, apoptosis and necrosis both *in vivo* and *in vitro*. Correlations between the method of preparation and toxicity have been established both *in vivo* and *in vitro* (Ni *et al.*, 2004; Pan *et al.*, 2009; Kang *et al.*, 2010; Hainfeld *et al.*, 2004; Balasubramanian *et al.*, 2010).

2.5.5 Common applications of AuNPs in cancer treatments

Radiation cancer therapy utilizes ionizing radiations such as X-rays, gamma rays and high energy particles to kill and stop the spread of cancer in many tumours while AuNPs have been used as radiosensitizers, such an approach is non-specific as most of the ionizing agents cannot differentiate tumours from normal cells and destroy type of cells (Mesbahi, 2010). Thus, AuNPs-mediated radiosensitization has led to enhanced photoelectric photon absorption. The size, dosage, surface coating and distance of AuNPs from cell organelles are of critical importance for effective radiosensitization (Jain *et al.*, 2012). Interactions between AuNPs low energy photons, and increased radiation side effects have been detected (Jain *et al.*, 2012; Mesbahi, 2010).
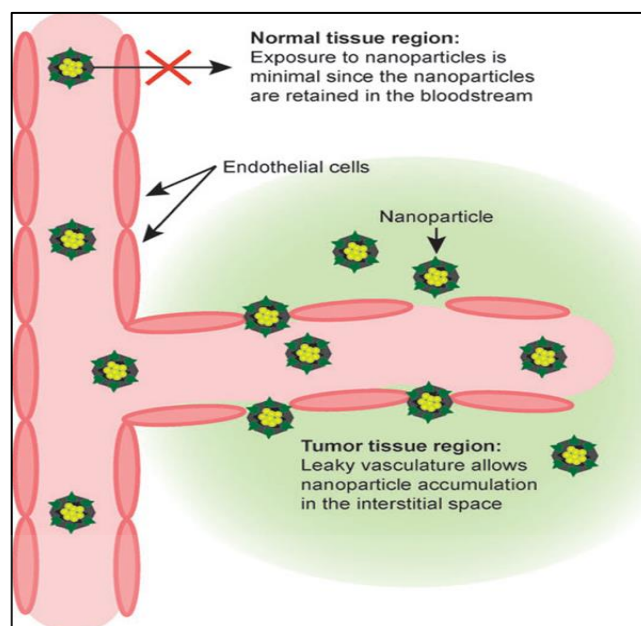
Figure 16: Schematic diagram showing enhanced permeability and retention of nanoparticles in tumors. Normal tissue vasculature is lined by tight endothelial cells, thereby preventing nanoparticle drugs from escaping or extravasation, whereas tumor tissue vasculature leaks and is hyperpermeable allowing preferential accumulation of nanoparticles in the tumor interstitial space, known as passive nanoparticle tumor targeting (Nie *et al*., 2007).

In pharmacological studies, AuNPs have been extensively used to improve drug delivery to tumours and subsequently cancer treatment efficiency. AuNPs proved to be effective when used as a delivery system, enhancing the anticancer therapeutic effects up to 50% when compared to the anticancer agents used alone in various cancer types, including pancreatic cancer models (Patra *et al*., 2010; Patra *et al*., 2008). When conjugated to either anticancer agents or anticancer agents bound to antibodies both *in vivo* and *in vitro*, AuNPs showed various appreciable therapeutic effects (Jain *et al*., 2012; Kullmann *et al*., 2009; Patra *et al*., 2010).

Developments in nanomedical research have led to metal nanoparticles-targeted cancer therapy (Jain *et al*., 2012). Light activation of Auger electrons were demonstrated when the effects of AuNPs in combination with various lasers were evaluated (Figure 17), and is known as thermal therapy. Similar to PDT, in this therapy the chosen laser should match the surface

resonance of the AuNPs, which depend mainly on their size, shape and methods of synthesis (El-Sayed *et al.*, 2005). Nanoshells are the most commonly used form of AuNPs as they are able to induce a shift in the resonance peak to the NIR (650-950 nm) (Lal *et al.*, 2008). The generated heat energy result from the excitation and relaxation of Auger electrons (Cherukuri *et al.*, 2010). Subsequent hyperthermia is the main cause of induced cell death and had been seen in various tumours. In the clinical setting, hyperthermia is often used in combination with other treatments. Increased local regulation and survival had also been identified when thermal therapy had been combined with radiation or chemotherapy (Issels *et al.*, 2010; van der Zee *et al.*, 2000). The main downfall of AuNPs-mediated thermotherapy include elusive specificity, difficulties in accessing and heating deeper tumours, as well as thermo-tolerance, usually seen after the first treatment (Wust *et al.,* 2002).

However, AuNPs showed good preclinical results as radiosensitizing agents in various tumour cells and using different radiation sources. Here AuNP mediated radiotherapy caused mitochondrial disturbance and subsequent cell damage (Taggart *et al.*, 2014). Irradiated AuNPs have the potential to kill cancer cells and cause minimal damage to neighboring cells. Light-activated AuNPs induced sudden photothermal cytotoxicity and high ROS within Burkitt lymphoma B and epithelial breast cancer cells (Minai *et al.*, 2013). Further investigations are required to determine AuNPs pharmacokinetics, biodistribution and cytotoxicity effects *in vivo*. Although AuNPs are biocompatible, certain preparations have the potential to cause cytotoxicity both *in vivo* and *in vitro*. As AuNPs have a high atomic number, they offer greater absorption of kilovoltage X-rays and greater contrast than other contrast agents (Jain *et al.*, 2012).
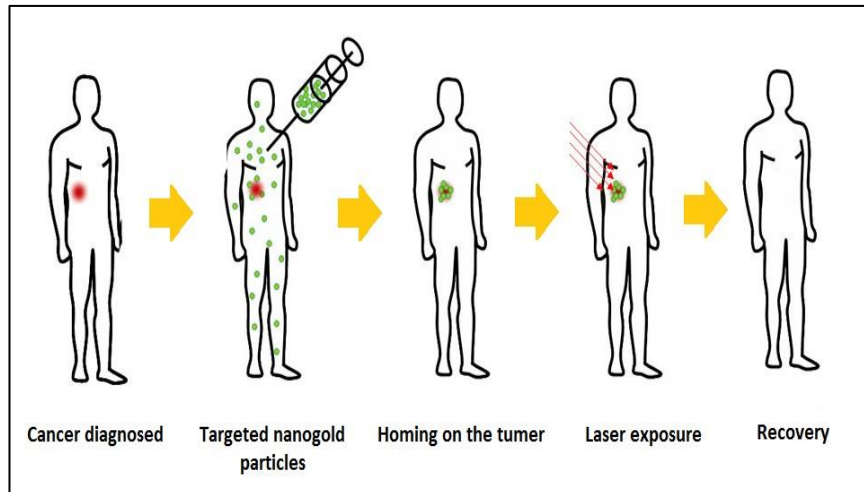
Figure 17: A schematic illustration of radiotherapy using nanoparticles. Once administrated, nanoparticles make their way to tumour sites, where they accumulate. Light is absorbed by the particle to heat the particle and surrounding tissue. Heat produced will kill cells and light may also be used to produce high energy oxygen molecules which will chemically react with and destroy cells (Wijesena, 2015).

CHAPTER THREE

METHODOLOGY

3.1 Study Design

A flow diagram showing an overview of this project is presented in Figure 18.
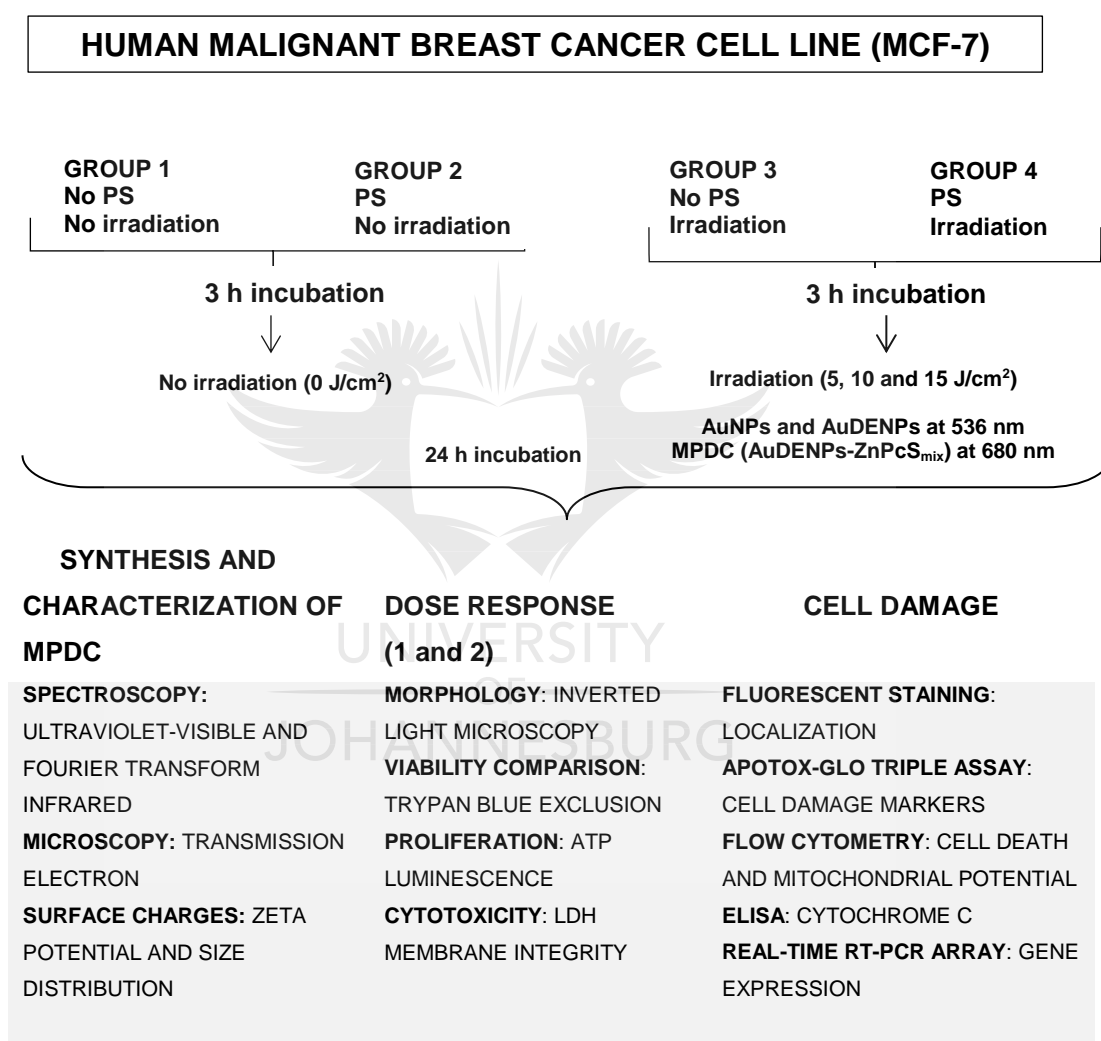
Figure 18: Flow diagram of AuNPs, AuDENPs and MPDC-mediated PDT. The project consisted of MPDC synthesis and characterization, dose response and cell damage studies. MCF-7 cell cultures were divided into 4 study groups. Group 1 was an untreated control, group 2 received PS but was not irradiated and group 3 was irradiated but received no PS. Irradiation was done with a (536 or 680 nm) diode laser set as for AuNPs/AuDENPs and MPDC respectively. Group 4 was irradiated and received PS. All samples were incubated for 24 h (except for PCR array, 3 h) and thereafter localisation, dose response and cell death studies were performed. PS refers to AuNPs, AuDENPs or MPDC. Dose response 1 was done with only nanoparticles and excludes morphology, while dose response 2 was performed with MPDC.

3.2 Cell Culture

A commercial cell-line was utilized throughout the course of the study. Therefore, this research did not fall within the guidelines set out in the Human Tissue Act 65 of 1983, with particular reference to the provision of the act; tissue which may and may not be used and the removal of tissue from living donors. The MCF-7 cells as a breast cancer cell line which was isolated in 1970 from a 69-year-old Caucasian woman. Herbert Soule and co-workers established the cell line in 1973 (Soule *et al.*, 1973).

The MCF-7 breast cancer cells (ATCC Number: HTB-22™, Lot Number: 60731981) were cultivated in Dulbecco's Modified Eagle Medium (DMEM, Gibco, 41966) medium. The culture media was enriched with 10% fetal bovine serum (FBS, Gibco, 10106-169) and 1% Penicillin-streptomycin (Sigma, P4333). Cells were incubated at 37°C in 5% CO_2 and 85% humidity. Upon reaching confluence, cells were washed twice with Hank's Balance Salt Solution (HBSS, Gibco, 14065-056) therefore TrypIE^{tm} Express (Gibco, 12604) was used to detach the cells from the culturing flasks using 1 ml/25 cm^2. For experimental purposes, $5x10^5$ MCF-7 cells (in 2 ml culture medium) were seeded in 3.4 cm diameter culture dishes and incubated at 37°C for 4 h to allow the cells to attach.

3.3 Photo-Irradiation

Cells were categorized into four groups and only cells from group 3 and 4 were irradiated (Figure 18). Once MCF-7 cells were attached to the culture dishes, AuNPs/AuDENPs or MPDC was added and cells were incubated at 37°C in 5% CO_2 and 85% humidity for 3 h prior to laser irradiation. In order to remove non-localized treatment agents, cells were washed and fresh media was added before laser irradiation. The PS used in this study was a mixture and mainly consisted of tetra, tri and disulfonated zinc phthalocyaines (Figure 19).
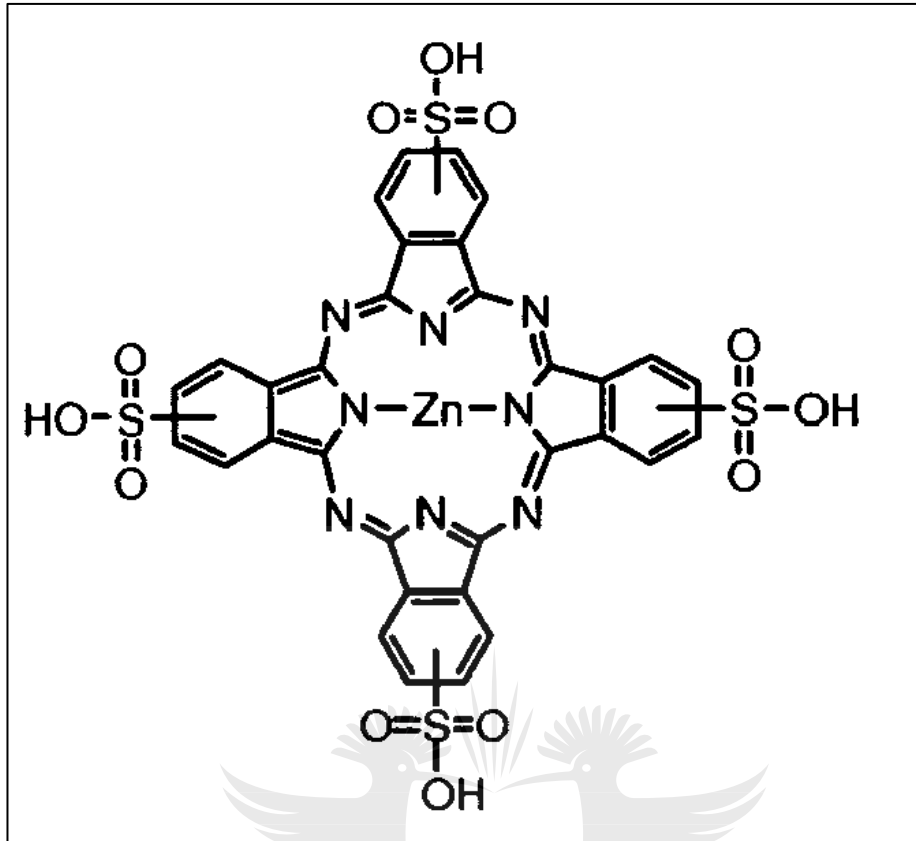
Figure 19: Chemical structure of tetrasulfonatede zinc phthalocyanine, one of the main components of ZnPcS$_{mix}$. The mixture consists of mono-, di-, tri- and tetrasulfonated mPcs (http://www.google.com.gt/patents/EP2222791B1?cl=en).

All laser irradiations were conducted in a dark room using 536 or 680 nm diode lasers for nanomaterials and ZnPcS$_{mix}$, respectively and Table 2 presents all the laser parameters used during the whole study. The lasers were provided by the National Laser Centre (South Africa). Briefly, Cells in the culture dishes, without lids on, were continuously irradiated from the top at different fluences (irradiation times). A FieldMate laser power meter was used to measure the output power of lasers and laser fluences were determined. Unirradiated cells (group 1 and 2) were kept in the dark at room temperature during irradiations. Dose was calculated as follows: Irradiance (J/cm^2) = time (s) x [power (W)/surface (cm^2)] (APPENDIX C).

Table 2: Laser parameters for irradiation.

Parameters	Diode laser	Diode laser
Manufacturer	Oriel Corporation	Optoelectronics Tech
Wavelength	680 nm	532 nm
Wave emission	continuous	continuous
Spot size	9.1 cm^2	9.1 cm^2
Output power	52 mW	642 mW
Power density	5.73 mW/cm^2	70.74 mW/cm^2
Fluences	5 J/cm^2	5 J/cm^2
	10 J/cm^2	10 J/cm^2
	15 J/cm^2	15 J/cm^2
Irradiation times	16 min 50 s	1 min 10 s
	33 min 40 s	2 min 21 s
	50 min 30 s	3 min 32 s

3.4 Synthesis and Characterization of MPDC

The chemical synthesis of AuNPs was carried out at room temperature and achieved via the Brust method. It is the most popular method for obtaining aqueous solutions of nanoparticles that are 5-30 nm in size. The method is a 2 phase method and was used mostly for thiol-stabilized metal nanoparticles in organic solvents, and in the range of 1-30 nm (El-Hussein *et al.*, 2015).

The Au dendrimer-encapsulated nanoparticles (DENs) were synthesized and characterized at the Chemistry Department, University of Johannesburg, South Africa, using G4-G6 PAMAM-NH2 dendrimers as templates and stabilizers. Sodium tetrahydridoborate (NaBH4) was used as a reducing agent for the synthesis of DENs. Binding studies were carried out in order to determine the maximum capacity of the dendrimer to which the metal ions can be added (Nemanashi and Meijboom, 2013).

The ZnPcS$_{mix}$ was synthesized and characterized at the Chemistry Department, University of Rhodes, South Africa. The photophysical and photochemical study identified phosphate buffered saline (PBS) as the preferred solvent over dimethyl sulphoxide (DMSO) and Triton X-100 to achieve the purpose of this study. Henceforth, ZnPcS$_{mix}$ was dissolved in sterile PBS to a final stock concentration of 5 mM, which was wrapped in foil for protection from direct light (Ogunsipe and Nyokong, 2005).

The final MPDC was obtained after incubating AuDENPs and ZnPcS$_{mix}$ in a nitrogen gas atmosphere for 48 h, with ZnPcS$_{mix}$ in excess. After characterization, a pre-determined volume of AuNPs, AuDENPs and MPDC (AuDENPs-ZnPcS$_{mix}$) was transferred into media to give the required final concentration (used for experimentation) and cells were incubated overnight at 37°C. Media was then removed and the cells were washed as described previously with HBSS to remove either AuNPs, AuDENPs or conjugate, which was not taken up by the cells. Elementary characterization analysis was performed before the conjugated compound was used for cell study.

3.4.1 Spectroscopy

The patterns of absorption (wavelengths absorbed and their extensions) and emission (wavelengths emitted and their intensities) are called spectra and the atomic or molecular interpretation of spectra is known as spectroscopy. Both ultra-violet visible (UV-Vis) and Fourier Transform Infrared (FTIR) spectroscopy, available at the Department of Applied Chemistry at the University of Johannesburg, were used to characterize MPDC.

UV-visible spectroscopy

UV illumination stimulates molecular vibration and electron transitions when atoms/molecules absorb electrons in the range of 160-780 nm. For a light medium, the light intensity is inversely proportional to the depth and the concentration of the sample. Spectrophotometry permits the identification of the absorption band of AuDENPs, $ZnPcS_{mix}$ and MPDC and to investigate the shift in the absorption band of PS after combination to AuNPs. The 2450 Spectrophotometer with a 1 cm matched quartz cell from Shimadzu Scientific Instruments, Kyoto, Japan was used to get the various UV-Vis absorption spectra.

Fourier Transform Infrared (FTIR) spectroscopy

The FTIR spectroscopic measurement of AuDENPs, $ZnPcS_{mix}$, and MPDC was recorded using a Bruker- TENSOR-FTIR spectrometer by making separate pellets of each sample with potassium bromide (KBr). Initially, for combining, the dendrimer (25 mg) was dissolved in 12 ml of DMSO, methanol and dimethylfuran (DMF) (1:1:1 ratio) solvent mixture. After 10 min of stirring, 100 mg of zinc-phtaocyanin was added and stirred for 48 h at room temperature under nitrogen. The resulting mixture was distilled under high vacuum to remove the solvents, and a stream of nitrogen was passed into the wet product for 1 h to get a pure, dry product which was characterized and used for further experiments.

3.4.2 Transmission electron microscopy (TEM)

Nano scaling characterization and visualization are achieved using different systems; scanning tunneling (STM), atomic force (AFM), scanning electron (SEM), high resolution transmission electron (HRTEM) and TEM. TEM is extensively used for medical applications. The TEM was performed at the SPECTRAU laboratory, University of Johannesburg, South Africa, and used for ultrastructural studies (size and shape) of the conjugate using the Jeol

JEM 2100 (Advanced Laboratory Services). It utilizes transmitted electrons through the objects being viewed to form images, and its best resolution is around 0.2 nm, which is 1,000 times better than the conventional light microscope. Samples were loaded by placing one drop of aqueous conjugate on a holey carbon-coated Copper grid (200 mesh) and allowing the solvent to evaporate in air.

3.4.3 Zeta potential

Zeta potential is the potential that exists at the periphery of a compound and is a function of the electrophoretic mobility of the compound. The development of a net charge at the surface of a compound affects its distribution and subcellular localization. A compound with a zeta potential more positive than +30 mV or more negative than -30 mV is considered to be stable. Zeta potential was performed to determine the surface charge of MPDC, size distribution and to investigate its stability.

The Zeta potential was measured in triplicate at the Department of Applied Chemistry, University of Johannesburg by using the Malvern Zetasizer Nano ZS (Malvern Instruments, Malvern, UK) at 25°C and at a 12° angle. Ten microliters of MPDC was transferred to a vessel containing an electrode and used for light scattering analysis, to determine the electrophoretic mobility and the net charge of the sample. Thereafter, the size distribution was also determined.

3.5 Dose Response using AuDENPs-ZnPcS$_{mix}$

To identify the treatment parameters that led to approximately 50% decreased cell viability, a dose response study was conducted using different laser irradiation fluences and MPDC concentrations. Laser fluences of 0, 5, 10 and 15 J/cm^2 and concentrations of 0, 0.1 and 0.3 µM of MPDC were used. Therefore, at this stage different laser light irradiation

fluences or concentrations were applied separately on individual samples without inducing photodynamic reactions and then in combination yielding photodynamic effects.

Morphological changes were observed using inverted light microscopy, cellular viability was determined with the trypan blue exclusion test, cellular proliferation with the adenosine triphosphate (ATP) luminescent assay and cellular membrane damage with the lactate dehydrogenase (LDH) colorimetric assay, all performed after 24 h incubation. The latter assays were performed in the dose response studies to determine the optimum photosensitizer concentration and laser irradiation fluence. Subcellular localization of MPDC was determined with the fluorescent microscope. This was performed in order to perform target-related assays.

The PDT or MPDC alone or irradiation alone; or untreated (no MPDC and no laser irradiation) cells were incubated for 24 h and morphological changes were observed under the microscope coupled to a digital camera. Supernatants from the cells were collected and dispensed into cell free 1.5-2 ml microcentrifuge tubes that were properly labelled and frozen for analysis if they were not to be used for cellular membrane damage. Cells were detached using the procedure described previously in this chapter and culture dishes were rinsed with HBSS to collect the remaining cells. Cells were spun at 2 500 rpm for 5 min and the supernatants were discarded. Cells were re-suspended in HBSS for performing the cell count with trypan blue, unless specified otherwise. Cells were used immediately to conduct biological assays.

3.5.1 Trypan blue exclusion test

A cell count using the trypan blue exclusion test was used to determine cellular viability. The principle of the assay is based on the selective exclusion of the vital dye by live/viable cells since live cells possess intact

membranes and appear translucent under the microscope. Dead cells take up the stain due to exposed or damaged membranes, and when visualized microscopically they appear blue.

In this test, 20 µl cell suspension was removed and added into a microcentrifuge tube followed by 20 µl of 0.4% trypan blue stain to make a 1:2 dilution. The mixture was loaded onto a cell haemocytometer specifically designed for use with the Countess™ automated cell counter (Invitrogen, Life Technology). Percentage viability and cell number was recorded from 15 squares of the haemocytometer and an average was calculated.

3.5.2 Cellular proliferation assay

Adenosine triphosphate (ATP) luminescent assay

The CellTiter-Glo® luminescent assay (G7570, Analytical Diagnostic Products, South Africa) was used to measure cellular proliferation by determining the cellular ATP content in metabolically active cells. The assay relies on the properties of a thermostable luciferase oxidative enzyme used for bioluminescence, to enable the reaction conditions that will simultaneously inhibit endogenous enzymes such as ATPase released during cell lysis as well as generating a stable luminescent signal. The stable luminescent signal generated by the enzyme is proportional to the amount of ATP present. The amount of ATP is directly proportional to the number of viable cells. The assay buffer was thawed, and together with the lyophilized substrate was allowed to equilibrate at room temperature prior to use.

A weight of 0.007 g substrate was dissolved into a volume of 1 ml assay buffer and mixed by vortexing the tube. The mixture was sufficient for 20 reactions (APPENDIX E). A volume of 50 µl of cells suspended in supplemented media was transferred into each flat bottomed 96-well coated luminescence microplate, and left to equilibrate at room temperature for 30 min. Thereafter, 50 µl of the solution was added into each well that

contained sample and the microplate was placed on an orbital shaker (Heidolph Polymax Orbital, Labotec, 1040) for 2 min to induce cell lysis by gentle shaking. After lysis induction, the plate was placed on the bench for 10 min to stabilize the luminescent signal. Luminescence was recorded using the Victor[3] microplate reader (Perkin-Elmer).

3.5.3 Cell membrane damage

Lactate dehydrogenase (LDH) cytotoxicity assay

The non-radioactive CytoTox96® (G400 Analytical Diagnostic Products, South Africa) cytotoxicity assay is a colorimetric analytical method that was used to measure LDH released from the cells. Lactate dehydrogenase catalyzes the interconversion between pyruvate and lactate via the interconversion of NADH and NAD^+. The principle of the assay is based on measuring the cytosolic enzyme, LDH, which is released upon cell lysis which correlates with the amount of damaged cells. The released LDH in the culture supernatant is measured with a 30 min coupled enzymatic reaction which results in the conversion of tetrazolium salt into a red formazan product which is read at the absorbance of 490 nm. The amount of colour formed is proportional to the number of lysed cells.

A volume of 1.2 ml of assay buffer was aliquoted into 1.5 ml eppendorf tubes and 0.012 g of substrate was added to the buffer; the mixture was sufficient to perform 24 reactions. Frozen supernatants were thawed in the water bath at 37°C for approximately 5 min. A blank or sample volume of 50 μl was transferred to the flat bottomed 96-well microplate, followed by an equal volume of the substrate mix. The microplate was covered with foil to prevent direct light penetration or interference and incubated in the dark for 30 min at room temperature. Thereafter, the reaction was stopped by adding 50 μl of the stop solution and the absorbance was read at 490 nm using the Victor[3] microplate reader (Perkin-Elmer).

3.6 Cell Damage

After completing the dose response study, the irradiation fluence of 10 J/cm^2 and the concentration of 0.3 μM MPDC were identified as the parameters to be used for the cell damage study. Post treatment, the incubation periods of 2, 3 and 24 h were considered for localization, gene expression and biological assays, respectively.

3.6.1 Localization

The cell damage study started with the determination of the subcellular localization of MPDC after uptake by MCF-7 cells. Cover slips were sterilized with 70% ethanol and passed over a flame from a Bunsen burner. After sterilization, the sterile cover slips were placed inside 3.4 cm diameter culture dishes and cells were cultured overnight. Thereafter, cells were rinsed with HBSS and incubated with MPDC (at a final concentration of 0.3 μM in supplemented media) for 2 h at 37°C with 5% CO$_2$ and 85% humidity. Next, cells were washed with warm HBSS to remove unabsorbed MPDC, stained with intracellular organelle fluorescent dyes to determine the localization site of conjugate and viewed with different filters as presented in Table 3. Fluorescence images were obtained using a live imaging fluorescent microscope (Carl Zeiss Axio Z1 cell observer).

3.5.2 Cell morphology analysis

Morphological changes were examined in all control and experimental groups 24 h after treatment. A CKX41 inverted light microscope (Olympus, Wirsam) connected to a camera was used to observe and capture qualitative changes with the analysis getIT software. Once digital images were captured, cells were then detached, collected and re-suspended for further biological analysis.

Table 3: The intracellular localization of MPDC was determined by incubating cells with the MPDC and then staining with the fluorescent dye. The fluorescent pattern was visualized under the fluorescent microscope and images were recorded.

Organelle	Fluorescent dye	Concentration	Filters
Mitochondria	MitoTracker (Green)	50 nM	$459_{Ex}/529_{Em}$
Lysosomes	LysoTracker (Green)	75 nM	$459_{Ex}/529_{Em}$
Nuclei	DAPI (Blue)	0.1 mg	$350_{Ex}/461_{Em}$

3.6.3 Apotox-Glo assay (viability, cytotoxicity and caspase activity)

The Apotox-Glo assay (G6320, Analytical Diagnostic Products, South Africa) was performed to assess cell viability, cytotoxicity and caspase activation. Firstly, the assay measures two protease activities for cell viability and cytotoxicity; glycyphenylalanyl- aminofluorocoumarin (GF-AFC) and bis-alanylalanyl-phenylalanyl-rhodamine 110 (bis-AAF-R110), respectively. Live cells show a decrease in AFC fluorescence, while dead cells show an increase in R110 fluorescence. GF-AFC and bis-AAF-R110 have different excitation and emission wavelengths and can thus be assayed in combination. Secondly, the assay contains a luciferase for determination of a luminescent caspase 3/7 signal and assists in monitoring cell death events, which are reflected by an increase in caspase 3/7 activity.

A density of 2×10^5 cells per well was seeded and 20 µl of viability/cytotoxicity reagent, containing both GF-AFC and bis-AAF-R110 substrates, was added to each well and placed on an orbital shaker (Heidolph Polymax Orbital, Labotec, 1040), set at 250 rpm for 1 min. The mixture in a 96-well plate was incubated for 1 h at 37°C before the fluorescence signals were recorded with $400_{Ex}/550_{Em}$ filters for viability and

$485_{Ex}/535_{Em}$ filters for cytotoxicity. Thereafter, caspase 3/7 activity was measured by adding 100 µl of the Caspase-Glo 3/7 reagent to all wells and the luminescence signal measured after 30 min of incubation at room temperature. All signal measurements were perfomed using the Victor[3] microplate reader (Perkin-Elmer).

3.6.4 Mitochondrial destabilization

Change in mitochondrial membrane potential or the depolarization of the mitochondrial transmembrane potential ($\Delta \Psi_m$) is associated with apoptosis. The 1st J-aggregate-forming cationic dye (JC-1) is a lipophilic cationic fluorochrome used to evaluate the status of the $\Delta \Psi_m$. Viable cells are able to take up the JC-1 stain via their plasma membrane and this uptake depends on the $\Delta \Psi_m$. Viable cells have polarized $\Delta \Psi_m$ and can take up the JC-1 leading to mitochondrial JC-aggregates, a red-spectral shift and a high red fluorescence emission, which is measured in the red channel on the flow cytometer. Damaged cells with depolarized mitochondria cannot take up JC-1 stains and do not fluoresce in the red fluorescence channel. JC-1 remains in its monomeric form in the cytoplasm and is not permeable to cells with depolarized mitochondria, and thus no red spectral shift.

Cells were detached as previously described, re-suspended in 1 ml HBSS and centrifuged at a speed of *400 x g* for 5 min at a temperature of 4°C. The supernatant was discarded and cells were re-suspended in 0.5 ml of a fresh JC-1 working solution and thoroughly mixed. Then the mixture was incubated at 37°C in a CO_2 incubator for 10 min, followed by the addition of 1 ml of 1 x assay buffer. The combination was mixed and centrifuged for 5 min at *400 x g*. Again, the supernatant was discarded, 0.5 ml of 1 x assay buffer was added, the solution was vortexed and centrifuged in the same manner. Cells were re-suspended in 0.5 ml 1 x buffer and the cells in the pellet and suspended by vortexing. Analysis was done using the FACSCAria flow cytometer (BD Biosciences).

3.6.5 Cytochrome C leakage

Cytochrome C is an apoptogenic component required for further apoptotic events such as caspase-3 activation and DNA fragmentation. Mitochondrial damage and leakage leads to the accumulation of cytochrome C in the cytosol of intact cells.

An Enzyme linked immunoassay (ELISA) (human cytochrome C Platinum ELISA kit) was used to detect the level of cytosolic cytochrome C in various treated samples. Cells were detached from the plate, re-suspended in HBSS, centrifuged for 15 min at a speed of 217 *xg* and the supernatant was discarded. Thereafter, cells were re-suspended in 1 ml of cold PBS and centrifuged for 5 min at 398 *xg*. Cells were then lysed by incubating with 0.5 ml of lysis buffer for 1 h at room temperature. Then, cells were centrifuged for 15 min at *200 x g* and a 50-fold dilution of the supernatant was done by removing 5 µl of the supernatant and adding it into to a 1.5 ml tube with 245 µl of 1 x assay buffer and stored at -80 °C.

Samples (lysate supernatants) were further diluted by making a 1:2 dilution in assay buffer, 150 µl of sample was added to an equal volume of 1 x assay buffer, and a volume of 100 µl was added to the wells. Blank wells contained 100 µl of 1 x assay buffer added in duplicate, and all standards and samples were also added in duplicate. A volume of 50 µl biotin-conjugated anti-human cytochrome C antibody was added to all the wells and the microplate was covered with an adhesive film and incubated for 2 h at room temperature. Thereafter, the microplate was rinsed three times with 400 µl of wash buffer and 100 µl of Streptavidin-HRP secondary antibody was added to all the wells. The microplate was covered with an adhesive film and incubated for 1 h at room temperature. After the wells were washed three times with 400 µl of wash buffer, 100 µl of tetramethyl-benzidine (TMB) substrate was added and the plate was incubated at room temperature for 10 min. Lastly, the reaction was stopped by adding 100 µl of stop solution

and the absorbance of each well was read at 450 nm using the Victor³ microplate reader (Perkin-Elmer).

3.6.6 Cell death detection

Apoptosis is an important physiological process as it participates in cellular homeostasis and removal of useless cellular contents. This mode of cell death has hallmark features that enable systematic differentiation from other modes of cell death. Phosphatidylserine is a membrane phospholipid protein, and when cells undergo apoptosis this protein is translocated from the inner to the outer leaflet of the plasma membrane, thereby exposing the phosphatidylserine to the external cellular environment. Annexin V is a 35-36 kDa Ca^{2+} dependent phospholipid-binding protein that has a high affinity for phosphatidylserine and therefore binds to cells with exposed phosphatidylserine.

Annexin V conjugated to fluorescein isothiocyanate (Annexin V-FITC) fluorochrome is currently used to detect apoptotic cells by flow cytometric analysis. Annexin V-FITC is more often used in conjunction with propidium iodide (PI), a crucial and specific dye used to stain necrotic cells. This is because viable cells exclude PI whereas dead cells take up the dye. Therefore, healthy cells with integral membranes are Annexin V-FITC and PI negative (FITC-/PI-), viable and early apoptotic cells are FITC positive- and PI negative (FITC+/PI-), necrotic cells are PI positive (FITC-/PI+), and late apoptotic cells stain positive for both FITC and PI (FITC+/PI+) (Grosse *et al.,* 2009).

Cells were re-suspended, rinsed twice with PBS and then re-suspended in a 1 x assay binding buffer. A volume of 100 µl was transferred into a 5 ml sterile Falcon tube and cells were concurrently incubated with 5 µl of Annexin V-FITC and PI. The mixtures were incubated in the dark for 5 min on ice. Then 400 µl of 1 x binding buffer was added to all the samples, which

were analyzed on the FACSCAria flow cytometer (BD Biosciences) by reading 10 000 events. Control samples were included and prepared for the assay as follow: cells only without any stain; cells stained with Annexin V-FITC only; cells stained with PI only; and positive control cells which included those stained with both Annexin V-FITC and PI (late apoptotic). An apoptosis positive control was prepared by inducing apoptosis with 1 µg/ml actinomycin D, and a necrosis positive control with 10% (v/v) hydrogen peroxide for 24 h.

3.6.7 Real-time Reverse Transcriptase Polymerase Chain Reaction

The real-time Reverse Transcriptase Polymerase Chain Reaction (RT-PCR) was used to study the amplification of gene products and expression. The RT-PCR was done using SYBR Green technology, which has an affinity for double-stranded genetic material and binds to nitrogenous bases of the genetic molecules to produce a fluorescent signal (Bustin *et al.*, 2005; Wang *et al.*, 2006).

Extraction of ribonucleic acid (RNA) and quantification

The RNeasy kit (74104, SABiosciences, South Africa) with QiAshredder homogenisers (79654, SABiosciences, South Africa) was utilized to isolate RNA from the MCF-7 cells. The isolated RNA is approximately 200 bases long and is obtained after the elution phase, which is achieved in a low ionic milieu (Lai *et al.*, 2007). The isolation was performed based on the binding affinity of the silica membrane and the speed of the microcentrifugation technology. The positively charged silica membrane facilitates the binding to the phosphate backbone of the nucleic acids in the presence of specific salt, which disrupts the non-covalent inetractions between water molecules.

Three hours after incubation, both treated and untreated cells were detached and rinsed with PBS to remove all traces of culture media. Cells were re-suspended in 600 ml of RLT buffer after they were spun down and the PBS was discarded. All extraction reagents and cell supsensions were loaded on the QIAcube (Invitrogen). At the end of the run, 30 µl of eluted RNA was collected and quantified using the Quant-iT™ RNA Assay kit (Q32852, Life Technologies, South Africa) on the Qubit™ fluorometer (Invitrogen). The working solution of the assay was prepared and Quant-iT™ RNA reagent was diluted in Quant-iT™ RNA buffer in a 1:200 ratio in thin-walled and clear 0.5 ml optical-grade PCR tubes and stored at room temperature. Standards 1 and 2 were prepared by loading 190 µl working solution into two tubes and 10 µl of each Quant-iT™ standard (1 and 2) was added to the suitable tube and mixed. For experiments purpose, 1 µl of the eluted RNA sample was diluted in 199 µl working solution and mixed. Both standard and sample tubes had a final volume of 200 µl and all tubes were incubated for 2 min. The two standard tubes were used to calibrate the Qubit™ fluorometer and the RNA sample concentration (µg/ml) was determined. The obtained concentration was multiplied by the total number of eluted volume (30 µl) and the total concentration of isolated RNA was determined.

RNA purity

One microliter of each isolated RNA sample was mixed with 99 µl buffer AE (19077, SABiosciences, South Africa) in a quartz cuvette to determine the quality of nucleic acids. The buffer consists of 10 mM Tris-Cl and 0.5 mM EDTA; pH 9.0. The absorbance of each sample was read using the Biomate 3 spectrophotometer (Thermospectronic, 335904P), and the ratio of the absorbance value at 206 nm over the value at 208 nm was calculated and purity was determined. All ratio values were between 1.8 and 2.0 (APPENDIX F).

Complementary DNA (cDNA) synthesis

Following RNA purity verification, the QuantiTect Reverse Transcription kit (Qiagen, 205311) was used to synthesize complementary DNA (cDNA) from isolated RNA samples. The QuantiTect Reverse Transcriptase, contained in this kit possesses a high affinity for RNA and is able to synthesize cDNA from as little as 10 pg RNA. A volume comprising of 30 ng of RNA was used for RNA reverse transcription into cDNA and used for the genomic DNA (gDNA) elimination reaction mixture prepared on ice and according to Table 4. The PCR Array is very sensitive and yields results with as little as 25 ng or as much as 5 µg total RNA per array.

Table 4: Genomic DNA elimination reaction and various components.

Component	Volume/reaction	Final concentration
gDNA wipeout buffer	2 µl	1X
Template RNA	Variable (30 ng)	
RNase free water	Variable	
Final volume	**14µl**	**-**

The final volume for gDNA elimination was 14 µl, tubes were incubated for 8 min at 42˚C and then placed on ice. Thereafter, a reverse transcription reaction with a final volume of 20 µl was prepared on ice by mixing Quantiscript Reverse Transcriptase, Quantiscript RT Buffer, RT Primer Mix and 14 µl of the gDNA elimination reaction as presented in Table 5. The reverse transcription reaction tubes were vortexed and incubated for 15 min at 42˚C. Then the reverse transcription reaction tubes were incubated for 3 min at 95˚C to deactivate Quantiscript Reverse Transcriptase. The real-time PCR array was performed and the synthesized cDNA used as a template or stored at -20˚C for later usage.

Table 5: Reverse transcription reaction and various components.

Component	Volume/reaction
Reverse-Transcription master mix	
Quantiscript Reverse Transcriptase	1μl
Quantiscript RT Buffer	4μl
RT Primer Mix	1μl
Template RNA	
gDNA elimination reaction	14μl
Final volume	**20 μl**

Gene expression

The purity of the cDNA samples was determined after obtaining the absorbance values and ratios ($A_{260/280}$ nm). One microliter of synthesized cDNA was mixed to 99 μl buffer AE (Qiagen, 19077) in a quartz cuvette and read using the Biomate 3 spectrophotometer. Ratios between 1.84 and 1.97 were obtained and used for gene expression analysis (APPENDIX F). The expression of 84 genes involved in death and senescence (Table 6) was studied and profiled using the Human Cell Death PathwayFinder™ PCR Array (SABiosciences, PAHS-212A) and Stratagene Mx3000p® instrument.

The RT² Profiler PCR Array System takes advantage of real-time PCR performance and combines it with the ability of microarrays to detect the expression of multiple genes simultaneously. The first 84 wells (A1 to G12) of the PCR plate each contained a different cell death gene and the remaining 12 wells consisted of housekeeping genes (H1 to H5) to normalize the PCR Array data, gDNA control (H6) to detect gDNA contaminant, Reverse Transcription control genes (RTC, H7 to H9) and Positive PCR control genes (PPC, H10 to H12) to assess the quality of the the reverse transcription and PCR efficiency, restively (Figure 20).

The cDNA samples were diluted with 92 µl of RNase-DNase free water (final volume 102 µl) and used to prepare an experimental cocktail by adding the SABiosciences RT^2 qPCR master mix and RNase-DNase free water in a 50 ml RNase-DNase free tube according to the manufacturer's protocol and sequence as per Table 7. The SABiosciences RT^2 qPCR Master mix used was precisely designed for the Stratagene Mx3000p® and contained RT^2 SYBR Green (detected dye) and ROX (reference dye) qPCR components.

Table 6: Functional gene grouping of the human cell death pathway finder profiler (updated from SABiosciences, PHAS-212A).

Cell death	Gene subunits
Pro-Apoptotic	ABL1, APAF1, BCL2L11, BIRC2 (c-IAP2), CASP1 (ICE), CASP2, CASP6, CASP7, CASP9, CD40 (TNFRSF5), CD40LG (TNFSF5), CFLAR (CASPER), DFFA, FASLG (TNFSF6), GADD45A, NOL3, TNFRSF10A (TRAIL-R).
Anti-Apoptotic	BCL2A1 (Bfl-1/A1), BIRC3 (c-IAP1), IGF1R, MCL1, TNFRSF11B, TRAF2, XIAP.
Apoptosis and Autophagy	AKT1, BAX, BCL2, BCL2L1 (BCL-X), CASP3, FAS (TNFRSF6), TNF, TP53.
Apoptosis and Necrosis	ATP6V1G2, CYLD, SPATA2, SYCP2, TNFRSF1A
Autophagy	APP, ATG12, ATG16L1, ATG3, ATG5, ATG7, BECN1, CTSB, CTSS, ESR1 (ERa), GAA, HTT, IFNG, IGF1, INS, IRGM, MAP1LC3A, MAPK8 (JNK1), NFKB1, PIK3C3 (VPS34), RPS6KB1, SNCA, SQSTM1, ULK1.
Necrosis	BMF, C1orf159, CCDC103, COMMD4, DEFB1, DENND4A, DPYSL4, EIF5B, FOXI1, GALNT5, GRB2, HSPBAP1, JPH3, KCNIP1, MAG, OR10J3, PARP1 (ADPRT1), PARP2, PVR, RAB25, S100A7A, TMEM57, TXNL4B.

Table 7: Experimental cocktail preparation for RT-PCR application.

Plate format:	96 well
2x SABiosciences RT^2 qPCR Master mix	1,350 µl
Diluted First Strand cDNA Synthesis Reaction	102 µl
Water	1,248 µl
Final Volume	**2,700 µl**
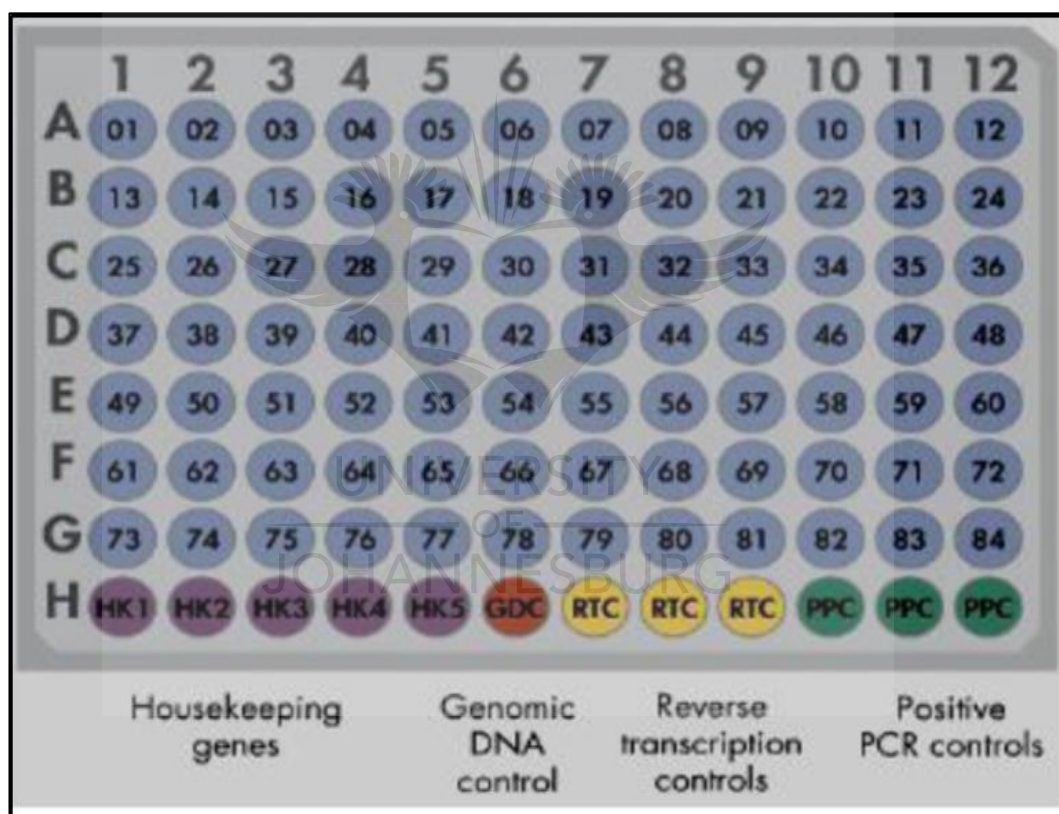
Figure 20: Layout of the catalogued 96well PCR Array. Wells A1 through G12 contain individual qPCR assays for the 84 genes relevant to the human cell death pathway. Wells H1 through H5 contain a panel of housekeeping genes (HK1-HK5) used for normalizing the PCR array data. Well H6 to H12 contain controls namely genomic DNA contamination (GDC), Reverse Transcription Controls (RTC), and Positive PCR Control (PPC).

Twenty five microliters of the the experimental cocktail was added to each well and the 96 well PCR Array plate was sealed with optical thin walled 8-

cap strips and centrifuged for 1 min at room temperature at 1,000 *xg* using a Heraeus Labofuge 400 centrifuge (Thermo Scientific) to remove all air bubbles. The run on the Stratagene Mx3000p® was programmed as follows: 1 cycle, 10 min at 95˚C to activate the HotStart DNA polymerase, and 40 cycles of 15 sec and 1 min at 95˚C and 60˚C respectively (the annealing step). During the annealing step of each cycle, SYBR Green intercalates and detects double stranded DNA from every well.

The target DNA sequence was amplified through a thermal process of repeated heating (for DNA melting) and cooling (for enzyme dependent replication) steps. During the DNA melting step, the double stranded helical molecule unwinded and separated into two single stranded DNA molecules, which were used as templates for amplication by DNA polymerase in the cooling step. SYBR Green is not specific and had the ability to detect any other double stranded DNA such as the target DNA in each well, primer dimers, contaminant DNA or products from misannealed primers. A melt curve analysis was programmed at the end of the PCR cycling (95˚C, 1 min; 65˚C, 2 min (optics off) and 65 to 95˚C at 2˚C per min (optics on)) and gave an indication of the amplication of each single product. During the heating step, the double stranded DNA molecules dissociated and altered to a hyperchromic form as the hydrogen bonds between the nitrogenous bases were being weakened and the absorbance intensity increased. The melting point depends on the G-C content of the nucleic and is the temperature at which 50% of hydrogen bonds are disrupted with capital for identification of a single peak at temperatures greater than 80˚C in each well.

Real-time PCR array data analysis

A loaded PCR Array plate was placed on the real-time thermal cycler and the program was run. The instrument software gave the threshold cycle (C_t) value for each well and all C_t values equal to or greater than 35 were considered as negative amplification (absence of amplicon). A gDNA control

well (well H6) with a C_t value greater than 35 designated absence of gDNA contamination and a C_t value lesser than 35 ($C_t<35$) designated gDNA impurity. C_t values of 20±2 (should not vary by more than 2 cycles between PCR Arrays being compared) for positive PCR control wells (PCC, wells H10 to H12) should be obtained, which indicated successful amplification. The average C_t values of all 5 housekeeping genes was used by the software to normalize the 84 genes studied and was subtracted from the gene of interest C_t value. All C_t values were exported to a blank Excel spread sheet and used with the SABioscience PCR array Data Analysis Template available from the SABioscience website with the suitable pathway-focused genes (PAHS-212A). The PCR Array Data Analysis software was used to obtain the calculations and interpretation of the control wells. The student t-test was used to obtain the degree of significance alteration of gene expression (p value) and results were presented in a tabular format, a scatter plot, a three-dimensional profile, and a volcano plot (when replicates are included).

Fold-change ($2^{\wedge}(\Delta\Delta C_t)$) was calculated by the software by dividing the normalized gene expression ($2^{\wedge}(\Delta C_t)$) of the test sample by the normalized gene expression ($2^{\wedge}(\Delta C_t)$) of the control sample. Fold-change values greater than one indicate a positive or an up-regulation, and the fold-regulation is equal to the fold-change, while fold-change values less than one indicate a negative or down-regulation. The fold-regulation is the negative inverse of the fold-change. The p values were calculated based on the Student's t-test of the replicate $2^{\wedge}(\Delta C_t)$ values for each gene in the control group and treatment groups. A value of $p<0.05$ was considered significant.

3.7 Statistical Analysis

Dose response study experiments were repeated six times (n=6), gene expression experiments were performed three times (n=3) and cell damage

experiments were repeated four times (n=4) on different MCF-7 cell populations. Each biochemical assay was done in duplicate, the average of which was used, and the mean, standard deviation, standard error and significant changes were calculated using SigmaPlot Version 11.0 software, manufactured by Systat Software Incorporation. The results were recorded for statistical analysis and the one-tailed Student t-test (difference between control and experimental group) was used for each independent variable. Statistical significance is shown as $p<0.05$(*), $p<0.01$(**) or $p<0.001$(***) when compared to the untreated control cell and graphs and tables are represented as the mean ± standard error.

CHAPTER FOUR

RESULTS

4.1 Dose Response using two Gold Nanoparticles

A dose response was conducted using two gold nanomaterials, namely gold nanoparticles (AuNPs) and gold encapsulated dendrimers (AuDENPs), to identify the optimal nanomaterials to be used and to determine its role prior to conjugation with $ZnPcS_{mix}$. Cells were treated with two concentrations (1 and 3 mM) of each gold nanomaterial and after 24 h cell viability, proliferation and cytotoxicity were assessed by means of the Trypan Blue exclusion assay, ATP luminescence assay and LDH cytotoxicity assay, respectively. Additionally, the temperature of all irradiated samples was monitored and remained constant during laser irradiation.

Results showed that cell viability decreased in a dose-dependent manner (Table 8) and that AuNPs induced a significant decrease ($p < 0.05$) in a light independent manner; when cells were treated with 1 and 3 mM AuNPs and compared to untreated control cells (0 J/cm^2 and 0 mM). All cells that received AuNPs and laser irradiation showed that cell viability decreased significantly ($p < 0.05$ and $p < 0.01$). The viability of AuDENP-treated cells also decreased in a dose-dependent manner, but only showed a significant decrease in cells treated with 1 mM at 15 J/cm^2, and 3 mM at both 10 and 15 J/cm^2 ($p < 0.05$).

With the cell proliferation assay, the level of ATP decreased similarly in a dose-dependent and light-independent manner. All cells treated with AuNPs showed a significant decrease in ATP luminescence ($p < 0.05$ and $p < 0.01$) when compared to the untreated control (0 J/cm^2 and 0 mM). AuDENP treatment was less severe when compared to AuNPs, and showed only light-dependent dose response. There was a significant decrease ($p < 0.05$) in all irradiated AuDENP-treated cells, with the exception of cells treated with 1 mM AuDENP and 5 J/cm^2 laser (Table 9).

Table 8: Percentage viability of treated and untreated MCF-7 cells using the Trypan Blue exclusion assay. Various concentrations of nanomaterials and laser fluences were applied during treatment. In comparison to untreated cells (0 mM and 0 J/cm^2), statistical differences are shown as *p<0.05 and **p<0.01.

Trypan Blue Viability Assay (%)

Laser Fluences	Control	Gold nanoparticle Concentration		Gold encapsulated dendrimer Concentration	
	0 mM	1 mM	3 mM	1 mM	3mM
0 J/cm^2	94 ± 1,06	74 ± 1,56*	72 ± 0,52*	95 ± 1,76	93 ± 1,48
5 J/cm^2	93 ± 3,21	71 ± 1,61*	70 ± 2,36**	86 ± 0,56	86 ± 0,59
10 J/cm^2	94 ± 2,67	72 ± 0,45*	69 ± 1,43**	84 ± 1,58	81 ± 1,75*
15 J/cm^2	97 ± 0,45	69 ± 2,86**	65 ± 1,34**	78 ± 0,75*	72 ± 0,63*

± represents standard error

Table 9: Proliferation of treated and untreated MCF-7 cells using the Adenosine Triphosphate luminescence assay (Relative Light Unit, RLU). Various concentrations of nanomaterials and laser fluences were applied during treatment. In comparison to untreated cells (0 mM and 0 J/cm^2), statistical differences are shown as *p<0.05 and **p<0.01.

Adenosine Triphosphate Proliferation Assay

Laser Fluences	Control	Gold nanoparticle Concentration		Gold encapsulated dendrimer Concentration	
	0 mM	1 mM	3 mM	1 mM	3 mM
0 J/cm^2	256431± 25	198983± 82*	193692± 58*	224558± 74	214785± 98
5 J/cm^2	254682± 64	175894± 64**	198752± 76*	211254± 45	197581± 65*
10 J/cm^2	264130± 52	198645± 12*	167985± 15**	193945± 65*	197455± 57*
15 J/cm^2	258791± 36	154896± 28**	157487± 45**	188543± 76*	178954± 36*

± represents standard error

Cellular membrane integrity was used to determine the degree of toxicity of each treatment (Table 10). AuNPs induced cytotoxicity with a significant increase in the levels of LDH in the culture media of MCF-7 cells treated with 3 mM AuNPs (p<0.05), as well as all irradiated AuNP-treated cells (p<0.05 and p<0.01) when compared to that of the untreated cells. AuDENPs did not show dark toxicity and led to a light-dependent cytotoxicity

(p<0.05) when laser fluences of 10 and 15 J/cm^2 laser fluences were used to activate AuDENPs.

Table 10: Cytotoxicity of treated and untreated MCF-7 cells using the Lactate Dehydrogenase Membrane Integrity assay (A_{490}nm). Various concentrations of nanomaterials and laser fluences were applied during treatment. In comparison to untreated cells (0 mM and 0 J/cm^2) statistical difference are shown as *p<0.05 and **p<0.01.

Lactate Dehydrogenase Membrane Integrity Assay

Laser Fluences	Control	Gold nanoparticle Concentration		Gold encapsulated dendrimer Concentration	
	0 mM	1 mM	3 mM	1 mM	3mM
0 J/cm^2	$0,331\pm 0,021$	$0,354\pm 0,045$	$0,383\pm 0,053*$	$0,345\pm 0,042$	$0,353\pm 0,075$
5 J/cm^2	$0,321\pm 0,035$	$0,389\pm 0,037*$	$0,392\pm 0,069*$	$0,363\pm 0,036$	$0,379\pm 0,048$
10 J/cm^2	$0,354\pm 0,025$	$0,401\pm 0,081*$	$0,397\pm 0,014*$	$0,412\pm 0,015*$	$0,405\pm 0,036*$
15 J/cm^2	$0,341\pm 0,065$	$0,458\pm 0,04**$	$0,462\pm 0,05**$	$0,395\pm 0,045*$	$0,443\pm 0,042*$

± represents standard error

4.2 Synthesis and Characteristics of MPDC

AuNP showed both light-independent and light-dependent cytodamage while AuDENPs only yielded to light-dependent cytodamage, and for this reason AuDENPs was chosen for conjugation. Both AuDENPs and ZnPcS$_{mix}$ (in excess) were mixed at a ratio of 1:37,86 (v/v), continually agitated and incubated in a nitrogen gas atmosphere for 48 h. Then, the solution was collected and analyzed to determine whether or not combination was successful. The resulting mixture was characterized by both UV-Vis and FTIR spectroscopy, TEM and zeta potential analysis.

4.2.1 Spectroscopy

UV-visible

The absorption spectra of AuDENPs, ZnPcS$_{mix}$ and their resulting mixture were obtained and analyzed. The peaks of absorption were obtained at 524 nm (black), 676 nm (bleu) and 674 nm (red) for AuDENPs, ZnPcS$_{mix}$ and

MPDC (AuDENPs-ZnPcS$_{mix}$), respectively. The absorption peak of MPDC is near the therapeutic window and would probably have optical properties similar to that of ZnPcS$_{mix}$ rather than that of AuDENPs.
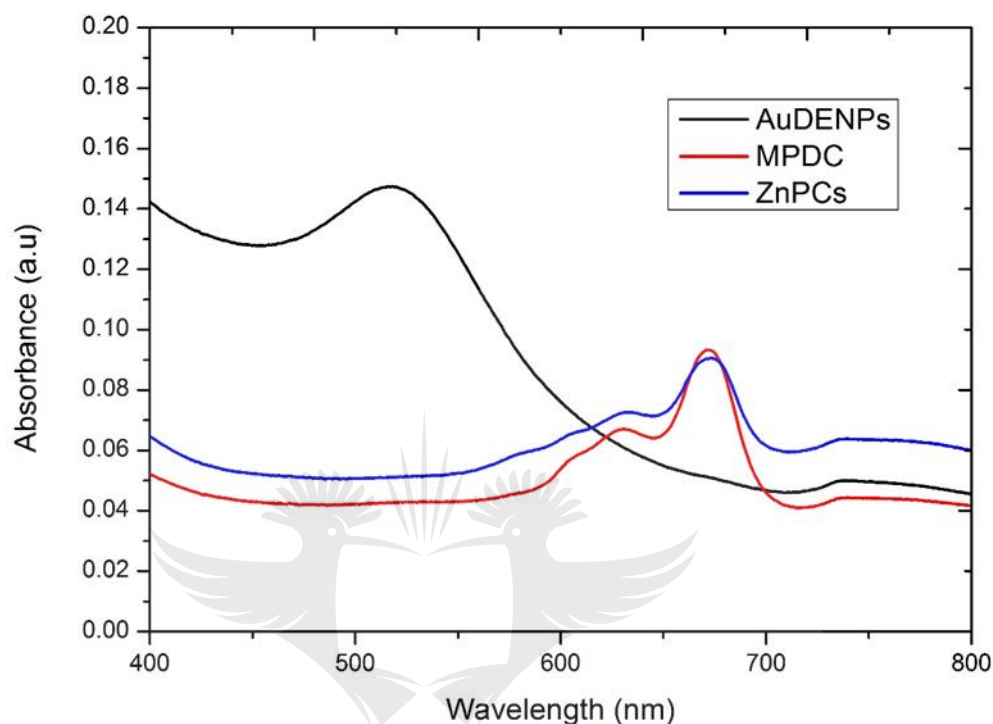
Figure 21: Absorption spectra. The respective absorption peaks of AuDENPs, ZnPcS$_{mix}$ and MPDC were at 524, 676 and 674 nm.

Fourier Transform Infrared (FTIR)

The FTIR spectra of AuDENPs, ZnPcS$_{mix}$ and MPDC were obtained and compared (Figure 22). The AuDENPs showed two major peaks at 3341.86 and 1640.23 (bottom spectrum). ZnPcS$_{mix}$ had five major peaks at 3907.58, 3529.39, 1638.50, 1400.46 and 638.35 (middle spectrum). The combined compound or MPDC (AuDENPs-ZnPcS$_{mix}$) had several peaks at similar positions as the previous ones indicated spectral shifts and formation of new functional groups (top spectrum). Thus, this confirmed a successful conjugation, MPDC and conjugate were used interchangeably in this study, consisting of AuDENPs and ZnPcS$_{mix}$. The 3126.12 peak related to the possible shift from 3341.86 (AuDENPs) or 3529.39 (ZnPcS$_{mix}$); the 1636.56

peak is as a result of the possible shift from 1640.23 (AuDENPs) and 1638.50 (ZnPcS$_{mix}$); the 1400.42 from 1400.43 (ZnPcS$_{mix}$), and the 501.19 from 638.35 (ZnPcS$_{mix}$).
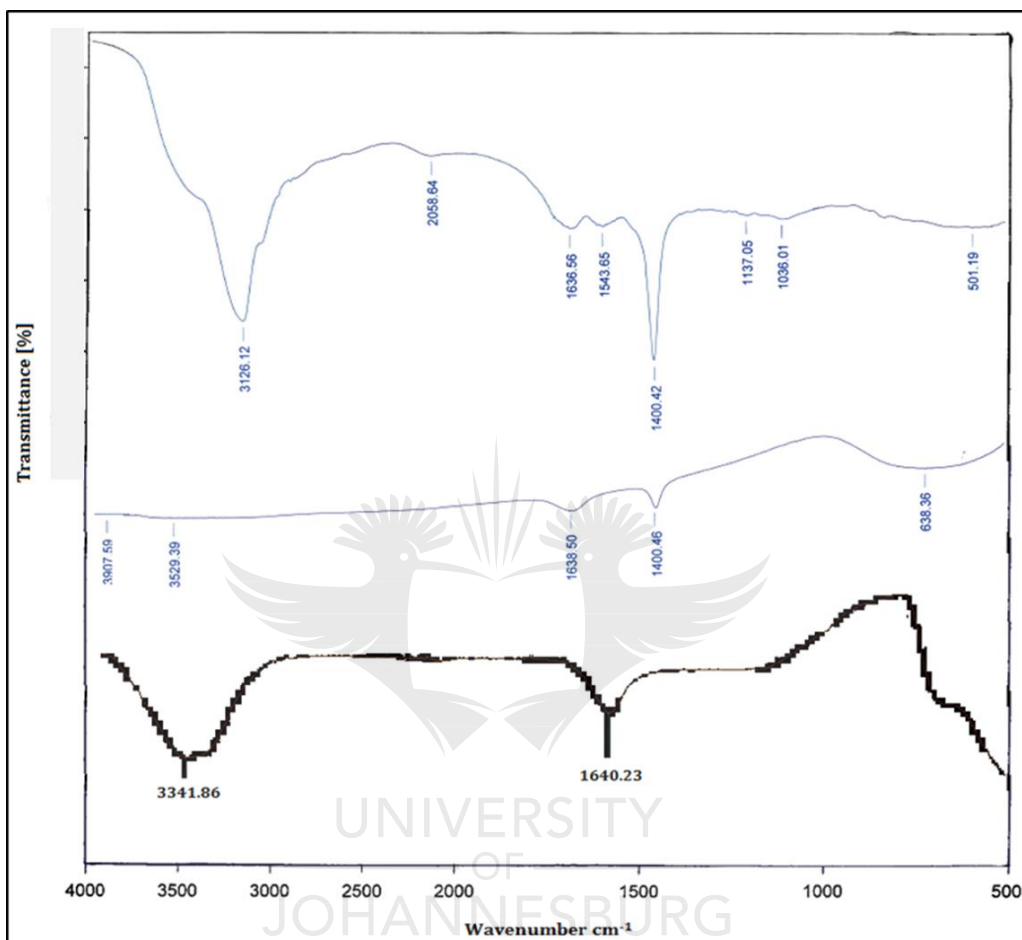
Figure 22: Comparative Infrared spectra of samples. The bottom spectrum of AuDENPs showed 2 peaks, the middle spectrum of ZnPcS$_{mix}$ had 5 peaks and the top spectrum of MPDC had 8 distinct peaks (new functional groups formed).

4.2.2 Transmission electron microscopy (TEM)

The size and the shape of MPDC (AuDENPs-ZnPcS$_{mix}$) was determined by means of TEM (Figure 23). The MPDC was spherical in shape with an average size of less than 5 nm. The small size of the conjugate would probably be an advantage as the effectivity of nanostructure is size-dependent and the smaller the size, the better the uptake and activity of NPs.
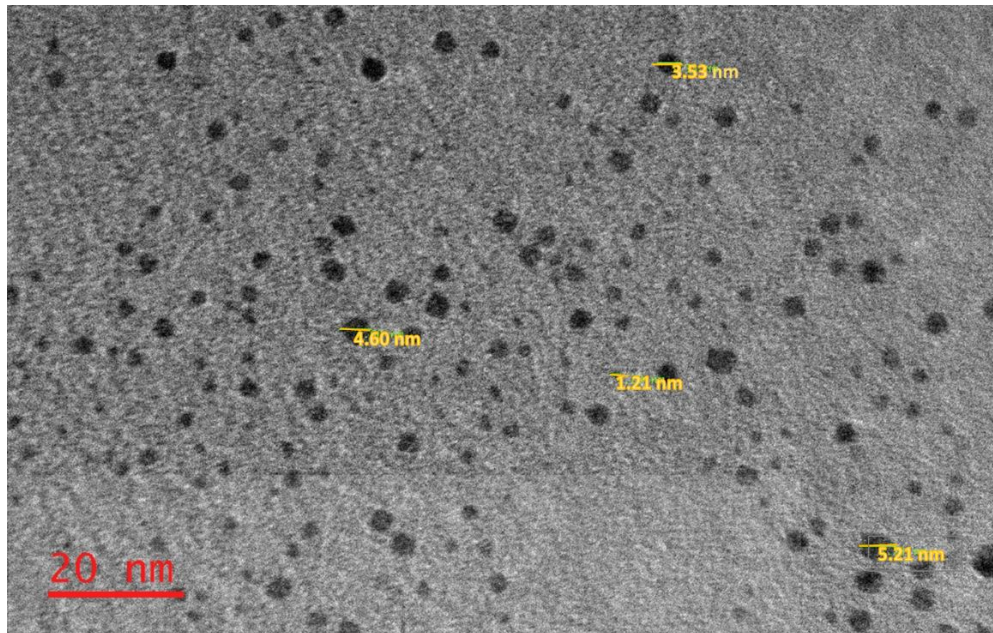
Figure 23: Transmission Electron Microscopy of MPDC (AuDENPs-ZnPcS$_{mix}$). The conjugate was spherical in shape with an average size of less than 5 nm (3.53, 4.60, 1.21 and 5.21 nm yellow scale).

4.2.3 Zeta potential analysis

Zeta potential was used to determine the surface charge of the obtained conjugate or MPDC. The surface charge was found to be +36 mV, which is greater than +30 mv, indicating that MPDC is stable. The size distribution indicated that more than 95% of MPDC had an average size of 4, 43 nm.

4.3 Dose Response using MPDC (AuDENPs-ZnPcS$_{mix}$)

After characterization, a second dose response was performed to determine the treatment parameters to be used in the cell damage study, which would lead to approximately a 50% decrease in cell population. Five concentrations (0.1; 0.3; 0.5; 0.7 and 0.9 µM) of MPDC were considered together with a laser fluence of 10 J/cm^2 as it was previously shown that AuDENPs were not activated with a laser fluence of less than 10 J/cm^2. After treatment, cells were incubated for 24 h and the Trypan Blue exclusion

assay, the ATP luminescence assay and the LDH assay were performed to evaluate percentage cell viability (%), proliferation (Relative Light Units, RLU) and degree of cytotoxicity (A_{490} nm), respectively. All treated MCF-7 cells were compared to the untreated control (0 µM MPDC and 0 J/cm^2) and statistical differences are shown as *$p<0.05$, **$p<0.01$ and ***$p<0.001$.

Results indicated that all PDT-treated cells showed a significant decrease in cell viability ($p<0.05$ and $p<0.001$) when compared to untreated control cells (Table 11). A similar observation was made when looking at the combined effects of MPDC and laser irradiation on the proliferation of MCF-7 cells ($p<0.05$ and $p<0.001$) (Table 11). With the exception of treatment with 0.1 µM MPDC and laser irradiation, MPDC plus laser irradiation yielded significant membrane damage or toxicity ($p<0.01$ and $p<0.001$) (Table 11). Concentrations of MPDC used in this second dose response experiment were very little when compared to the first dose response study (more than 1,000 times less than the amount of AuNPs and AuDENPs alone). Treated cells became more sensitive to the treatment; MPDC was effective in prompting decrease in viability and in proliferation with enhanced cytotoxic effects. The treatment combination of 0.3 µM MPDC and 10 J/cm^2 was identified as the one that led to a decrease below the 50% cell viability. Thus, it was used to study cell damage effects.

4.4 Cell damage

Multiple particle delivery complex at a concentration of 0.3 µM and laser irradiation at a fluence of 10 J/cm^2 were used to treat MCF-7 cells. This cell damage study was performed to determine the photodynamic effects of MPDC after incubation. Before evaluating these effects on cell morphology, viability, toxicity, enzymatic (caspase 3/7) activity, mitochondrial damage, protein presence, cell death induction and gene expression following PDT, the subcellular localization of MPDC was determined in MCF-7 cells.

Table 11: Evaluation of cell viability, proliferation and cytotoxicity of MCF-7 cells treated with MPDC and a laser fluence of 10 J/cm^2. Statistical difference are shown as *p<0.05, **p<0.01 and ***p<0.001, respectively. The experiments were repeated four times (n=4).

	Untreated	MPDC (µM)				
	0.0 µM	0.1	0.3	0.5	0.7	0.9
	0 J/cm^2	10 J/cm^2				
TB (%)	91±1.8	78±3.0*	53±2.1 ***	40±1.2 ***	29±3.8 ****	11±2.7 ***
ATP (RLU)	25897 ±222	22242 ±724*	14469 ±250***	11258 ±557***	8608 ±542***	6786 ±352***
LDH (A$_{490}$nm)	0.401 ±.005	0.404 ±.006	0.476** ±.004	0.491** ±.0001	0.632*** ±.001	0.767*** ±.0002

± represents standard error,

4.4.1 Localization

MCF-7 cells were treated with MPDC and incubated for 2 h before they were treated and stained for fluorescent microscopy to identify the subcellular localization of MPDC. The fluorescent images showed colocalization of both mitotracker and MPDC as the appearance of a yellowish colour; merged colour between the green mitotracker and red MPDC. Distinct blue nuclei remained clearly identifiable in the merged image and indicated that MPDC did not primarily localize in the nuclei (Figure 24). An analogous observation was made when cells were stained with DAPI and lysotracker. The intermediate yellowish colour between the green of the lysotracker and the red of MPDC was detected, and indicated colocalization of MPDC and lysosomes. The blue nuclei remained as such in the merged image and demonstrated that MPDC did not localize in the nuclei.
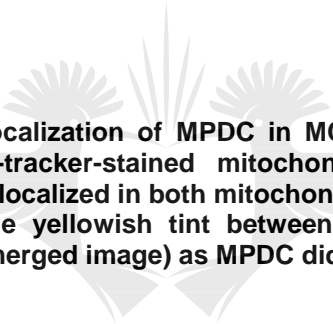
Figure 24: Subcellular localization of MPDC in MCF-7 cells. DAPI-stained nuclei (blue), Mito- and Lyso-tracker-stained mitochondria and lysosomes (green), respectively. MPDC (red) localized in both mitochondria and lysosomes and is seen as the emergence of the yellowish tint between green and red. Distinct blue fluorescence was seen (merged image) as MPDC did not localize in the nuclei but in the perinuclear area.

4.4.2 Morphology

Morphological features of MCF-7 cells were assessed after treatment with conjugate alone, laser irradiation alone and PDT (Figure 25) and compared to those of the untreated MCF-7 cells. Neither irradiated cells nor conjugate-treated cells showed detectable morphological changes. However, PDT-treated cells changed from their initial appearance, became irregular and some rounded off, detached from the culture flask and appeared as free floating structures.
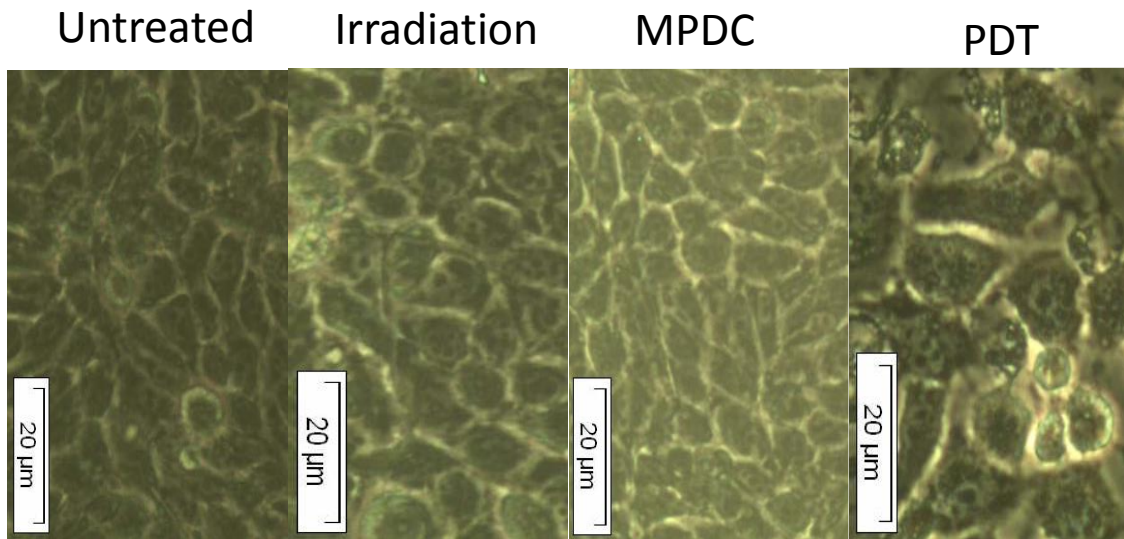
Figure 25: Morphology of untreated, irradiated, MPDC-treated and PDT-treated MCF-7 cells. No morphological change was noted in irradiated or MPDC-treated cells when compare to untreated cells. The morphology of PDT-treated MCF-7 cells changed, include an elongation of cells, decrease in cell number, detachment and rounding off (200x magnification).

4.4.3 Apoptox-Glo assay

The Apoptox-Glo assay was performed and results of treated cells were compared to those of untreated cells. Neither irradiation alone nor treatment with MPDC or conjugate were able to induce a change in cell viability (Figure 26), cytotoxicity (Figure 27) and caspase activity (Figure 28). Thus, MPDC alone as well as irradiation alone did not produce toxic effects. In combination with laser irradiation (10 J/cm^2), MPDC caused marked changes including decreased viability (p<0.01), increased cytotoxicity (p<0.01) and enhanced caspase activity (p<0.001). MPDC had a photodamaging ability as it only showed a light-dependent toxicity.
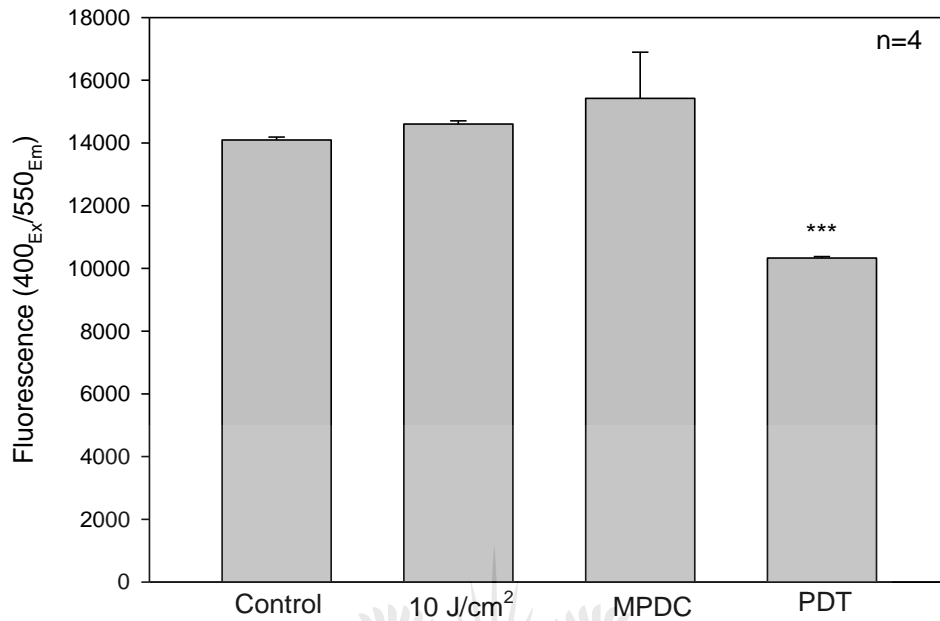
Figure 26: Apoptox-Glo Cell viability assay in MCF-7 cells using 400/550 ex/em filters. When compared to untreated control cells, the fluorescent signal of both laser-irradiated and MPDC-treated cells did not indicate any major change in cell viability. The irradiated conjugate exhibited a significant decrease in cell viability as ** (p<0.01).
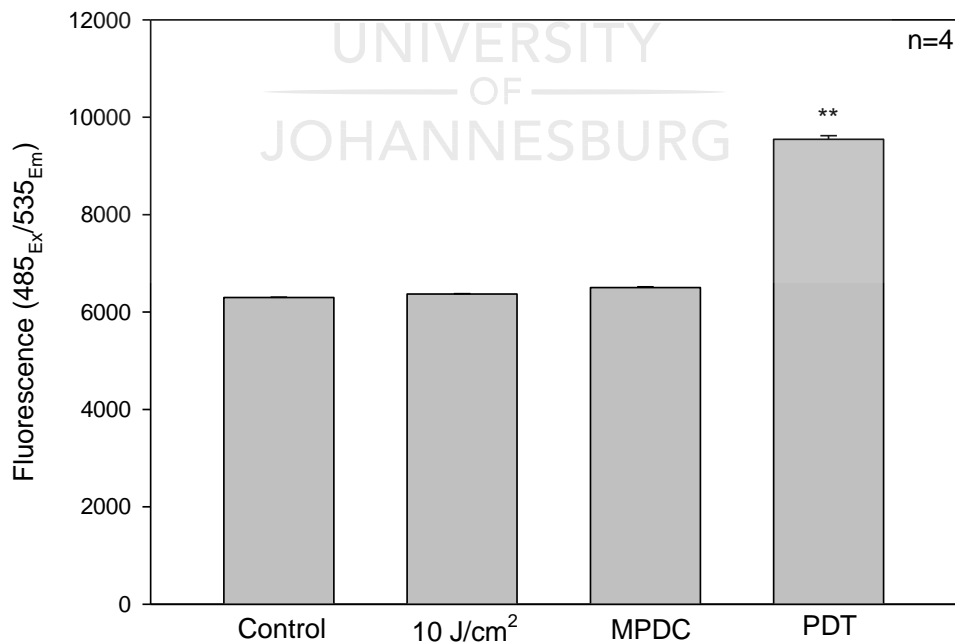
Figure 27: Apoptox-Glo Cytotoxicity assay in MCF-7 cells using 485/535 ex/em filters. When compared to untreated control cells, the fluorescent signal of both laser-irradiated and MPDC-treated cells did not present any major increased toxicity. The irradiated MPDC exhibited an increase in cytotoxicity, shown as ** (p<0.01).

Caspase 3/7 Assay
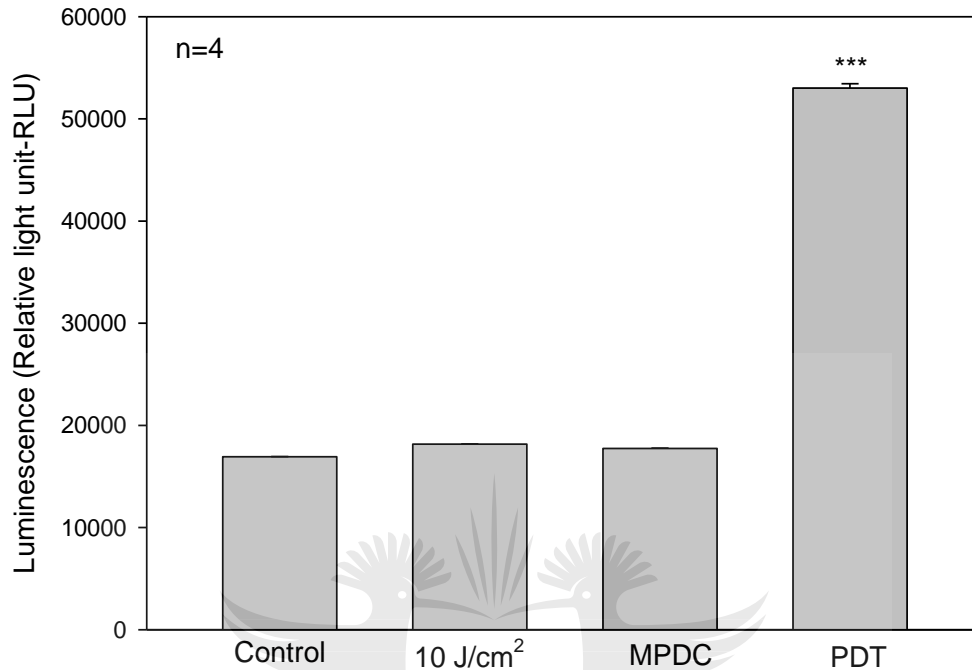
Figure 28: Apoptox-Glo Caspase luminescence assay in MCF-7 cells. When compared to untreated control cells, the luminescent signal of both laser-irradiated and MPDC-treated cells did not present any major increased caspase activity. The irradiated MPDC displayed a high luminescent signal, thus an enhanced caspase activity and is indicated as * ($p < 0.001$).**

4.4.4 Mitochondrial destabilization

Mitochondrial damage or destabilization was evaluated post-PDT in MCF-7 cells. The percentage of both polarized (black) and depolarized (grey) mitochondrial membrane potential in each treated cell group was determined and compared to the respective percentage of the untreated control cells (Figure 29). After 24 h of incubation with the JC-1 fluorometric stain, no change in mitochondrial membrane potential (polarized and depolarized cells) was detected when cells were treated with irradiation alone or MPDC alone. However, a change in both the polarized cell population and the depolarized cell population was noticeable with PDT-treated cells. The PDT-treated cells showed both an increase in the percentage of depolarized mitochondrial membrane and a decrease in the

percentage of polarized membranes (p<0.01). Thus, loss of mitochondrial membrane potential or damage was seen with light-activated MPDC.

Mitochondrial Membrane Potential
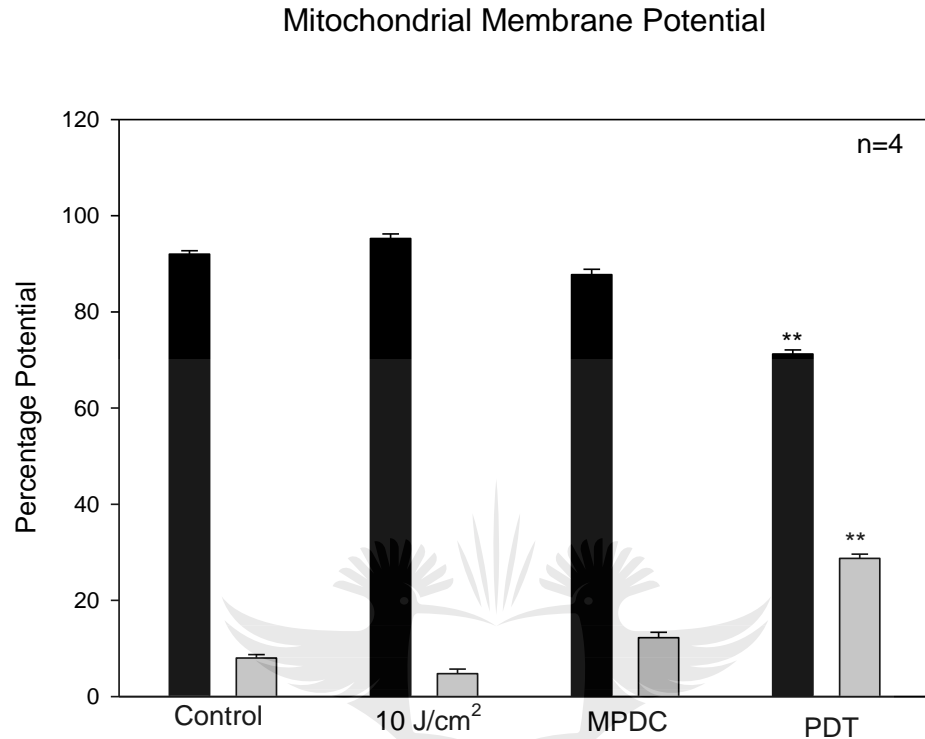
Figure 29: Evaluation of mitochondrial membrane potential using flow cytometric analysis of JC-1 fluorometric stain. Percentage of polarized (black) and depolarized (grey) mitochondrial membrane potential were determined and compared to the percentage of the corresponding mitochondrial membrane potential of untreated control cells. Only the PDT-treated cells showed a change in mitochondrial membrane potential ([**]p<0.01).

4.4.5 Cytochrome C

The level of cytochrome C was determined 24 h after the treatment. The release of cytochrome C from the mitochondria is a critical event in cell damage. An ELISA was performed to detect and compare the amount of release of cytochrome C in untreated and treated cells. The results revealed that in the absence of laser irradiation, MPDC is unable to trigger such a damaging event (Figure 30). Laser irradiation alone was also not enough to lead to an increase in cytochrome C. MPDC coupled with laser irradiation was able to initiate cell damage and lead to an augmented amount of cytochrome C (p<0.001).

Cytochrome C
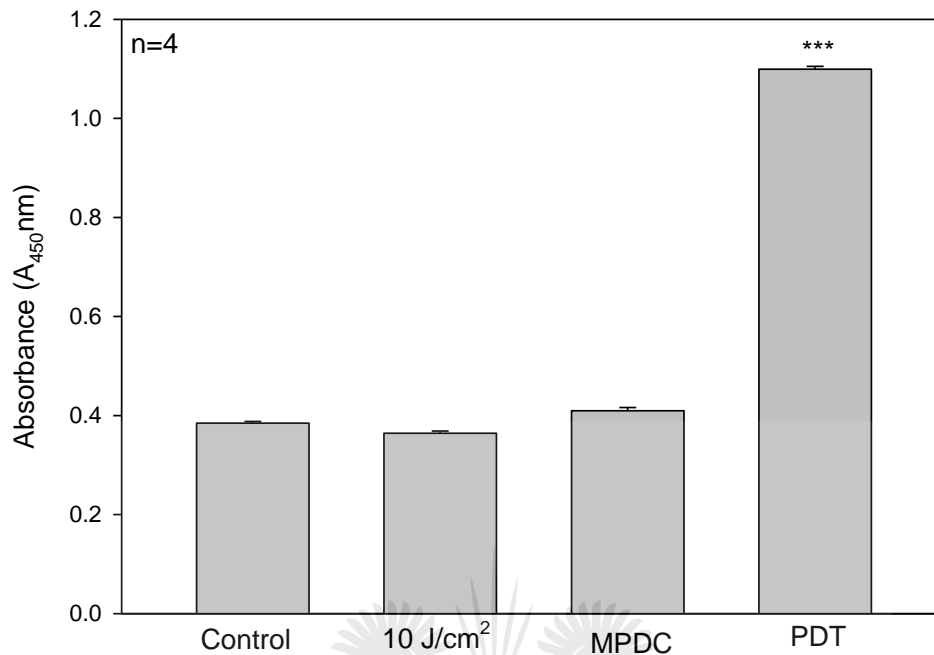
Figure 31: Estimation of cytochrome C levels in untreated and treated MCF-7 cells. Cells treated with laser alone or MPDC alone did not lead to an increased colorometric signal when compared to the untreated cells. PDT-treated cells showed a significant increase shown as *** (p<0.001) and evidence of undergoing cell damage.

4.4.6 Cell death detection

Another flow cytometric analysis using Annexin V-FITC and PI was performed to determine the foremost mode of cell death in MCF-7 cells following PDT. Twenty four hours after treatment with PDT, MCF-7 cells were stained and prepared for analysis. Additional controls were included in this experiment and consisted of MCF-7 cells treated with Actinimycin D and Hydrogen peroxide (H_2O_2) acting as apoptotic and necrotic controls, respectively. Different populations of cells were obtained: normal (negative for both Annexin V and PI), early apoptotic (positive for Annexin V and negative for PI), late apoptotic (positive for both Annexiv V and PI) and necrotic (positive for PI and made up of cells that were subjected to intensive damage).

When cells were treated with Actinomycin D or H_2O_2, a significant change ($p<0.05$, $p<0.01$ and $p<0.001$) was seen with all cell populations when compared to their respective population type of the untreated control cells. These treatments were able to induce cell death with apoptotic being more pronounced with Actinomycin D as expected (Table 12).

Table 12: Percentage of various cell populations after flow cytometric analysis. The lowest percentage of cell death (apoptotic and necrotic) and highest percentage of normal population were obtained with untreated cells. These apoptotic populations significantly increased (around 63%, accumulated percentage) in Actinomycin D-treated cells, and the highest percentage of necrotic population (42%) was seen with hydrogen peroxide (H_2O_2)-treated cells. Experiments were repeated four times (n=4) and significant differences are indicated as *($p<0.05$) and ***($p<0.001$) when compared to the respective population type of the untreated control cells.

Cell populations	Untreated cells	Actinomycin-D-treated cells	H_2O_2-treated cells
Normal	89 ±2.05	26±1.34***	9±2.52***
Early apoptotic	7 ±1.69	34±0.49***	16±2.62*
Late apoptotic	3 ±2.65	29±0.12***	33±1.55***
Necrotic	1±1.23	11±1.63*	42±1.02***

± represents standard error

Cells treated with laser irradiation alone or MPDC (conjugate) alone did not result in a significant change when compared to their respective population of untreated cells (Table 13). Only PDT-treated cells showed a significant change with all populations ($p<0.05$, $p<0.01$ and $p<0.001$), with the apoptotic population being the most prominent (59%, accumulated percentage).

4.4.7 Gene expression

The gene expression profile was assessed 3 h after treatment and by means of Real-time RT-PCR to detect the regulation of 84 genes, all involved in cell death. An additional 12 genes were integrated and consisted of 5 housekeeping genes to standardize the genes of interest, a gDNA control, positive PCR control genes (in triplicate) and reverse transcriptase

control genes (in triplicate). Results obtained from the reverse transcriptase control was not considered as the SABioscience RT^2 First kit was not used when performing cDNA synthesis. Some of these controls are not in the results panel of expressed genes. Nucleic acid purity was done through the course of the experiment and values were between 1.84 and 1.93.

Table 13: Percentage of various cell populations after flow cytometric analysis. The lowest percentage of cell death (apoptotic and necrotic) were obtained with untreated and irradiated controls. These apoptotic populations significantly increased (around 65%) in MPDC- and PDT-treated cells. Experiments were repeated four times (n=4) and significant differences are shown as *(p<0.05), **(p<0.01) and ***(p<0.001***) when compared to the respective population type of the untreated control cells.

Cell populations	Untreated cells	Irradiated cells	MPDC-treated cells	PDT-treated cells
Normal	89 ±2.05	91±1.11	86±0.32	32±1.06***
Early apoptotic	7 ±1.69	6±0.29	9±2.12	29±1.56**
Late apoptotic	3 ±2.65	2±2.45	4±3.05	30±1.74**
Necrotic	1±1.23	1±2.15	1±1.84	9±2.33*

± represents standard error

Gene expression profiles of MPDC alone and PDT on MCF-7 cells

MCF-7 cells were treated with 0.3 µM MPDC alone and incubated for 3 h before RNA isolation was performed for real-time RT-PCR. Neither of the up-regulated or down-regulated genes were significantly expressed (Figure 31).The gene expression analysis of PDT-treated MCF-7 cells was performed after RNA was isolated and cDNA synthesised. Results showed that BAX (p<0.05), BCL2 (p<0.05), CASP2 (p<0.001) and ULK-1 (p<0.05) were significantly up-regulated when compared to the untreated control cells. None of the down-regulated genes was found to be significant (Figure 32).
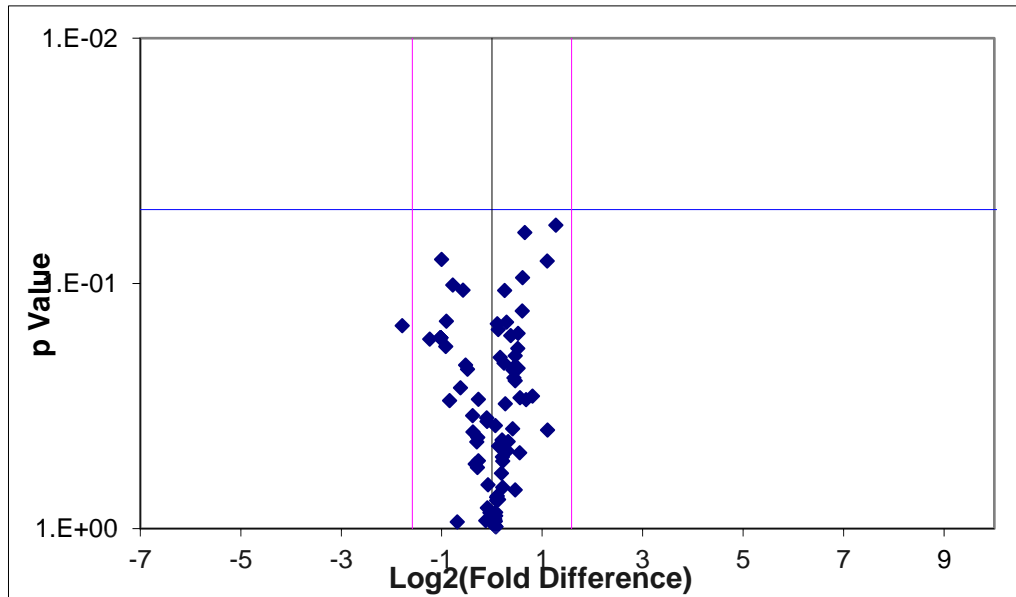
Figure 31: Gene expression profile of MPDC-treated cells was analyzed using the Human Cell Death Pathway Finder Profiler™ PCR Array System. Treatment did not have an effect on the gene expression and none of the genes were significantly regulated as represented in the volcano plot. In the volcano plot, the horizontal line designates the target threshold (p=0.05) and vertical lines, the fold change (central) and target fold change threshold (peripheral) in gene expression.
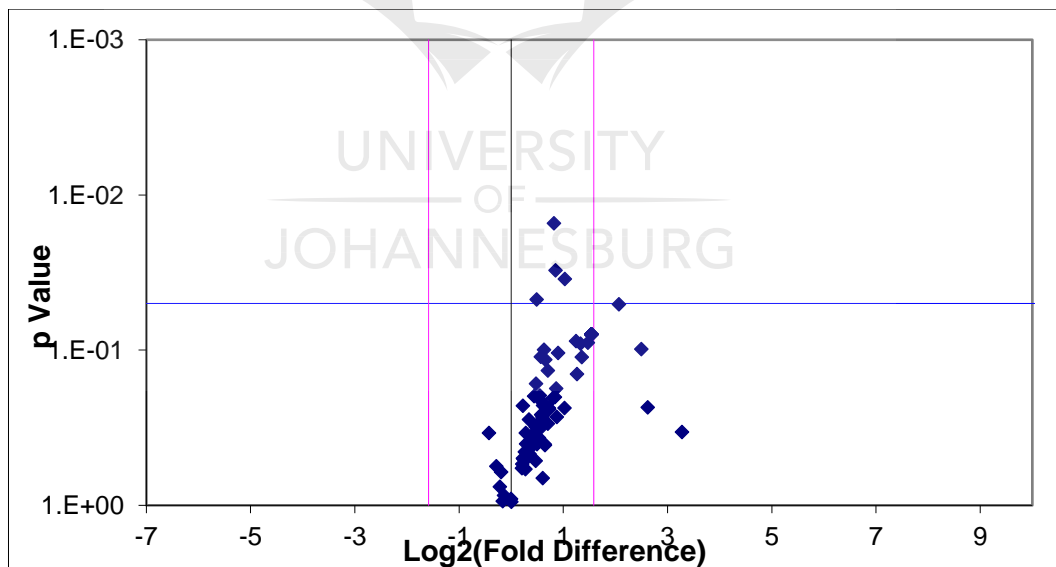
Figure 32: Gene expression profiles of PDT-treated MCF-7 cells with 0.3 µM MPDC and 10 J/cm² was analyzed using the Human Cell Death Pathway Finder Profiler™ PCR Array System. MPDC-mediated PDT-induced changes in gene expression and BAX, BCL-2, CASP-2 and ULK-1 genes were significantly up-regulated as represented in the volcano plot. In the volcano plot, the horizontal line designates the target threshold (p=0.05) and vertical lines, the fold change (central) and target fold change threshold (peripheral) in gene expression.

CHAPTER FIVE

DISCUSSION AND CONCLUSION

AgNPs have characteristics and have been explored in ink-jet printing, cosmetics, domestic appliances and fighting microbial contamination (Hussain *et al.*, 2006; El-Chaghaby and Ahmad, 2011). AgNPs are good antibacterial agents with multiple functionalities, which have made them potential agents for biomedical applications. These nanomaterials possess antitumor activity and can damage both neurons and undifferentiated cells (Hussain *et al.*, 2006; Haghsh *et al.*, 2012).

In preliminary studies, the effects of AgNPs and AuNPs together with low intensity laser irradiation were tested in both breast and lung cancer cell lines (MCF-7 and A549, respectively). Irradiated AgNPs caused decreased cell viability and proliferation, increased cytotoxicity and induced cell death, and these effects were more pronounced in MCF-7 cells than in A549 cells. Moreover, observed antitumor activity of irradiated AgNPs were far greater than those observed with the irradiated AuNPs. It was suggested that an alteration on the structure of AuNPs should be made in order to improve its photodynamic effects. Size reduction and conjugation were identified as possibilities to be explored for the suggested improvement, and in the case of conjugation the role of AuNPs should be determined prior to evaluation of photodynamic capacity of the conjugates (Mfouo-Tynga *et al.*, 2014; Hussein *et al.*, 2015).

Subsequently, this present study started with the determination of the roles and comparison of photodynamic effects of two gold nanomaterials, namely AuNPs and a fourth generation AuDENP; both of spherical shape with a diameter of less than 10 nm. Many chemotherapeutic agents are now being conjugated (Multiple particle delivery complex, MPDC) in order to minimize the shortcomings of the free-drug counterparts and to enhance their

therapeutic capabilities (Cho *et al.*, 2008, Li, 2002). Polymer-based drug carriers are synthesized via dissimilar routes and these molecular carriers include polymeric NPs, micelles or dendrimers. Dendrimers are hyper-branched macromolecules and used mostly as delivery systems in targeted therapies. They are easily functionalized and have a high ligand density and good biodistribution (Cho *et al.*, 2008). It is well established that many NPs have photothermal and non-photothermal toxicity (Lee *et al.*, 2014; Jelveh and Chithrani, 2011; Selim and Hendi, 2012; Qu *et al.*, 2012), yet in the present case, no substantial change in temperature was noted during irradiation, therefore invalidating the possibility of photothermal toxicity of nanomaterials.

The photodynamic effects of AuNPs in MCF-7 cells on cell viability, cytotoxicity and proliferation were determined. Here, AuNPs (1 and 3 mM) were able to cause cell damage and successfully led to a decrease in viability (Table 8) and proliferation (Table 9), and an increase in cytotoxicity (Table 10) after light activation at 0, 5, 10 and 15 J/cm^2 using a 536 nm diode laser. However , a major downfall was seen and seemed to disqualify AuNPs as a potential agent to be used in photodynamic reactions or as a PS. Major cell damage was noted at both concentrations and in the absence of light (0 J/cm^2) where both viability and proliferation significantly decreased ($p<0.05$). A meaningful increase in cytotoxicity was also noted ($p<0.05$) when cells were treated with 3 mM AuNPs in the absence of light. Other cell studies using AuNPs had shown a correlation between the presence of AuNPs and induction of cell organelle damage, ROS production and subsequent cell death. It was also recently established that even when used alone, AuNPs have the potential to cause cell damage (Schlinkert *et al.*, 2015; Khanna *et al.*, 2015; Mkandawire *et al.*, 2015).

This disqualifies AuNPs as an ideal PS for PDT as good PSs have minimal dark toxicity. As a consequence AuDENPs were considered, and in this improved form (AuDENPs) the nanomaterials did not induce significant dark

toxicity when compared to the untreated control (0 mM AuDENPs and 0 J/cm^2). When no significant change in cell viability, proliferation and cytotoxicity were noted. However, cellular changes were observed and appeared to be the result of both AuDENPs and laser irradiation at a fluence of 10 J/cm^2 or higher.

Comparison between AuNPs and AuDENPs showed that the latter was most suitable for conjugation with the sulfonated ZnPcS$_{mix}$ and would be used as delivery agents rather than therapeutic agents. In other studies involving similar compounds in conjugates that yielded good therapeutic effects, AuDENPs were used as delivery agents (Goodman *et al*., 2004; Murphy *et al*., 2008). Another investigative study with similar AuNPs conjugated to various sulfonated mPCs and looking at the photophysical properties, confirmed that conjugation did not negatively affect the PS or lower fluorescence quantum yield with similar fluorescence lifetimes compared to their free-mPC counterparts (Nombona *et al*., 2011). It was proved that nanomaterials have the ability to enter various cell types and their functionalization renders them able to distinguish between cell types (Huefner *et al*., 2014).

Currently, third generation PSs for PDT are being assembled by combining second generation PSs to specific molecules such as antibodies and liposomes. The aim is to increase the therapeutic outcome by adding to the already improved second generation additional beneficial features from the combined molecules. Phthalocyanines are now established as an effective PS *in vitro*, and have been evaluated and show good therapeutic effects in early stages of clinical trials (Borgetti-Jeffreys *et al*., 2007; Baron *et al*., 2010; Kinsella *et al*., 2011). The emergence of nano-oncology has enhanced the specificity to neoplastic tissues. Recent pre-clinical and clinical advancements have demonstrated that NPs increase the passive accumulation of anticancer agents in tumours, and when administrated systemically there is enhanced drug-delivery to the tumour. Clearly, NPs will

continue to have an impact in oncology and attract more attention (Rink *et al.*, 2013).

There are few studies reporting on the use of spherical AuNPs in combination with mPCs for cancer therapy. In this present study, AuDENPs were combined to ZnPcS$_{mix}$. The UV-Vis spectroscopy results showed that MPDC had one absorption peak at 674 nm, which is more closely related to the absorption of ZnPcS$_{mix}$ (676 nm) than that of AuDENPs (524 nm). This has therapeutic importance as MPDC absorb light in the NIR region of the spectrum, the therapeutic window. Combination preserves the photodynamic capability of ZnPcS$_{mix}$ and supports about the role of AuDENPs as delivery agents rather than therapeutic agents in a light mediated therapy. MPDC has similar promising optical properties, which it undoubtedly inherited from ZnPcS$_{mix}$.

In order to confirm the chemical conjugation, FTIR spectroscopy was performed to identify any bond-shift. It transpired that AuDENPs presented with two distinct peaks and ZnPcS$_{mix}$ with five main peaks. MPDC had several peaks including at new ones (new functional groups) and bond-shifted peaks. One at about 3126.12, which was comparable to the position of the ZnPcS$_{mix}$ peak at 3529.39 or the 3341.86 peak of AuDENPs. Another peak was seen at around 1636.66, comparable to the position of the 1638.50 peak of ZnPcS$_{mix}$ or the peak at 1640.23. A third peak was seen at 1400.42, and was comparable to the 1400.46 peak of ZnPcS$_{mix}$. A final peak was seen at 501.19, and was comparable to the peak at 638.36 of ZnPcS$_{mix}$. It could be presumed that the resulting compounds are made of combined AuDENPs and ZnPcS$_{mix}$.

Subsequent to that, the size and the shape of MPDC was determined. MPDC or conjugated was of a spherical shape with an average size not exceeding 5 nm in diameter. It has been shown that fourth generation

dendrimers usually have a diameter around 5 nm (Oliveira *et al.*, 2010; Divsar *et al.*, 2009; Kim *et al.*, 2004).

Zeta potential measurements revealed that MPDC was positively charged with a zeta potential and 95% MPDC had a diameter less than 5 nm. This showed stability and indicated that hybrid compounds have amino terminals accessible for protonation. Similar findings were presented by Shi and collaborators (2006), when they examined the stability of various generations of gold dendrimeric compounds with the same ratio of terminal nitrogen ligands and gold atoms. They found that those hybrid molecules provided new platforms for interaction with biological ligands and were stable with zeta potential values between +26 to +41 mV, and were found to be useful for biosensing and targeted cancer therapy (Shi *et al.*, 2006).

Several concentrations of MPDC or conjugated made up of AuDENPs-ZnPcS$_{mix}$ were used in a second dose response study, which was aimed at determining the concentration of the conjugate to be used for further cell assessments with a laser fluence of 10 J/cm^2. At this laser fluence, significant cytodamage was obtained when compared to 5 J/cm^2 in the first dose response. In a previous study, it was demonstrated that MCF-7 cells were very sensitive to ZnPcS$_{mix}$ and this PS was able to induce cytotoxic effects in MCF-7 cells at a much lower concentration when compared to A549 lung cancer cells (Manoto *et al.*, 2012; Mfouo-Tynga *et al.*, 2013). AgNPs had more severe effects on MCF-7 cells than on A549 cells (El-Hussein *et al.*, 2014).

With concentrations of 1 mM and 3 mM, irradiated AuDENPs were not able to induce a decrease in viability around the 50% mark. At a concentration of 0.5 µM, laser activated ZnPcS$_{mix}$ led to a cell viability decrease of around 50%. Comparatively, at a concentration of 0.3 µM laser activated MPDC led to approximately 50% cell viability, which was 1.6 times less than that of ZnPcS$_{mix}$ and more than 10,000 less than that of AuDENPs. Combination

provided a compound that yields more with much less. This combination improved the efficiency of cancer treatment *in vitro*. A study conducted by Cho *et al.* (2008) reported that when bound to ligands or antibodies, cancer nanotherapeutic agents, which had specific characteristic features such as enhanced permeability and retention effects, were able to overcome the limitations seen with conventional treatments and improve therapeutic outcomes by increasing the drugs solubility, biodistribution, targeting, therapeutic indices and reducing drug resistance effect.

Before the cell damage sub-study was performed, fluorescent microscopy was done to determine the subcellular localization of MPDC in MCF-7 cells. Subcellular localization of any PS has critical importance for the subsequent induction of cytodamage. Many agents used in photodynamic reactions for cancer therapy have been reported to localize in the plasma membrane, mitochondria, lysosomes, ER and Golgi apparatus (Calzavara-Pinto *et al.*, 2007). Most PSs, including $ZnPcS_{mix}$, localized in the mitochondria and lysosomes and not in the nuclear regions. For this reason, MPDC in this study was stained with mitotracker, lysotracker and DAPI to determine whether it localizes primarily in mitochondria, lysosomes and or in nuclei. Fluorescent analysis revealed that both mitochondria and lysosomes were sites of subcellular localization prior to laser irradiation. This finding aligned with previous observations made when ZnPC compounds were found to accumulate in these two organelles and not in nuclei (Vitar *et al.*, 2008; Mfouo-Tynga *et al.*, 2013; El-Hussein *et al.*, 2012). Thus, the $ZnPcS_{mix}$ component of MPDC seemed to dictate its subcellular localization once taken up by MCF-7 cells.

Mitochondria, often referred to as the power house of cells, provides the necessary energy for cellular metabolic activities. Thus, PSs that localize in these specific organelles have the tendency to damage and stimulate apoptotic-like events in treated cells. Such PSs were found to be amphiphilic compounds with cationic moieties and to localize both in mitochondria and

lysosomes (Karioti and Bilia, 2010; Repnik and Turk, 2010; Kessel and Luo, 2001). Berg and colleagues (1991) demonstrated the association between porphyrin-derived compounds that localize in lysosomes and the induction of cell damage.

Inverted light microscopy analysis was performed following treatment with both MPDC and laser irradiation in MCF-7 cells. Only the laser-activated MPDC in the PDT-treated cells showed a significant change in cell morphology as compared to the untreated control cells. Some cells were detached from the culture surface and appeared as free-floating structures, indication of cell damage and confirming the ability of MPDC to yield cytodamaging effects in cancer cells. Lee and co-workers (2009) confirmed cell morphological changes when conjugated AuNPs were used in lung cancer targeted therapy. Another similar analysis was conducted and indicated that using AuNPs-targeted therapy in liver and lung cancer led to morphological change and the appearance of apoptotic like characteristic morphological features (Singh *et al.*, 2014).

The Apoptox-Glo assay was performed to determine cell viability, cytotoxicity and caspase activity after treatment. It was revealed that light-activated MPDC prompted decreased cell viability and increased toxicity and caspase activity in MCF-7 cells. This showed that MPDC in its active form was able to induce significant damaging effects. Other studies have reported similar findings using various conjugated AuNPs in various cancer cell lines. Decreased cell viability of breast, bladder and prostate cancer cells was seen after irradiation of drug-coated with AuNPs for fibroblast growth factor-1 targeted cancer therapy (Szlachcic *et al.*, 2012). Both 5 and 10 nm AuNPs compounds were endocytosed by A549 lung cancer cells and led to the inhibition of cell growth and increased cytotoxicity. These effects seemed to disappear when 20 and 40 nm sized compounds were utilized (Liu *et al.*, 2014). In another targeted therapy, decreased viability, increased anti-proliferative and pro-apoptotic activity (such as increase caspase

activity) were identified as the induced tumour suppressor response in breast cancer cells (Selcuklu *et al*., 2012).

Results from this study showed that mitochondrial integrity was not maintained after MPDC-mediated PDT in MCF-7 cells, as both a change in the percentage of polarized and depolarized mitochondrial membrane potential was detected and indicated mitochondrial damage. A number of studies have reported that treatments using drugs, which localize in mitochondria, damage these cellular organelles and lead to cell death through apoptotic pathways. Wen and co-workers (2013) reported that cancer treatment that targeted mitochondria led to dysfunctioning mitochondria with a shift in energy generation from oxidative phosphorylation to glycolysis, and noted high levels of ROS in various cell lines. Treatment provoked a change in mitochondrial membrane potential, ROS levels and intracellular levels of ATP (Le bras *et al*., 2006). Pancratistin, an anti-cancer agent, triggered a decrease in mitochonrial membrane potential and led to the initiation of apoptosis in colorectal carcinoma cell lines (Griffin *et al*., 2011).

Nanoparticles containing therapeutic agents led to depolarization of the mitochondrial membrane potential, translocation of AIF and activation of caspase activity (Eloy *et al*., 2012). Rhodamine[123] accumulated in mitochondria and this accumulation lead to the disruption of mitochondrial membrane potential in kidney and breast cancer cells (Summerhayes *et al*., 1982; Bernal *et al*., 1982). A similar disruption in mitochondrial membrane potential was seen with treatments using compounds such as RH1, edelfosine, doxobicin and curcumin as anti-cancer agents (Park *et al*., 2011; Mollinedo *et al*., 2011; Kuznetsov *et al*., 2011; Gogada *et al*., 2011a).

Mitochondrial damage has been linked to the release of cytochrome C. In this study, we used ELISA to determine the level of cytochrome C. It was found that the release of cytochrome C significantly increased after

treatment with MPDC and laser irradiation in the PDT-treated cells. This concurs with work done by Heiligtag and associates (2002) when cerulenin, an anti-cancer agent, was able to damage mitochondria, which led to the release of cytochrome C and the induction of apoptosis. The induced release of cytochrome C is an important event for the activation of apoptotic cascades and caspase-dependent cell death (Gogada *et al.*, 2011b; Valero *et al.*, 2011). The release of cytochrome C from the mitochondria was detected and seemed to be critical for the initiation of cell death (Robertson *et al.*, 2002).

Mitochondrial damage and subsequent events to the induction of cell death in an apoptotic manner. Annexin-V FITC and PI flow cytometric analysis was conducted and confirmed apoptosis as the main induced cell death response after MPDC-mediated PDT in MCF-7 cells. The induction of apoptosis after mitochondrial damage is of no surprise as many previous studies confirmed the induction of apoptosis after treating cells with various mitochondrial-damaging and anti-cancer agents in PDT (Mroz *et al.*, 2011). Photodynamic therapy treatment that causes mitochondrial damage promotes apoptosis through the release of cytochrome C, AIF and other apoptogenic proteins such as caspases (Ribeiro *et al.*, 2004). Hypericin-mediated PDT that led to the initiation of apoptosis was demonstrated in a human hepatocellular liver carcinoma cell line (HepG2) after analyzing Annexin V- FITC/PI-stained cells using flow cytometry (Barathan *et al.*, 2013). A large number of morphological changes including cell shrinkage, chromatin condensation, and nuclear fragmentation were detected and identified as typical apoptotic features in three cell lines (HeLa, HaCaT and MCF-7) when using cationic conjugated compounds containing ZnPC in PDT. It was concluded that those cells had undergone apoptosis, which was detected 3 h after PDT (Acedo *et al.*, 2014).

Investigation into the expression of genes involved in cell death pathways was done 3 h after PDT as a final assessment of the efficacy of MPDC and

to determine the genes which were primarily affected. It transpired that out of the 84 genes examined, only 4 genes (BAX, BCL-2, CASP-2 and ULK-1) were significantly up-regulated in the PDT treated cells. Bax is an apoptosis regulator protein and member of the Bcl-2 family. It was among the first genes to be associated with pro-apoptotic activity. Its activation activity has been linked to the loss in mitochondrial membrane potential and the release of cytochrome C. Down-regulation or mutation of this protein leads to the suppression of apoptosis (Hassan *et al.*, 2012; Oltvai *et al.*, 1993). It exits as a cytosolic protein in normal cells, but upon induction of apoptotic signals it undergoes a conformational change and become associated with organelle membranes, in particular mitochondrial membranes (Pierrat *et al.*, 2001). Curcumin-induced upregulation of BAX and cancer cell death through the mitochondrial-mediated apoptotic pathway (Wen *et al.*, 20103).

BCL-2 is another Bcl-2 family member protein and determines the commitment of cells to apoptosis (Czabotar *et al.*, 2014). Bcl-2 (B-cell lymphoma 2) regulates apoptosis by inducing or inhibiting apoptosis but it is principally considered as an anti-apoptotic effector and classified as an oncogene. In response to mitochondrial damage, release of cytochrome C, caspase activation and additional apoptotic events, BCL-2 is overexpressed to control these activities (MacManus and Linnick, 1997).

Caspase 2 (CASP-2) is an apoptosis-related cysteine peptidase and is involved in the initiation of apoptosis by participating in the formation of the CARD domain, RIP-associated Ich-1/Ced-3-homologue protein with a death domain (RAIDD), apoptosis repressor with caspase recruitment domain (ARC), and death effector filament-forming Ced-4-like apoptosis protein (DEFCAP). Nuclear damage is critically important for the expression of caspase-2 (Zhivotovsky and Orrenius, 2005). Additionally, caspase-2 can interact with the p53-induced protein with a death domain to form the PIPPosome, which is an activation platform for other proteases (Manzl *et al.*, 2009; Tinel and Tschopp, 2004). Robertson and colleagues (2002)

found that caspase-2 additionally induces genetic damage and the induction of mitochondrial apoptotic pathway.

The fourth gene, ULK-1, that was upregulated is associated with autophagy, which is both a survival and cell death mechanism. This proved that MPDC mediated-PDT cell death through several pathways as shown by ULK-1 expression, also known as the autophagy initiation kinase Unc-51-like kinase (ULK1)/ATG1. ULK-1 is an autophagy initiator protein which is indispensable for autophagic complex formation (Alers *et al.*, 2011). This complex consists of ULK1, ATG13 and ATG17 and leads to the formation of autophagosomes in the absence of mTOR signal (Mizushima, 2010; Jung *et al.*, 2009). Autophagy has a cell death role and it was demonstrated that Ulk-1 also plays a role in ATP depletion and death in the presence of both PARP1 activity and H_2O_2 (vigorous damage). The same study showed autophagy pro-death activity of Ulk-1 in response to ROS generation (Joshi *et al.*, 2015). The schematic representation of induced gene expression and cell death events of this present study is presented in figure 33.

In conclusion, the search for improved and ideal PSs is indisputably encouraged for more effective cancer therapy. Firstly, the AuNPs successfully accumulated in MCF-7 cells, but yielded both light-dependent and light-independent (in the dark or without irradiation) cytotoxicity. Secondly, AuDENPs only offered the desired light-dependent cell destruction and was consequently utilized in combination with ZnPcS$_{mix}$ for potential improved efficiency of PDT. Finally, the combination yielded a successful and stable hybrid agent with potent photodynamic abilities. The resulted MPDC localized in both mitochondria and lysosomes, and was able to induce subsequent cytodamaging effects. MCF-7 cells became more sensitive to the treatment after combination and the cellular damage included increased cytotoxicity, increased caspase activity, promotion of apoptotic-like events and upregulation of genes involved in apoptotic

pathways. Combination improved the therapeutic outcomes by achieving better targeted therapy or better delivery to cancer cells, and increased cancer cell sensitivity to the newly combined anti-cancer agent.
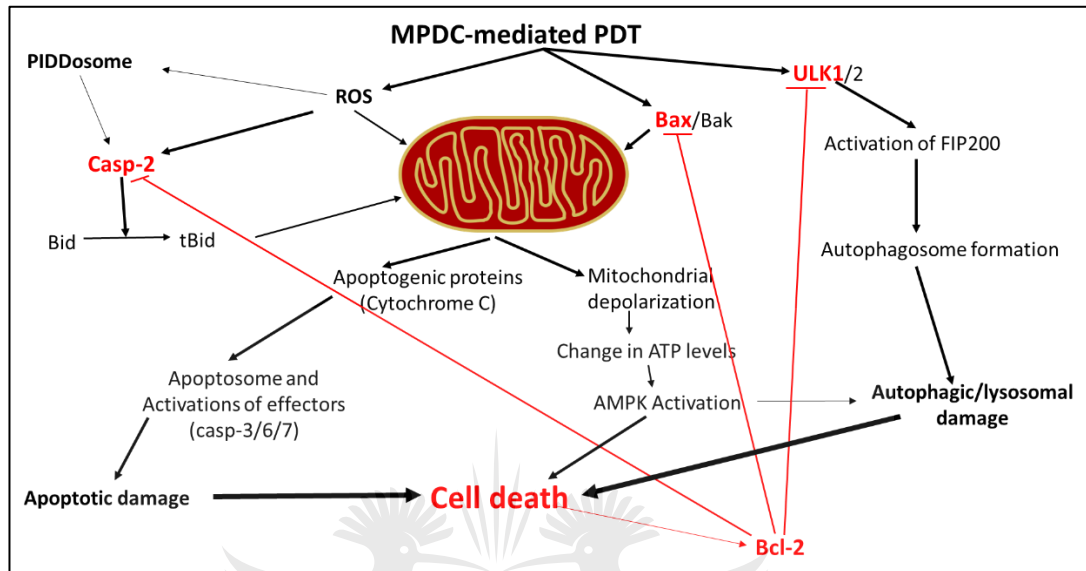
Figure 33: The primary response of MPDC-mediated PDT on the expression of genes involved in cell death pathways was the up-regulation of Ulk-1, Bax, Casp-2 and Bcl-2 genes. The Ulk-1 protein protonates and activates the FIP200. ULK is part of a protein complex containing Atg13, Atg17 and FIP200 (autophagosome), which drives the subsequent cellular damage and death. The Bax protein directly affects the mitochondria while the Cas-2 protein is activated by reactive oxygen species (ROS) and then Casp-2 transforms a mitochondrial damaging protein into its truncated and activated form (tBid). The p53-induced death domain associated protein (PIDD) can also convert pro-Casp-2 into the active Casp-2. Apoptogenic proteins (such as Cytochrome C) released from mitochondria participate in the assemblage of the apoptosome, activation of other effectors (Casp-3/6/7) and cell death. Mitochondrial damage and depolarization induce change in cellular ATP levels, activation of the 5' adenosine monophosphate activated protein kinase (AMPK) and AMPK-induced cell death. This cell death response stimulates Bcl-2 protein to prevent further cell damage.

REFERENCES

Abrahamse H., Kresfelder T., Horne T., Cronje M. and Nyokong T. (2006). Apoptotic inducing ability of a novel photosensitizing agent, Ge sulfophthalocyanine, on oesophageal and breast cancer cell lines. Proc. SPIE 6139, Optical Methods for Tumor Treatment and Detection: Mechanisms and Techniques in Photodynamic Therapy XV, 613904, March 06, 2006; David Kessel, San Jose, CA, January 21, 2006.

Acedo P., Stockert J.C., Cañete M. and Villanueva A. (2014). Two combined photosensitizers: a goal for more effective photodynamic therapy of cancer. *Cell Death Discovery* **5(3)**: e1122.

Adeli M., Soleyman R., Beiranvand Z. and Madani F. (2013). Carbon nanotubes in cancer therapy: a more precise look at the role of carbon nanotube-polymer interactions. *Chemical Society Reviews* **42(12)**:5231-5256.

Agostinis P., Berg K., Cengel K.A., Foster T.H., Girotti A.W., Gollnick S.O., Hahn S.M., Hamblin M.R., Juzeniene A., Kessel D., Korbelik M., Moan J., Mroz P., Nowis D., Piette J., Wilson B.C. and Golab J. (2011). Photodynamic Therapy of Cancer: An Update. *CA: A Cancer Journal for Clinicians* **61**: 250-281.

Albain K.S., Barlow W.E., Ravdin P.M., et al. (2009). Adjuvant chemotherapy and timing of tamoxifen in postmenopausal patients with endocrine-responsive, node-positive breast cancer: A phase 3, open-label, randomised controlled trial. *Lancet* **374**:2055–2063.

Allen C.M., Sharman W.M. and van Lier J.E. (2001). Current status of phthalocyanines in the photodynamic therapy of cancer. *Journal of Porphyrins Phthalocyanines* **5**:161-169.

Allen N.E., Beral V., Casabonne D., et al. (2009). Moderate alcohol intake and cancer incidence in women. *Journal of the National Cancer Institute* **101(5)**: 296–305.

Allison R.R., Downie G.H., Cuenca R., Hu X.H., Childs C.J. and Sibata C.H. (2004). Photosensitizers in clinical PDT. *Photodiagnosis and Photodynamic Therapy* **1**:27–42.

America Cancer Society (2011). Cancer in Africa. Atlanta: American Cancer Society; 2011. http://www.cancer.org. Retrieved 2013-10-04.

American Cancer Society (2014). Cancer Facts & Figures 2014. Atlanta: American Cancer Society; 2014. http://www.cancer.org. Retrieved 2015-09-26.

American Cancer Society (2014). Evolution of cancer treatments: Surgery. http://www.cancer.org/cancer/cancerbasics/thehistoryofcancer/the-history-of-cancer-cancer-treatment-surgery. Retrieved 2015-10-12.

American Cancer society (2014). What is Cancer? http://www.cancer.org/cancer/cancerbasics/what-is-cancer. Retrieved 2015-02-23.

American Society of Clinical Oncology, ASCO, (2015). Stages of Cancer. http://www.cancer.net/navigating-cancer-care/diagnosing-cancer/stages-cancer. Retrieved 2015-02-26.

Annam Pharma, (2013). Technology: Dendrimers. http://www.annampharma.com/dendrimers.html, Retrieved 2015-09-21.

Arwert E.N, Hoste E. and Watt F.W. (2012). Epithelial stem cells, wound healing and cancer. *Nature Reviews Cancer* **12(3)**:170-180.

Aslan B., Ozpolat B., Sood A.K. and Lopez-Berestein G. (2013). Nanotechnology in cancer therapy. *Journal of Drug Targeting* **21(10)**: 904–913.

Balasubramanian S.K., Jittiwat J., Manikandan J., Ong C.N., Yu L.E. and Ong W.Y. (2010). Biodistribution of gold nanoparticles and gene expression changes in the liver and spleen after intravenous administration in rats. *Biomaterials* **31**:2034–2042.

Banerjee R. (2001). Liposomes: applications in medicine. *Journal of Biomaterials Applications* **16**:3-21.

Bangham A.D., Standish M.M. and Watkins J.C. (1965). Diffusion of univalent ions across lamellae of swollen phospholipids. *Journal of Molecular Biology* **13**:238–252.

Barathan M., Mariappan V., Shankar E.M., Abdullah B.J.J., Goh K.L. and Vadivelu J. (2013). Hypericin-photodynamic therapy leads to interleukin-6 secretion by HepG2 cells and their apoptosis via recruitment of BH3 interacting-domain death agonist and caspases. *Cell Death and Disease* **4**:e697; doi: 10.1038.

Barker A.D., Sigman C.C., Kelloff G.J., et al. (2009) I-SPY 2: An adaptive breast cancer trial design in the setting of neoadjuvant chemotherapy. *Clinical Pharmacology and Therapeutics* **86**:97–100.

Baron E.D., Malbasa C.L., Santo-Domingo D., Fu P., Miller J.D., Hanneman K.K., Hsia A.H., Oleinick N.L., Colussi V.C. and Cooper K.D. (2010). Silicon phthalocyanine (Pc 4) photodynamic therapy is a safe modality for cutaneous neoplasms: results of a phase 1 clinical trial. *Lasers in Surgery and Medicine* **42(10):**728-735.

Barrett P.A.; Dent C.E. and Linstead R.P. (1934). Phthalocyanines. Part VII. Phthalocyanine as a co-ordinating group. A general investigation of the metallic derivatives. *Journal of the Chemical Society* **179**:1718-1736.

Bednarski M., Dudek M., Knutelska J., Nowiński L., Sapa J., Zygmunt M., Nowak G., Luty-Błocho M., Wojnicki M., Fitzner K. and Tęsiorowski M. (2015). The influence of the route of administration of gold nanoparticles on their tissue distribution and basic biochemical parameters: *In vivo* studies. *Pharmacological reports* **67(3)**:405-409.

Benn C.A. (2009) Breast cancer rise alarming, www.health24.com, Retrieved 2010-03-31.

Bentolila L.A., Ebenstein Y. and Weiss S. (2009). Quantum dots for *in vivo* small-animal imaging. *Journal of Nuclear Medicine* **50**:493-496.

Berg K., Madslien K., Bommer J.C., Oftebro R., Winkelman J.W. and Moan J. (1991). Light induced relocalization of sulfonated meso-tetraphenylporphines in NHIK 3025 cells and effects of dose fractionation. *Photochemistry and Photobiology* **53**:203-210.

Bernal S.D., Lampidis T.J., Summerhayes I.C. and Chen L.B. (1982). Rhodamine-123 selectively reduces clonal growth of carcinoma cells in vitro. *Science* **218**:1117–1119.

Birkenfeld A. and Kase N.G. (1994). Functional anatomy and physiology of the female breast. *Obstetrics and Gynecology Clinics of North America* **21(3)**:433-44.

Blumberg B.S. (1984). Hepatitis B virus and the control of hepatocellular carcinoma. *IARC Scientific Publications* **(63)**:243-261.

Bonnet F., Lewden C., May T., Heripret L., Jougla E., Bevilacqua S., Costagliola D., Salmon D., Chêne G. and Morlat P. (2014). Malignancy-related causes of death in human immunodeficiency virus-infected patients in the era of highly active antiretroviral therapy. *Cancer* **101**:317-324.

Borgatti-Jeffreys A., Hooser S.B., Miller M.A. and Lucroy M.D. (2007). Phase I clinical trial of the use of zinc phthalocyanine tetrasulfonate as a photosensitizer for photodynamic therapy in dogs. *American Journal of Veterinary Research* **68(4)**:399-404.

Brackett C. and Gollnick S. (2011). Photodynamic therapy enhancement of anti-tumour immunity. *Journal of Photochemistry and Photobiology B: Biology* **83(5)**:1063-1068.

Brada M., Pijls-Johannesma M. and De Ruysscher D. (2007). Proton therapy in clinical practice: Current clinical evidence. *Journal of Clinical Oncology* **25(8)**:965–970.

Brancaleon L. and Moseley H. (2002). Laser and non-laser light sources for photodynamic therapy. *Lasers in Medical Science* **17**:173–186.

British Broadcasting Corporation (2006). Weight link to breast cancer risk. www.news.bbc.co.uk/2/hi/health/5171838.stm. Retrieved 2015-03-10

Brown S.B, Brown E.A. and Walker I. (2004). The present and future role of photodynamic therapy in cancer treatment. *Lancet Oncology* **5(8)**:497-508.

Buzea C., Pacheco-Blandino I.I. and Robbie K. (2007). Nanomaterials and nanoparticles: Sources and toxicity. *Biointerphases* **2(4)**: MR17 - MR172

Byers R.J. and Hitchman E.R. (2011). Quantum dots brighten biological imaging. *Progress in Histochemistry and Cytochemistry* **45**: 201-237.

Caan B.J., Kwan M.L., Hartzell G., Castillo A., Slattery M.L., Sternfeld B. and Weltzien E. (2006). Post-diagnosis weight gain and breast cancer recurrence in women with early stage breast cancer. *Breast Cancer Research Treatment* **99(1)**: 47–57.

Cadenas E. and Davies K.J. (2000). Mitochondrial free radical generation, oxidative stress and aging. *Free Radical Biology and Medicine* **29**:222–230.

Cai W. and Chen X. (2007). Nanoplatforms for targeted molecular imaging in living subjects. *Small* **3**:1840–1854.

Cai W., Ting Gao T., Hong H. and Sun J. (2008). Applications of gold nanoparticles in cancer nanotechnology. *Nanotechnology, Science and Applications* **(1)**: doi:10.2147/NSA.S3788.

Calzavara-Pinton P.G, Venturini M. and Sala R. (2007) Photodynamic therapy: update 2006. Part 1. Photochemistry and Photobiology. *Journal of the European Academy of Dermatology and Venereology* **21**: 293-302

Campidelli S., Ballesteros B., Filoramo A., Diaz D., de la Torre G., Torres T., Rahman G.M.A., Aminur E.C., Kiessling D., Werner F., Sgobba V., Guldi D.M., Cioffi C., Prato M., Bourgoin J.P. (2008). Facile decoration of functionalized single-wall carbon nanotubes with phthalocyanines. *Journal of the American Chemical Society* **130**:11503-11509.

Cancer Institute NSW (2014). What are the different stages of cancer? http://www.cancerinstitute.org.au. Retrieved 2015-02-25.

Cancer Research UK (2014). Worldwide Cancer. Cancer Statistics. http://publications.cancerresearchuk.org. Retrieved 2015-02-26.

Casaluce F., Sgambato A., Rossi A. and Mulshine J.L. (2012). The US FDA has approved Abraxane for the treatment of non-small-cell lung cancer. Aurora: a new light for targeted therapy in small-cell lung cancer. *Lung Cancer* **1**:251–254.

Castano A.P., Demidova T.N. and Hamblin M.R. (2004). Mechanisms in Photodynamic Therapy: Part One – Photosensitizers, Photochemistry and Cellular Localization. *Photodiagnosis & Photodynamic Therapy* **1(4)**: 279-293.

Cavalier-Smith T. (1987). The origin of eukaryotic and archaebacterial cells. *Annals of New York Academy of Sciences* **503**: 17–54.

Center for Responsible Nanotechnology (2002). What is Nanotechnology? http://www.crnano.org/whatis.htm, Retrieved 2015-03-02.

Centre for Disease Control and Prevention (2015). The Global Burden of Cancer. http://www.cdc.gov/cancer/international/burden.htm. Retrieved 2015-11-03.

Chaidogiannos G., Petraki F., Glezos N., Kennou S. and Nešpůrek S. (2009). Low voltage operating OFETs based on solution-processed metal phthalocyanines. *Applied Physics A* **96 (3)**: 763. doi:10.1007/s00339-009-5268-1

Chang E., Thekkek N., Yu W.W., Colvin V.L. and Drezek R. (2006). Evaluation of quantum dot cytotoxicity based on intracellular uptake. *Small* **2**:1412–1417.

Chaturvedi S., Dave P.N. and Shah N.K. (2012). Applications of nano-catalyst in new era. *Journal of Saudi Chemical Society* **16**:307–325.

Chemistry About (2009) Porphyrin chemical structure, www.chemitry.about.com, Retrieved 2009-09-17.

Chen Q., Huang Z., Chen H., Beckers J. and Hetzel F.W. (2002). Improvement of tumor response by manipulation of tumor oxygenation during photodynamic therapy. *Journal of Photochemistry and Photobiology B: Biology* **76**:197–203.

Cherukuri P. and Curley S.A. (2010). Use of nanoparticles for targeted, noninvasive thermal destruction of malignant cells. *Methods in Molecular Biology* **624**:359–373.

Chiarugi P. and Cirri P. (2003). Redox regulation of protein tyrosine phosphatases during receptor tyrosine kinase signal transduction. *Trends in Biochemical Sciences* **28**:509–514.

Chlebowski R.T., Blackburn G.L., Thomson C.A., Nixon D.W., Shapiro A., Hoy M.K., Goodman M.T., Giuliano A.E., Karanja N., McAndrew P., Hudis C., Butler J., Merkel D., Kristal A., Caan B., Michaelson R., Vinciguerra V., Del Prete S., Winkler M., Hall R., Simon M., Winters B.L. and Elashoff R.M. (2006). Dietary fat reduction and breast cancer outcome: interim efficacy results from the Women's Intervention Nutrition Study (WINS). Journal of the National Cancer Institute **98 (24)**:1767–1776.

Cho K., Wang X., Nie S., Chen Z. and Shin D.M. (2008). Therapeutic nanoparticles in drug delivery in cancer. *Clinical Cancer Research* **14(5)**:1310-1316.

Cho Y., McQuade T., Zhang H., Zhang J. and Chan F.K.M. (2011). RIP1-Dependent and Independent Effects of Necrostatin-1 in Necrosis and T cell Activation. *PLoS ONE* **6(8)**: e23209.

CIA (2010). The World Factbook. https://www.cia.gov/library/publications/the-world-factbook/. Retrieved 2015-03-02.

Cid J.J., Yum J.H., Jang S.R., Nazeeruddin M.K., Martinez- Ferrero E., Palomares E., Ko J., Graetzel M. and Torres T. (2007). Molecular cosensitization for efficient panchromatic dye-sensitized solar cells. *Angewandte Chemie International Edition* **46**:8358-8362.

Collaborative Group on Hormonal Factors in Breast Cancer (1997). Breast cancer and hormone replacement therapy: collaborative reanalysis of data from 51 epidemiological studies of 52,705 women with breast cancer and 108,411 women without breast cancer. *Lancet* **350(9084)**: 1047–1059.

Cook M.J., Chambrier I., Cracknell S.J., Mayes D.A. and Russell D.A. (1995). Octa-alkyl zinc phthalocyanines: Potential photosensitizers for use in the photodynamic therapy of cancer. *Journal of Photochemistry and Photobiology B: Biology* **62**:542-545.

Coupienne I., Fettweis G. and Piette J. (2011a). RIP3 expression induces a death profile change in U2OS osteosarcoma cells after 5-ALA-PDT. *Lasers in Surgery and Medicine* **43**:557–564.

Coupienne I., Fettweis G., Rubio N., Agostinis P. and Piette J. (2011b). 5-ALA-PDT induces RIP3-dependent necrosis in glioblastoma. *Photochemical & Photobiological Sciences* **10**: 1868–1878.

Curado M.P., Edwards B.K., Shin H.R., et al. (2007), eds. Cancer Incidence in Five Continents, Vol. IX. Lyon: IARC; *IARC Scientific Publications* No. 160.

Czabotar P.E., Lessene G., Strasser A. and Adams J.M. (2014). Control of apoptosis by the BCL-2 protein family: implications for physiology and therapy. *Nature Reviews Molecular Cell Biology* **15**:49–63.

Daniel M.C. and Astruc D. (2004). Gold nanoparticles: assembly, supramolecular chemistry, quantum-size-related properties, and applications toward biology, catalysis, and nanotechnology. *Chemical Reviews* **104**:293–346.

D'Autrèaux B. and Toledano M.B. (2007). ROS as signalling molecules: mechanisms that generate specificity in ROS homeostasis. *Nature Reviews Molecular Cell Biology* **8**:813–824.

De Jong W.H. and Borm P.J.A. (2008). Drug delivery and nanoparticles: Applications and hazards. *International Journal of Nanomedicine* **3(2)**:133-149.

de la Torre G., Vazquez P. and Torres T. (2004). Role of structural factors in the nonlinear optical properties of phthalocyanines and related compounds. *Chemical Reviews* **104**:3723-3750.

Divsar F., Nomani A., Chaloosi M. and Haririan I. (2009). Synthesis and characterization of gold nanocomposites with modified and intact polyamidoamine dendrimers. *Microchimica Acta* **165(3)**:421-426.

Dougherty T.J. (1993). Photodynamic Therapy. *Journal of Photochemistry and Photobiology B: Biology* **58**:895.

Drobizhev M., Makarov N.S., Stepanenko Y. and Rebane A. (2006). Near-infrared two-photon absorption in phthalocyanines: enhancement of lowest gerade-gerade transition by symmetrical electron-accepting substitution. *Journal of Chemical Physics* **124**:224701.

Dröge W. (2002). Free radicals in the physiological control of cell function. *Physiological Reviews* **82**:47–95.

Edelstein A.S. and Cammarata, R.C. (1998). Nanomaterials: Synthesis, Properties, and Applications, second ed. CRC Press.

El-Chaghaby G.A. and Ahmad A.F. (2011). Biosynthesis of silver nanoparticles using *Pistacia lentiscus* leaves extract and investigation of their antimicrobial effect. *Oriental Journal of Chemistry* **27(3)**:929–936.

El-Hussein A., Mfouo-Tyng I., Abdel-Harith M. and Abrahamse H. (2015). Comparative study between the photodynamic ability of gold and silver nanoparticles in mediating cell death in breast and lung cancer cell lines. *Journal of Photochemistry and Photobiology B: Biology* **153**:67–75.

El-Hussein., Harith M. and Abrahamse H. (2012). Assessment of DNA damage after photodynamic therapy using a metallophthalocyanine photosensitizer. *International Journal of Photoenergy* **12**:1-12

Eloy L., Jarrousse A.S., Teyssot M.L., et al. (2012). Anticancer activity of silver-N-heterocyclic carbine complexes. Caspase-independent induction of apoptosis via mitochondrial apoptosis-inducing factor (AIF). *Chem Med Chem.* **7(5)**:805–814.

El-Sayed I.H., Huang X. and El-Sayed MA. (2005). Surface plasmon resonance scattering and absorption of anti-EGFR antibody conjugated gold nanoparticles in cancer diagnostics: applications in oral cancer. *Nano Letters* **5**:829–834.

El-Tamer M.B., Ward B.M., Schifftner T., Neumayer L., Khuri S. and Henderson W. (2007). Morbidity and Mortality Following Breast Cancer Surgery in Women. *Annals of Surgery* **245(5)**: 665–671.

Erental A., Sharon I. and Engelberg-Kulka H. (2012). Two Programmed Cell Death Systems in *Escherichia coli*: An Apoptotic-Like Death Is Inhibited by the mazEF-Mediated Death Pathway. *PLOS Biology* **10(3)**: e1001281.

Fadeel B. and Orrenius S. (2005). Apoptosis: a basic biological phenomenon with wide-ranging implications in human disease. *Journal of Internal Medicine* **258**:479-517.

Ferlay J., Shin H.R., Bray F., Forman D., Mathers C.D., Parkin D. (2008). GLOBO-CAN 2008, Cancer Incidence and Mortality Worldwide: IARC Cancer-Base No.10 [Internet]. Lyon, France: International Agency for Research on Cancer; Available from: http://globocan.iarc.fr.

Firdous S., Nawaz M., Ikram M. and Ahmed M. (2012). *In vitro* study of cell death with 5-aminolevulinic acid -based photodynamic therapy to improve the efficiency of cancer treatment. *Laser Physics* **22(3)**:626–633.

Folse H.J. and Roughgarden J. (2010). What is an individual organism? A multilevel selection perspective. *The Quarterly review of biology* **85 (4)**:447–472.

Franceschi S. and Raza S.A. (2009). Epidemiology and prevention of hepatocellular carcinoma. *Cancer Letters* **286(1)**:5-8.

Gallucci B.B. (1985). Selected concepts of cancer as a disease. From the Greeks to 1900. *Oncology Nursing Forum* **12**:67–71.

Gannon C.J., Cherukuri P., Yakobson B.I., Cognet L., Kanzius J.S., Kittrell C., Weisman R.B., Pasquali M., Howard K. Schmidt H.K., Smalley R.E. and Curley S.A. (2007). Carbon Nanotube-enhanced Thermal Destruction of Cancer Cells in a Noninvasive Radiofrequency Field. *Cancer* **110**:2654–2665.

Garg A.D., Maes H., Romanoa E. and Agostinis P. (2015). Autophagy, a major adaptation pathway shaping cancer cell death and anticancer immunity responses following photodynamic therapy. *Photochemical & Photobiological Sciences.* DOI: 10.1039/C4PP00466C

Giorgi C., Bonora M., Sorrentino G., Missiroli S., Poletti F., Suski J.M., Ramirez F.G., Rizzuto R., Di Virgilio F., Zito E., Pandolfi P.P., Wieckowski M.R., Mammano F., Del Sal G. and Pinton P. (2015a). p53 at the endoplasmic reticulum regulates apoptosis in a Ca_2+-dependent manner. *Proceedings of the National Academy of Sciences of the United States of America* **112(6)**:1779-1784.

Giorgi C. Bonora M., Missiroli S., Poletti F., Ramirez F.G., Morciano G., Morganti C., Pandolfi P.P., Mammano F. and Pinton, P. (2015b). Intravital imaging reveals p53-dependent cancer cell death induced by phototherapy via calcium signaling. *Oncotarget* **6(3)**:1435-1445.

Gogadaa R., Amadori M., Zhang H., Jones A., Verone A., Pitarresi J., Jandhyam S., Prabhu V., Black J.D. and Chandra D. (2011). Curcumin induces Apaf-1-dependent, p21-mediated caspase activation and apoptosis. *Cell Cycle* **10(23)**:4128–4137.

Gogadab R., Prabhu V., Amadori M., Scott R., Hashmi S., and Chandra D. (2011). Resveratrol induces p53-independent, X-linked inhibitor of apoptosis protein (XIAP)-mediated bax protein oligomerization on mitochondria to initiate cytochrome c release and caspase activation. *Journal of Biological Chemistry* **286(33)**:28749–28760.

Goodman C.M., McCusker C.D., Yilmaz T. and Rotello V.M. (2004). Toxicity of gold nanoparticles functionalized with cationic and anionic side chains. *Journal of Biological Chemistry* **15**:897-904.

Gradishar W.J., Tjulandin S., Davidson N., Shaw H., Desai N., Bhar P., Hawkins M. and O'Shaughnessy J. (2005). Phase III trial of nanoparticle albumin-bound paclitaxel compared with polyethylated castor oil-based paclitaxel in women with breast cancer. *Journal of Clinical Oncology* **23**:7794–803.

Gralow J.R., Burstein H.J., Wood W., et al.(2008). Preoperative therapy in invasive breast cancer: Pathologic assessment and systemic therapy issues in operable disease. *Journal of Clinical Oncology* **26**:814–819.

Green D.R. and Kroemer G. (2004).The pathophysiology of mitochondrial cell death. *Science* **305**:626–629.

Griffin C., Karnik A., McNulty J. and Pandey S.(2011). Pancratistatin selectively targets cancer cell mitochondria and reduces growth of human colon tumor xenografts. *Molecular Cancer Therapeutics* **10(1)**:57–68.

Guan Xiang D., Tetsuji M., Michiaki S., Shin S., Hiroaki F. and Migaku T. (2010). Evidence of localized surface plasmon enhanced magneto-optical effect in nanodisk array. *Applied Physics Letters* **96(8)**: e081915.

Guillaud G., Simon J. and Germain J.P. (1998). Metallophthalocyanines: Gas sensors, resistors and field effect transistors. *Coordination Chemistry Reviews* **31**:178-180.

Hainfeld J.F., Slatkin D.N. and Smilowitz H.M. (2004). The use of gold nanoparticles to enhance radiotherapy in mice. *Physics in Medicine and Biology* **49**:N309–N315.

Hamblin M.R. and Mróz, P. (2008). Advances in Photodynamic Therapy: Basic, Translational, and Clinical. Artech House; MA, USA: 2008.

Hanahan D. and Weinberg R.A. (2000). The hallmarks of cancer. *Cell* **100**:57-70.

Hassan M., Watari H., AbuAlmaaty A., Ohba Y. and Sakuragi N. (2014). Apoptosis and Molecular Targeting Therapy in Cancer. *BioMed Research International* ID150845:doi.org/10.1155/2014/150845.

He M., Rosen J., Mangiameli D. and Libutti S.K. (2007). Cancer development and progression. *Advances in Experimental Medicine and Biology* **593**:117-133.

He X., Gao J., Gambhir S.S., et al. (2010). Near-infrared fluorescent nanoprobes for cancer molecular imaging: status and challenges. *Trends in Molecular Medicine* **16**:574-583.

Heiligtag SJ, Bredehorst R, David KA. (2002). Key role of mitochondria in cerulenin-mediated apoptosis. *Cell Death & Differentiation* **9(9)**:1017–1025.

Herbst M. (2015). Fact Sheet on the Top Ten Cancers per Population Group. http://www.cansa.org.za/files/2015/05/Fact-Sheet-Top-Ten-Cancers-per-Population-Group-May-2015.pdf. Retrieved 2015-11-03.

Hilderbrand S.A. and Weissleder R. (2010). Near-infrared fluorescence: application to *in vivo* molecular imaging. *Current Opinion in Chemical Biology* **14**:71-79.

Hogan N.M. and Joyce M.R. (2012). Surgical Management of Locally Recurrent Rectal Cancer. *International Journal of Surgical Oncology* doi:10.1155/2012/464380.

Holmes M.D., Chen W.Y., Feskanich D., Kroenke C.H. and Colditz G.A. (2005). Physical activity and survival after breast cancer diagnosis. *Journal of the American Medical Association* **293 (20)**:2479–2486.

Horiba, (2015), Dendrimer particles size analysis. http://www.horiba.com/scientific/products/particlecharacterization/applications/pharmaceuticals/dendrimers/. Retrieved 2015-09-22.

Huang Z. (2005). A review of progress in clinical photodynamic therapy. *Technology in Cancer Research & Treatment* **4**:283-293.

Huang Z., Chen Q., Shakil A., et al. (2003). Hyperoxygenation enhances the tumor cell killing of Photofrin-mediated photodynamic therapy. *Photochemical & Photobiological Sciences* **78**:496–502.

Huang Z., Xu H., Meyers A.D., Musani A.I., Wang L., Tagg R., Barqawi A.B. and Chen Y.K. (2008). Photodynamic therapy for treatment of solid tumors – potential and technical challenges. *Technology in Cancer Research & Treatment* **7(4)**: 309–320.

Huefner A., Septiadi D., Wilts B.D., Patel I.I., Kuan W.L., Fragniere A., Barker R.A. and Mahajan S. (2014). Gold nanoparticles explore cells: Cellular uptake and their use as intracellular probes. *Methods* **68(2)**:354-363.

Hunter D.J., Spiegelman D., Adami H.O., Beeson L., van den Brandt P.A., Folsom A.R., Fraser G.E., Goldbohm R.A., Graham S., Howe G.R., *et al.* (1996). Cohort studies of fat intake and the risk of breast cancer--a pooled analysis. *New England Journal of Medicine* **334(6)**:356–361.

Hussain S.M., Javorina A.K., Schrand A.M., Duhart H.M., Ali S.F. and Schlager J.J. (2006). The interaction of manganese nanoparticles with PC-12 cells induces dopamine depletion. *Toxicological Sciences* **92(2)**:456–463.

Hutchison G.J., Valentine H.R., Loncaster J.A., et al. (2004). Hypoxia-inducible factor 1alpha expression as an intrinsic marker of hypoxia: correlation with tumor oxygen, pimonidazole measurements, and outcome in locally advanced carcinoma of the cervix. *Clinical Cancer Research* **10**:8405–8412.

Iannuzzi M., Tran F., Widmer R., Dienel T., Radican, K., Ding, Y., Hutter J., and Gröning O. (2014). Site-selective adsorption of phthalocyanine on h-BN/Rh(111) nanomesh. *Physical Chemistry Chemical Physics* **16(24)**:e12374. doi:10.1039/C4CP01466A.

IFI claims patentservices. Improved shading process. (http://www.google.com.gt/patents/EP2222791B1?cl=en). Retrieved 2016-07-17.

Institute of Medicine (2012). Breast Cancer and the Environment: A Life Course Approach. Washington, D.C: National Academies Press. pp. 52–53.

Issels R.D., Lindner L.H., Verweij J., Wust P., Reichardt P., Schem B.C., et al. (2010) Neo-adjuvant chemotherapy alone or with regional hyperthermia for localised high-risk soft-tissue sarcoma: a randomised phase 3 multicentre study. *Lancet Oncology* **11**:561–70.

Jain K., Paranandi K.S., Sridharan S. and Basu A. (2013). Autophagy in breast cancer and its implications for therapy. *American Journal of Cancer Research* **3(3)**:251-265.

Jain S., Hirst D.G. and O'Sullivan J.M. (2012). Gold nanoparticles as novel agents for cancer therapy. *British Journal of Radiology* **85(1010)**:101-113.

Jelveh S. and Chithrani D.B. (2011). Gold Nanostructures as a Platform for Combinational Therapy in Future Cancer Therapeutics. *Cancers* **3(1)**:1081-1110.

Jemal A., Center M.M., Desantis C. and Ward E.M. (2010). Global Patterns of Cancer Incidence and Mortality Rates and Trends. *Cancer Epidemiology Biomarkers & Prevention* **19(8)**:1893-1907.

Joshi A., Iyengar R., Joo J.H., Li-Harms X.J., Wright C., Marino R., Winborn B.J., Phillips A., Temirov J., Sciarretta S., Kriwacki R., Peng J., Shelat A. and Kundu M. (2015). Nuclear ULK1 promotes cell death in response to oxidative stress through PARP1. *Cell Death & Differentiation* doi: 10.1038/cdd.2015.88.

Jumaa H., Hendriks R.W. and Reth M. (2005). B-cell signaling and tumorigenesis. *Annual Review of Immunology* **23**:415-445.

Jung C.H., Jun C.B., Ro S.H., Kim Y.M., Otto N.M., Cao J., et al. (2009). ULK-Atg13-FIP200 complexes mediate mTOR signaling to the autophagy machinery. *Molecular Biology of the Cell* **20 (7)**:1992–2003.

Jung S.N., Yang W.K., Kim J., Kim H.S., Kim E.J., Yun H., Park H., Kim S.S., Choe W., Kang I. and Ha J. (2008). Reactive oxygen species stabilize hypoxia-inducible

factor-1 alpha protein and stimulate transcriptional activity via AMP-activated protein kinase in DU145 human prostate cancer cells. *Carcinogenesis* **29(4)**:713-721.

Juzenas P. and Juzeniene A. (2010). Reduction of cutaneous photosensitivity by application of ointment containing ferrous or cobaltous ions concomitant with the use of topical protoporphyrin IX precursors. *Photodiagnosis and photodynamic therapy* **7**:152-157.

Juzeniene A., Juzenas P., Ma L.W., Iani V. and Moan J. (2004). Effectiveness of different light sources for 5-aminolevulinic acid photodynamic therapy. *Lasers in Medical Science* **19**:139–149.

Kadakia K.C., Moynihan T.J., Smith T.J. and Loprinzi C.L. (2012). Palliative communications: addressing chemotherapy in patients with advanced cancer. *Annals of Oncology* **23(3)**: 29-32.

Kadish K.M., Smith K.M. and Guilard R. The Porphyrin Handbook; Academic Press: San Diego, CA, USA, 2003; Volumes 15-20.

Kanavos P. (2006). The rising burden of cancer in the developing world. *Annals of Oncology* **17(8)**:15-23.

Kang B., Mackey M.A. and El-Sayed M.A. (2010). Nuclear targeting of gold nanoparticles in cancer cells induces DNA damage, causing cytokinesis arrest and apoptosis. *Journal of the American Chemical Society* **132**:1517–1519.

Kang, R., Zeh H.J., Lotze M.T. and Tang D. (2011). The Beclin 1 network regulates autophagy and apoptosis. *Cell Death Differentiation* **18**:571-580.

Kardinal C. and Yarbro J.A. (1979). Conceptual history of cancer. *Seminars in Oncology* **6**:396-408.

Karioti A and Bilia A.R. (2010) Hypericins as potential leads for new therapeutics. *International Journal of Molecular Sciences* **11**:562-594.

Kavanagh B.D. and Timmerman R.D. (2006). Stereotactic radiosurgery and stereotactic body radiation therapy: An overview of technical considerations and clinical applications. *Hematology/Oncology Clinics of North America* **20(1)**:87–95.

Kesharwani P., Jain K. and Jain N.K. (2014). Dendrimer as nanocarrier for drug delivery. *Progress in Polymer Science* **39(2)**:268–307.

Kessel D., Luo Y., Mathieu P. and Reiners J.J. (2000). Determinants of the apoptotic response to lysosomal damage. *Photochemistry and Photobiology* **71**: 196-200.

Khanna P., Ong C., Bay H.B. and Baeg G.H. (2015). Nanotoxicity: An Interplay of Oxidative Stress, Inflammation and Cell Death. *Nanomaterials* **5(3)**:1163-1180.

Kim K.S., Cho C.H., Park E.K., Jung M.H., Yoon K.S. and Park, H.K. (2012). AFM-Detected Apoptotic Changes in Morphology and Biophysical Property Caused by Paclitaxel in Ishikawa and HeLa Cells. *PLoS ONE* **7(1)**: e30066.

Kim Y.G, Oh S.K., and Crooks R.M. (2004). Preparation and Characterization of 1-2 nm Dendrimer-Encapsulated Gold Nanoparticles Having Very Narrow Size Distributions. *Chemistry of Materials* **16**:167-172.

Kinsella T.J., Baron E.D., Colussi V.C., Cooper K.D., Hoppel C.L., Ingalls S.T., Kenney M.E., Li X., Oleinick N.L., Stevens S.R. and Remick S.C. (2011). Preliminary clinical and pharmacologic investigation of photodynamic therapy with the silicon phthalocyanine photosensitizer Pc 4 for primary or metastatic cutaneous cancers. *Frontiers in Oncology* **1**:14-21.

Kroemer G., Galluzzi L., Vandenabeele P., Abrams J., Alnemri E.S., Baehrecke E.H., Blagosklonny M.V., El-Deiry W.S., Golstein P., Green D.R., Hengartner M., Knight R.A., Kumar S., Lipton S.A., Malorni W., Nuñez,G., Peter M.E., Tschopp J., Yuan J., Piacentini M., Zhivotovsky B. and Melino G. (2009). Classification of cell death. *Cell Death Differentiation* **16(1)**: 3–11.

Kroenke C.H., Chen W.Y., Rosner B., Holmes M.D. (2005). Weight, weight gain, and survival after breast cancer diagnosis. *Journal of Clinical Oncology* **23 (7)**:1320–1328.

Kullmann F., Hollerbach S., Dollinger M., Harder J., Fuchs M., Messmann H., Messmann H., Trojan J., Gäbele E., Hinke A., Hollerbach C. and Endlicher E. (2009). Cetuximab plus gemcitabine/oxaliplatin (GEMOXCET) in first-line

metastatic pancreatic cancer: a multicentre phase II study. *British Journal of Cancer* **100**:1032–1036.

Kuznetsov A.V., Margreiter R., Amberger A., Saks V. and Grimm M. (2011). Changes in mitochondrial redox state, membrane potential and calcium precede mitochondrial dysfunction in doxorubicin-induced cell death. *Biochimica et Biophysica Acta* **1813(6)**:1144–1152.

Lal S., Clare S.E. and Halas N.J. (2008). Nanoshell-enabled photothermal cancer therapy: impending clinical impact. *Accounts of Chemical Research* **41**:1842–1851.

Lam M., Lee Y.J., Deng M., Hsia A.H., Morrissey K.A., Yan C., Azzizudin K., Oleinick N.L., McCormick T.S., Cooper K.D. and Baron E.D. (2010). Photodynamic Therapy with the Silicon Phthalocyanine Pc 4 Induces Apoptosis in Mycosis Fungoides and Sezary Syndrome. *Advances in Hematology* doi:10.1155/2010/896161.

Lam M.G., de Klerk J.M., van Rijk P.P. and Zonnenberg B.A. (2007). Bone seeking radiopharmaceuticals for palliation of pain in cancer patients with osseous metastases. *Anti-cancer Agents in Medicinal Chemistry* **7(4)**:381–397.

Le Bras M., Borgne-Sanchez A., Touat Z., et al. (2006). Chemosensitization by knockdown of adenine nucleotide translocase-2. *Cancer Research* **66(18)**:9143–9152.

Lee C.W.1., Chen M.J., Cheng J.Y. and Wei P.K. (2009). Morphological studies of living cells using gold nanoparticles and dark-field optical section microscopy. *Journal of Biomedical Optics* **14(3)**:034016. doi: 10.1117/1.3147390.

Lee J., Chatterjee D.K., Lee M.H. and Krishnan S. (2014). Gold nanoparticles in breast cancer treatment: promise and potential pitfalls. *Cancer Letters* **347(1)**:46-53.

Lemasters J.J. (2005). Dying a thousand deaths: redundant pathways from different organelles to apoptosis and necrosis. *Gastroenteritis* **129(1)**:351-60.

Li C. (2002). Poly (L-glutamic acid) anticancer drug conjugates. *Advanced Drug Delivery* **54**:695-713.

Ligibel J. (2011). Obesity and Breast Cancer. *Oncology* **25(11)**: 994–1000.

Link S. and El-sayed M.A. (2000). Shape and size dependence of radiance, non-radiative and photothermal properties of gold nanocrystals. *International Review in Physical Chemistry* **19(3)**:409-453.

Lis D. and Cecchet F. (2014). Localized surface plasmon resonances in nanostructures to enhance nonlinear vibrational spectroscopies: towards an astonishing molecular sensitivity. *Journal of Nanotechnology* **5**:2275-2292.

Liu Z., Wu Y., Guo Z., Liu Y., Shen W., Zhou P. and Lu X. (2014). Effects of Internalized Gold Nanoparticles with Respect to Cytotoxicity and Invasion Activity in Lung Cancer Cells. *PLoS ONE* **9(6)**:e99175. doi:10.1371/journal.pone.0099175.

Lubick N. and Betts K. (2008). Silver socks have cloudy lining. *Environmental Science & Technology* **42(11)**:e3910.

Mackay J., Jemal A., Lee N.C. and Parkin D.M. (2006). The Cancer Atlas. Atlanta: American Cancer Society; 2006.

MacManus J.P. and Linnik M.D. (1997). Gene Expression Induced by Cerebral Ischemia: An Apoptotic Perspective. *Journal of Cerebral Blood Flow and Metabolism* **17**:815–832.

Madaan K., Kumar S., Poonia N., Lather V. and Pandita D. (2014). Dendrimers in drug delivery and targeting: Drug-dendrimer interactions and toxicity issues. *Journal of Pharmacy and Bioallied Sciences* **6(3)**:139–150.

Maeda H., Greish K. and Fang J. (2006). The EPR effect and polymeric drugs: a paradigm shift for cancer chemotherapy in the 21st century. Polymer therapeutics II. Heidelberg, Berlin: Springer; 2006.

Magrez A., Kasas S., Salicio V., Pasquier N., Seo J.W., Celio M., Catsicas S., Schwaller B. and Forró L. (2006). Cellular toxicity of carbon-based nanomaterials. *Nano Letters* **6**:1121–1125

Majumdar P., Nomulaa R. and Zhao J. (2014). Activatable triplet photosensitizers: magic bullets for targeted photodynamic therapy. *Journal of Materials Chemistry C* **2(30)**:5982-5997.

Malone K.E., Daling J.R., Thompson J.D., O'Brien C.A., Francisco L.V. and Ostrander E.A. (1998). BRCA1 mutations and breast cancer in the general population: analyses in women before age 35 years and in women before age 45 years with first-degree family history. *Journal of the American Medical Association* **279(12)**: 922–929.

Mang T.S. (2004). Lasers and light sources for PDT: past, present and future. *Photodiagnosis and photodynamic therapy* **1**:43–48.

Manifold R.N. and Anderson C.D. (2011). Increased cutaneous oxygen availability by topical application of hydrogen peroxide cream enhances the photodynamic reaction to topical 5-aminolevulinic acid-methyl ester. *Archives of Dermatological Research* **303**:285-292.

Manoto S.L. and Abrahamse H. (2011). Effect of a newly synthesized Zn sulfophthalocyanine derivative on cell morphology, viability, proliferation, and cytotoxicity in a human lung cancer cell line (A549). *Lasers in Medical Science* **26(4)**:523-530.

Manoto S.L., Houreld N.N. and Abrahamse H. (2013). Phototoxic effect of photodynamic therapy on lung cancer cells grown as a monolayer and three dimensional multicellular spheroids. *Lasers in Surgery and Medicine* **45(3)**:186–194.

Manoto S.L., Sekhejane P.R., Houreld N.N. and Abrahamse H. (2012). Localization and phototoxic effect of zinc sulfophthalocyanine photosensitizer in human colon (DLD-1) and lung (A549) carcinoma cells *(in vitro)*. *Photodiagnosis and photodynamic therapy* **9(1)**:52-59.

Manzl C., Krumschnabel G., Bock F., Sohm B., Labi V., Baumgartner F., Logette E., Tschopp J. and Villunger A.(2009). Caspase-2 activation in the absence of PIDDosome formation. *Journal of Cell Biology* **185(2)**:291-303.

Matsumura Y. and Maeda H. (1986). A new concept for macromolecular therapeutics in cancer chemotherapy: mechanism of tumoritropic accumulation of proteins and the antitumor agent smancs. *Cancer Research* **46**:6387–6392.

Mesbahi A. (2010). A review on gold nanoparticles radiosensitization effect in radiation therapy of cancer. *Reports of Practical Oncology and Radiotherapy* **15**:176-180.

Mfouo-Tynga I., Houreld N.N. and Abrahamse H. (2012). The primary subcellular localization of Zinc phthalocyanine and its cellular impact on viability, proliferation and structure of breast cancer cells (MCF-7). *Journal of Photochemistry and Photobiology B: Biology* **120**:171-176.

Mfouo-Tynga I., Houreld N.N. and Abrahamse H. (2014). Induced Cell Death Pathway Post Photodynamic Therapy Using a Metallophthalocyanine Photosensitizer in Breast Cancer Cells. *Photomedicine and Laser Surgery* **32(4)**:205-211.

Michaud M., Martins I., Sukkurwala A.Q., Adjemian S., Ma Y., Pellegatti P., Shen S., Kepp O., Scoazec M., Mignot G., Rello-Varona S., Tailler M., Menger L., Vacchelli E., Galluzzi L., Ghiringhelli F., di Virgilio F. Zitvogel L. and Kroemer, G. (2011). Autophagy-dependent anticancer immune responses induced by chemotherapeutic agents in mice. *Science* **334**:1573-1577.

Minai L., Yeheskely-Hayon D. and Yelin D. (2013). High levels of reactive oxygen species in gold nanoparticle-targeted cancer cells following femtosecond pulse irradiation. *Scientific Reports* **3**:2146-2153.

Mizushima N. (2010). The role of the Atg1/ULK1 complex in autophagy regulation. *Current Opinion in Cell Biology* **22(2)**:132–139.

Mizushima N. and Klionsky D.J. (2007). Protein turnover via autophagy: implications for metabolism. *Annual Review of Nutrition* **27**:19-40.

Mkandawire M.M., Lakatos M., Springer A., Clemens A., Appelhans D., Krause-Buchholz U. Pompe W., Rodel G. and Mkandawire (2015). Induction of apoptosis in human cancer cells by targeting mitochondria with gold nanoparticles. *Nanoscale* **7(24)**:10634-10640.

Moan J. (1990). Properties for optimal PDT sensitizers. *Journal of Photochemistry and Photobiology B: Biology* **5**:521-524.

Mollinedo F., Fernandez M., Hornillos V., J Delgado, Amat-Guerri F., Acuña A.U., Nieto-Miguel T., Villa-Pulgarín J.A., González-García C., Ceña V., and Gajate C. (2011). Involvement of lipid rafts in the localization and dysfunction effect of the anti-tumor ether phospholipid edelfosine in mitochondria. *Cell Death and Disease* **2(5)**:e158.

Mosoyan G., Nagi C., Marukian S., Teixeira A., Simonian A., Resnick-Silverman L., DiFeo A., Johnston D., Reynolds S.R., Roses D.F. and Mosoian A.(2013). Multiple Breast Cancer Cell-Lines Derived from a Single Tumor Differ in Their Molecular Characteristics and Tumorigenic Potential. *PLoS ONE* **8(1)**: e55145.

Mostafa M.H., Sheweita S.A. and O'Connor P.J. (1999). Relationship between schistosomiasis and bladder cancer. *Clinical Microbiology Reviews* **12(1)**:97-111.

Mroz P., Yaroslavsky A., Kharkwal G.B. and Hamblin M.R. (2011). Cell Death Pathways in Photodynamic Therapy of Cancer. *Cancers* **3**:2516-2539.

Murphy C.J., Gole A.M., Stone J.W., Sisco P.N., Alkilany A.M., Goldsmith E.C. and Baxter S.C. (2008). Gold nanoparticles in biology: beyond toxicity to cellular imaging. *Accounts of Chemical Research* **41**:1721-1730.

National Cancer Institute. (2015). What Is Cancer? http://www.cancer.gov/about-cancer/what-is-cancer. Retrieved 2015-11-03.

Nel A., Xia T., Madler L. and Li N. (2006). Toxic potential of materials at the nanolevel. *Science* **311**:622–627.

Nemanashi M. and Meijboom R. (2013). Synthesis and characterization of Cu, Ag and Au dendrimer-encapsulated nanoparticles and their application in the reduction of 4-nitrophenol to 4-aminophenol. *Journal of Colloid and Interface Science* **389**:260–267.

Newcomb P.A., Storer B.E., Longnecker M.P., Mittendorf R., Greenberg E.R., Clapp R.W., Burke K.P., Willett W.C. and MacMahon B. (1994). Lactation and a reduced risk of premenopausal breast cancer. *New England Journal of Medicine* **330(2)**:81–87.

Nie S., Xing Y., Kim G.J. and Simons J.W. (2007). Nanotechnology applications in cancer. *Annual Review of Biomedical Engineering* **9**:257-288.

Nikoletopoulou V., Markaki M., Palikaras K. and Tavernarakis N. (2013). Crosstalk between apoptosis, necrosis and autophagy. *Biochemica et Biophysica Acta* **1833**:3448-3459.

Noda S.E., Lautenschlaeger T., Siedow M.R., et al. (2009). Technological advances in radiation oncology for central nervous system tumors. *Seminars in Radiation Oncology* **19(3)**:179–186.

Nombona N., Antunes E., Litwinski C. and Nyokong T. (2011). Synthesis and photophysical studies of phthalocyanine-gold nanoparticles conjugates. *Dalton Transactions* **40**:11876-11884.

Nyst H.J., van Veen R.L., Tan I.B., Peters R., Spaniol S., Robinson D.J., Stewart F.A., Levendag P.C., and Sterenborg H.J.C.M. (2007). Performance of a dedicated light delivery and dosimetry device for photodynamic therapy of nasopharyngeal carcinoma: Phantom and volunteer experiments. *Lasers in Surgery and Medicine* **39**:647–653.

Ocama P., Kagimu M.M., Odida M., Wabinga H., Opio C.K., Colebunders B., van Ierssel S. and Colebunders R. (2008). Factors associated with carcinoma of the oesophagus at Mulago Hospital, Uganda. *African Health Sciences* **8(2)**:80-84.

Oleinick N.L. and Evans H.H. (1998). The photobiology of photodynamic therapy: cellular targets and mechanisms. *Radiation Research* **150(5)**:S146-S156.

Oliveira J.M., Salgado A.J., Sousa N., Mano J.F. and Reis R.L. (2010). Dendrimers and derivatives as a potential therapeutic tool in regenerative medicine strategies. *Progress in Polymer Science* **35**:1163–1194

Oltvai Z.N., Milliman C.L. and Korsmeyer S.J. (1993). Bcl-2 heterodimerizes *in vivo* with a conserved homolog, Bax, that accelerates programmed cell death. *Cell* **74(4)**:609–619.

Ortel B., Shea C.R. and Calzavara-Pinton P. (2009). Molecular mechanisms of photodynamic therapy. *Frontiers in Bioscience* **14**:4157-1472.

Pala V., Krogh V., Muti P., Chajès V., Riboli E., Micheli A., Saadatian M., Sieri S., and Berrino F. (2001). Erythrocyte membrane fatty acids and subsequent breast

cancer: a prospective Italian study. *Journal of the National Cancer Institute* **93(14)**:1088–1095.

Pan Y., Leifert A., Ruau D., Neuss S., Bornemann J., Schmid G., Brandau W., Simon U., Jahnen-Dechent W. (2009). Gold nanoparticles of diameter 1.4 nm trigger necrosis by oxidative stress and mitochondrial damage. *Small* **5**:2067–2076.

Park M.T., Song M.J., Oh E.T., et al. (2011). The anti-tumour compound, RH1, causes mitochondria-mediated apoptosis by activating c-Jun N-terminal kinase. *British Journal of Pharmacology* **163(3)**:567–585.

Parkin D.M. (2006). The global health burden of infection-associated cancers in the year 2002. *International Journal of Cancer* **118**:3030-3044.

Parkin D.M. (2008). The global burden of urinary bladder cancer. *Scandinavian Journal of Urology and Nephrology* **218**:12-20.

Parkin D.M., Nambooze S., Wabwire-Mangen F., Wabinga H.R. (2010). Changing cancer incidence in Kampala, Uganda, 1991-2006. *International Journal of Cancer* **126(5)**:1187-1195.

Parkin D.M., Sitas F., Chirenje M., Stein L., Abratt R., Wabinga H. (2008). Part I: Cancer in Indigenous Africans-burden, distribution, and trends. *Lancet Oncology* **9(7)**:683-692.

Patel A.S., Lin L., Geyer A., Haspel J.A., An C.H., Cao J., Rosas I.O. and Morse D. (2012). Autophagy in Idiopathic Pulmonary Fibrosis. *PLoS ONE* **7(7)**:e41394.

Patel R.R. and Arthur D.W. (2006). The emergence of advanced brachytherapy techniques for common malignancies. *Hematology/Oncology Clinics of North America* **20(1)**:97–118.

Patra C.R., Bhattacharya R., Wang E., Katarya A., Lau J.S., Dutta S., Muders M., Wang S., Buhrow S.A., Safgren S.L., Yaszemski M.J., Reid J.M., Ames M.M., Mukherjee P., Mukhopadhyay D. (2008). Targeted delivery of gemcitabine to pancreatic adenocarcinoma using cetuximab as a targeting agent. *Cancer Research* **68**:1970–1978.

Patra C.R., Bhattacharya R., Mukhopadhyay D., and Mukherjee P. (2010). Fabrication of gold nanoparticles for targeted therapy in pancreatic cancer. *Advanced Drug Delivery Reviews* **62**:346–361.

Peng C-L., Lai P-S., Lin F-H., Wu S.Y-H.mand Shieh M-J. (2009) Dual Chemotherapy and Photodynamic Therapy in HT-29 Human Colon Cance Xenograft Model using SN-38-Loaded Chlorin-Core Star Block Copolymer micelles. *Biomaterials* **30(21)**:36-44.

Pepper J.W. and Herron M.D. (2008). Does biology need an organism concept? *Biological Reviews* **83(4)**: 621–627.

Peracchio C., Alabiso O., Valente G. and Isidoro C. (2012). Involvement of autophagy in ovarian cancer: a working hypothesis. *Journal of Ovarian Research* **5**:22-32.

Pierrat B., Simonen M., Cueto M., Mestan J., Ferrigno P. and Heim J. (2001). SH3GLB, a new endophilin-related protein family featuring an SH3 domain. *Genomics* **71(2)**: 222–234.

Pinzon J.R., Plonska-Brzezinska M.E., Cadona C.M., Athans A.J., Gayathri S.S., Guldi D.M., Herranz M.A., Martin N., Torres T. and Echegoyen L. (2008). Sc3N@C80-ferrocene electrondonor/acceptor conjugates as promising materials for photovoltaic applications. *Angewandte Chemie International Edition* **47**:4173-4176.

Plaetzer K., Krammer B., Berlanda J., Berr F. and Kiesslich T. (2009). Photophysics and Photochemistry of Photodynamic Therapy. *Lasers in Medical Sciences* **24(2)**: 259-268.

Pradeu, T. (2010). What is an organism? An immunological answer. *History and Philosophy of the Life Sciences* **32(2–3)**: 247–267.

Prentice R.L., Caan B., Chlebowski R.T., Patterson R., Kuller L.H., Ockene J.K., Margolis K.L., Limacher M.C., Manson J.E., Parker L.M., Paskett E., Phillips L., Robbins J., Rossouw J.E., Sarto G.E., Shikany J.M., Stefanick M.L., Thomson C.A., Van Horn L., Vitolins M.Z., Wactawski-Wende J., Wallace R.B., Wassertheil-Smoller S., Whitlock E., Yano K., Adams-Campbell L., Anderson G.L., Assaf A.R.,

Beresford S.A., Black H.R., Brunner R.L., Brzyski R.G., Ford L., Gass M., Hays J., Heber D., Heiss G., Hendrix S.L., Hsia J., Hubbell F.A., Jackson R.D., Johnson K.C., Kotchen J.M., LaCroix A.Z., Lane D.S., Langer R.D., Lasser N.L. and Henderson M.M. (2006). Low-fat dietary pattern and risk of invasive breast cancer: the Women's Health Initiative Randomized Controlled Dietary Modification Trial. *Journal of the American Medical Association* **295(6)**:629–642.

Protani M. et al (2010). Effect of obesity on survival of women with breast cancer: systematic review and meta-analysis. *Breast Cancer Research and Treatment* **123(3)**:627–635.

Qu X., Yao C., Wang J., Li Z. and Zhang Z. (2012). Anti-CD30-targeted gold nanoparticles for photothermal therapy of L-428 Hodgkin's cell. *International Journal of Nanomedicine* **7**:6095-6103.

Raab O. (1990) Uber die wirkung, fluorescirender stoffe auf infusorien. *Zeitschrift Fur Biologie* **39**:524-546.

Rada B. and Leto T.L. (2008). Oxidative innate immune defenses by Nox/Duox family NADPH oxidases. *Contributions to Microbiology* **15**:164-187.

Rai S., Paliwal R., Gupta P.N., Khatri K., Goyal A.K., Vaidya B., *et al.* (2008). Solid lipid nanoparticles (SLNs) as a rising tool in drug delivery science: one step up in nanotechnology. *Current Nanoscience* **4**:30-44.

Reddy P., Meyer-Weitz A. and Yach D. (1996). Smoking status, knowledge of health effects and attitudes towards tobacco control in South Africa. *South African Medical Journal* **86(11)**:1389-1393.

Regehly M. (2008). Photoinduced transfer processes in complex carrier systems for photodynamic therapy. http://edoc.hu-berlin.de/dissertationen/regehly-martin-2008-07-16/HTML/chapter2.html, Retrieved 2015-10-02.

Ribeiro J.N., da SilvaI A.D. and Jorge R.A. (2004). Involvement of mitochondria in apoptosis of cancer cells induced by photodynamic therapy. *Jornal Brasileiro de Patologia e Medicina Laboratorial* **40(6)**:383-390.

Rink J.S., Plebanek M.P., Tripathy S. and Thaxton C.S. (2013). Update on Current and Potential Nanoparticle Cancer Therapies. *Current Opinion in Oncology* **25(6)**:646–651.

Robertson J.D., Enoksson M., Suomela M., Zhivotovsky B. and Orrenius S. (2002). Caspase-2 acts upstream of mitochondria to promote cytochrome c release during Etoposide-induced apoptosis. *Journal of Biological Chemistry* **277(33)**:29803-29809.

Rooijen V.N. and Nieuwmegen V.R. (1980). Liposomes in immunology: multilamellar phosphatidylcholine liposome as a simple biodegradable and harmless adjuvant without any immunogenic activity of its own. *Immunological communications* **9**:243–256.

Sak K. (2012). Chemotherapy and Dietary Phytochemical Agents. *Chemotherapy Research and Practice* doi:10.1155/2012/282570.

Samkoe K.S., Clancy A.A., Karotki A., Wilson B.C. and Cramb D.T. (2007). Complete blood vessel occlusion in the chick chorioallantoic membrane using two-photon excitation photodynamic therapy: implications for treatment of wet age-related macular degeneration. *Journal of Biomedical Optics* **12**:e034025.

Sanz-Moreno V. and Marshall C.J. (2010). The plasticity of cytoskeletal dynamics underlying neoplastic cell migration. *Current Opinion in Cell Biology* **22**:690-696.

Schlinkert P., Casals E., Boyles M., Tischler U., Hornig E., Tran N., Zhao J., Himly M., Riediker M., Oostingh G.J., Puntes V. and Duschl A. (2015). The oxidative potential of differently charged silver and gold nanoparticles on three human lung epithelial cell types. *Journal of Nanobiotechnology* **13**:1-18.

Schneider M., Norman R., Steyn N., Bradshaw D. (2007). Estimating the burden of disease attributable to low fruit and vegetable intake in South Africa in 2000. *South African Medical Journal* **97(8 Pt 2)**:717-723.

Selcuklu S.D., Donoghue M.T., Rehmet K., de Souza Gomes M., Fort A., Kovvuru P., Muniyappa M.K., Kerin M.J., Enright A.J. and Spillane C.(2012). MicroRNA-9 inhibition of cell proliferation and identification of novel miR-9 targets by

transcriptome profiling in breast cancer cells. *Journal of Biological Chemistry* **287(35)**:e29516-28.

Selim M.E and Hendi A.A. (2012). Gold nanoparticles induces apoptosis in MCF-7 human breast cancer cells. *Asian Pacific Journal of Cancer Prevention* **13**:1617-1620.

Seotsanyana-Mokhosi I., Kresfelder T., Abrahamse H. and Nyokong T. (2006). The effect of Ge, Si and Sn phthalocyanine photosensitizers on cell proliferation and viability of human oesophageal carcinoma cells. *Journal of Photochemistry and Photobiology B: Biology* **83(1)**:55–62.

Serra A., Pineiro M., Pereira N., Gonsalves A.R., Laranjo M. and Abrantes M. (2008). A look at clinical applications and developments of photodynamic therapy. *Oncology Reviews* **2(4)**:235-249.

Shafey O., Eriksen M., Ross H., Mackay J. (2009). The Tobacco Atlas Third Edition. Atlanta, GA: American Cancer Society 2009.

Shi X., Ganser T.R., Sun K., Balogh L.P. and Baker Jr J.R. (2007). Characterization of crystalline dendrimer-stabilized gold nanoparticles. *Nanotechnology* **17**:1072–1078.

Shukla R., Bansal V., Chaudhary M., Basu A., Bhonde R.R. and Sastry M. (2005). Biocompatibility of gold nanoparticles and their endocytotic fate inside the cellular compartment: a microscopic overview. *Langmuir* **21**:10644–10654.

Shun-rong J., Chen L., Bo Z., Feng Y., Jin X., Jiang L., Chen J., De-liang F., Quan-xing N. and Xian-jun Y. (2010). Carbon nanotubes in cancer diagnosis and therapy. *Biochimica et Biophysica Acta* **1806(1)**:29–35.

Sibata C.H., Colussi V.C., Oleinick N.L. and Kinsella T.J. (2001). Photodynamic Therapy in Oncology. *Expert Opinion on Pharmacotherapy* **2**:917–927.

Singh M., Kumar M., Manikandan S., Chandrasekaran N., Mukherjee A. and Kumaraguru A.K. (2014). Drug Delivery System for Controlled Cancer Therapy Using Physico-Chemically Stabilized Bioconjugated Gold Nanoparticles Synthesized from Marine Macroalgae, Padina Gymnospora. *Nanomedicine Nanotechnology* doi.org/10.4172/2157-7439.S5-009.

Sitas F., Urban M., Bradshaw D., Kielkowski D., Bah S., Peto R. (2004). Tobacco attributable deaths in South Africa. *Tobacco Control* **13(4)**:396-399.35

Smith A.M., Mancini, Michael C.; Nie S. (2009). Bioimaging: Second window for in vivo imaging. *Nature Nanotechnology* **4(11)**:710–711.

Soberman R.J. (2003). The expanding network of redox signaling: new observations, complexities, and perspectives. *Journal of Clinical Investigation* **111**:571–574.

Sonestedt E., Ericson U., Gullberg B., Skog K., Olsson H. and Wirflt E. (2008). Do both heterocyclic amines and omega-6 polyunsaturated fatty acids contribute to the incidence of breast cancer in postmenopausal women of the Malmö diet and cancer cohort? *International Journal of Cancer* **123(7)**:1637–1643.

Soule H.D., Vazquez J., Long A., Albert S. and Brennan M. (1973). A human cell line from a pleural effusion derived from a breast carcinoma. *Journal of the National Cancer Institute* **51(5)**:1409–1416.

Springer T., Ermini M.L., Spackova B., Jablonku J. and Homola J. (2014). Enhancing sensitivity of surface plasmon resonance biosensors by functionalized gold nanoparticles: size matters. *Analytical Chemistry* **86(20)**:10350-10356.

Statistics South Africa (2012). Census 2011 Census in brief. http://www.statssa.gov.za/Census2011/Products. Retrieved 2015-03-03.

Steele S.R., Goetz L.H., Minami S., Madoff R.D., Mellgren A.F. and Parker S.C. (2006). Management of recurrent rectal prolapse: surgical approach influences outcome. *Diseases of the Colon & Rectum* **49(4)**:440-445.

Sudhakar A. (2009). History of Cancer, Ancient and Modern Treatment Methods. *Journal of Cancer Science & Therapy* **1(2)**:1–4.

Summerhayes I.C., Lampidis T.J., Bernal S.D., et al. (1982). Unusual retention of rhodamine 123 by mitochondria in muscle and carcinoma cells. *Proceedings of the National Academy of Sciences of the United States of America* **79**:5292–5296.

Swavey S. and Tran M. (2013). Porphyrin and Phthalocyanine Photosensitizers as PDT Agents: A New Modality for the Treatment of Melanoma. In Recent Advances

in the Biology, Therapy and Management of Melanoma, book edited by Lester M. Davids, ISBN 978-953-51-0976-1, Published: February 13, 2013 under CC BY 3.0 license.

Szlachcic A., Pala K., Zakrzewska M., Jakimowicz P., Wiedlocha A. and Otlewski J. (2012). FGF1-gold nanoparticle conjugates targeting FGFR efficiently decrease cell viability upon NIR irradiation. *International Journal of Nanomedicine* **7**:5915-5927.

Taggart L.E., McMahon S.J., Currell F.J., Prise K.M., and Butterworth K.T. (2014). The role of mitochondrial function in gold nanoparticle mediated radiosensitisation. *Cancer Nanotechnology* **5(1)**:5-17.

Taniguchi N. (1974). On the Basic Concept of Nanotechnology. Proc. Int. Conf. Prod. Eng. Tokyo, Part 2 (Tokoyo: JSPE), 18.

Tholouli E., Sweeney E., Barrow E., et al. (2008). Quantum dots light up pathology. *Journal of Pathology* **216**: 275-285.

Tinel A. and Tschopp J. (2004). The PIDDosome, a protein complex implicated in activation of caspase-2 in response to genotoxic stress. *Science* **304(5672)**: 843–846.

Torchilin V. (2005). Recent advances with liposomes as pharmaceutical carriers. *Nature Reviews Drug Discovery* **4**:145–160.

Torchilin V. (2006). Multifunctional nanocarriers. *Advanced Drug Delivery Reviews* **58(14)**:1532–1555.

Torchilin V. (2011). Tumor delivery of macromolecular drugs based on the EPR effect. *Advanced Drug Delivery Reviews* **63**:131–135.

True L.D. and Gao X. (2007). Quantum dots for molecular pathology: their time has arrived. *Journal of Molecular Diagnostics* **9**:7-11.

Tsujimoto Y. and Shimizu S. (2005). Another way to die: autophagic programmed cell death. *Cell Death & Differentiation* **12(2)**:1528-1534.

Turrens JF (2003). Mitochondrial formation of reactive oxygen species. *Journal of Physiology* **552(2)**: 335–344.

Tynga I. and Abrahamse H., Caspase-8 properties, functions and regulation during Photodynamic Therapy. In: Advances in Genetics Research, K.V. Urbano ed., Nova Sciences Publishers, 2012, volume 9, chapter 4, pp.107-119.

Vakrat-Haglili Y., Weiner L., Brumfeld V., et al. (2005). The microenvironment effect on the generation of reactive oxygen species by Pd-bacteriopheophorbide. *Journal of the American Chemical Society* **127**:6487–6497.

Valero J.G., Sancey L., Kucharczak J., et al. (2011). Bax-derived membrane-active peptides act as potent and direct inducers of apoptosis in cancer cells. *Journal of Cell Science* **124(4)**:556–564.

van der Zee J., Gonza´lez D., van Rhoon G.C., van Dijk J.D.P., van Putten W.L.J. and Hart A.A.M. (2000). Comparison of radiotherapy alone with radiotherapy plus hyperthermia in locally advanced pelvic tumours: a prospective, randomised, multicentre trial. *Lancet* **355**:1119–1125.

Vasenka J., Manne S., Giberson R., Marsh T. and Henderson E. (1999). Colloidal Gold Particles as an Incompressible AFM Imaging Standard for Assessing the Compressibility of Biomolecules. *Biophysical Journal* **65**:992-997.

Vaupel P. and Mayer A. (2007). Hypoxia in cancer: significance and impact on clinical outcome. *Cancer Metastasis Review* **26**:225–239.

Vaupel P., Höckel M. and Mayer A. (2007). Detection and characterization of tumor hypoxia using pO2 histography. *Antioxidants & Redox Signaling* **9**:1221–1235.

Veldeman L., Madani I., Hulstaert F. et al. (2008). Evidence behind use of intensity-modulated radiotherapy: A systematic review of comparative clinical studies. *Lancet Oncology* **9(4)**:367–375.

Velloso N.V., Muehlmann L.A., Longo J.P.F., Silva J.R.D., Zancanela D.C., Tedesco A.C., Azevedo R.B.D. (2012). Aluminum-phthalocyanine chloride-based photodynamic therapy inhibits PI3K/Akt/Mtor pathway in oral squamous cell carcinoma cells in vitro. *Chemotherapy* **1(5)**:107-111.

Vittar N.B.R., Prucca C.G., Strassert C., Awruch J. and Rivarola V.A. (2008) Cellular inactivation and antitumour efficacy of a new zinc phthalocyanine with potential use in photodynamic therapy. *International Journal of Biochemistry and Cell Biology* **40**: 2192- 2205.

Vitug A.F. and Newman L.A. (2007). Complications in breast surgery. *Surgical Clinics of North America* **87**:431–451.

Von Minckwitz G., Untch M., Blohmer J.U., et al. Gunter von Minckwitz, Michael Untch, Jens-Uwe Blohmer, Serban D. Costa S.D., Holger Eidtmann H., Peter A. Fasching P.A., Gerber B., Eiermann W., Hilfrich J., Huober J., Jackisch C., Kaufmann M., Konecny G.E., Denkert C., Nekljudova V., Mehta K. and Loibl S. (2012) Definition and impact of pathologic complete response on prognosis after neoadjuvant chemotherapy in various intrinsic breast cancer subtypes. *Journal of Clinical Oncology* **30**:1796–1804.

Von Tappeiner H. and Jesionek A. (1903). Therapeutische versuche mit fluorescierenden stoffen. *Munchener Medizinische Wochenschrift* **47**:2042–2044.

Von Tappeiner H. and Joblauer A. (1904). Uber die wirkung der photodynamischen (fluorescierenden) staffe auf protozoan und enzyme. *Deutsches Archiv für klinische Medizin* **80**:427–487.

Vorobiof D.A., Sitas F. and Vorobiof G. (2001). Breast cancer incidence in South Africa. *Journal of Clinical Oncology* **19(18)**:125S-127S.

Wang Y. and Chen L. (2011). Quantum dots, lighting up the research and development of nanomedicine. *Nanomedicine* **7**: 385-402.

Weersink R.A., Bogaards A., Gertner M., et al. (2005). Techniques for delivery and monitoring of TOOKAD (WST09)-mediated photodynamic therapy of the prostate: clinical experience and practicalities. *Journal of Photochemistry and Photobiology B: Biology* **79**:211–222.

Wei L. (2012). Nanoparticles for cancer treatment. *Medicine & Health Rhode Island* **95(9)**:249-295.

Wen S., Zhu D. and Huang P. (2013). Targeting cancer cell mitochondria as a therapeutic approach. *Future Medicinal Chemistry* **5(1)**: 53–67.

Whitacre C.M., Feyes D.K., Satoh T., Grossmann J., Mulvihill J.W., Mukhtar H. and Oleinick N.L. (2000). Photodynamic therapy with the phthalocyanine photosensitizer Pc 4 of SW480 human colon cancer xenografts in athymic mice. *Clinical Cancer Research* **6(5)**:2021-2027.

Woodhams J.H., Macrobert A.J. and Bown S.G. (2007). The role of oxygen monitoring during photodynamic therapy and its potential for treatment dosimetry. *Photochemical & Photobiological Sciences* **6**:1246–1256.

World Health Organization. World Cancer Report. Lyon: International Agency for Research on Cancer; 2008.

Wust P., Hildebrandt B., Sreenivasa G., Rau B., Gellermann J., Riess H., et al. (2002). Hyperthermia in combined treatment of cancer. *Lancet Oncology* **3**:487–497.

Xie Z. and Klionsky D.J. (2007). Autophagosome formation: core machinery and adaptation. *Nature Cell Biology* **9**:1102-1109.

Xue L.Y., Chiu S.M. and Oleinick N.L. (2010). Atg7 deficiency increases resistance of MCF-7 human breast cancer cells to photodynamic therapy. *Autophagy* **6(2)**: 248-255.

Yager J.D. and Davidson N.E. (2006). Estrogen carcinogenesis in breast cancer. *New England Journal of Medicine* **354 (3)**: 270–282.

Yang X., Sarvestani S.K., Moeinzadeh S., He X. and Jabbari E. (2013). Effect of CD44 Binding Peptide Conjugated to an Engineered Inert Matrix on Maintenance of Breast Cancer Stem Cells and Tumorsphere Formation. *PLoS ONE* **8(3)**: e59147.

Yu L., Wan, F., Dutta S., Welsh S., Liu Z., Freundt E., Baehrecke E.H. and Lenardo M. (2006). Autophagic programmed cell death by selective catalase degradation. *Proceedings of the National Academy of Sciences of the United States of America* **103(13)**:4952-4957.

Yuan J. and Kroemer G. (2010). Alternative cell death mechanisms in development and beyond. *Genes & Development* **24(23)**:2592-2602.

Zeng S., Baillargeat D., Ho-Pui H. and Ken-Tye Y. (2014). Nanomaterials enhanced surface plasmon resonance for biological and chemical sensing applications. *Chemical Society Reviews* **43 (10)**: 3426–3452.

Zhivotovsky B. and Orrenius S. (2005). Caspase-2 function in response to DNA damage. *Biochemical and Biophysical Research Communications* **331(3)**:859–867.

Zhou M., Wang L., Su W., Tong L., Liu Y., Fan Y., Luo N., Zheng Y., Zhao H., Xiang R. and Li Z. (2012). Assessment of therapeutic efficacy of liposomal nanoparticles mediated gene delivery by molecular imaging for cancer therapy. *Journal of Biomedical Nanotechnology* **8(5)**:742-750.

Zhu T.C. and Finlay J.C. (2008). The Role of Photodynamic Therapy (PDT) Physics. *Medical Physics.* **35(7)**: 3127-3136.

Ziegler J., Newton R., Bourboulia D., et al. (2003). Risk factors for Kaposi's sarcoma: a case-control study of HIV-seronegative people in Uganda. *International Journal of Cancer* **103(2)**:233-240.

Zirakzadeh A., Hu J., Kinn J., Marits P., Sherif A. and Winqvist O. (2013). The effect of chemotherapeutic drugs on human B lymphocytes. *Journal for ImmunoTherapy of Cancer* **1(1)**:P252.

APPENDICES

APPENDIX A

ETHICAL CLEARANCE

FACULTY OF HEALTH SCIENCES

ACADEMIC ETHICS COMMITTEE

AEC74-01-2013

25 November 2013

TO WHOM IT MAY CONCERN:

STUDENT: **MFOUO-TYNGA, IS**

STUDENT NUMBER: **200504361**

TITLE OF RESEARCH PROJECT: Combined Effects Of Zinc Phthalocyanine-Antibody-Gold Nanoparticles Conjugates And Low Intensity Laser Irradiation (LILI) In Human Breast And Lung Cancer Cells

DEPARTMENT OR PROGRAMME: **DTECH: Biomedical Technology**

SUPERVISOR: **Prof H Abrahamse**   **CO-SUPERVISOR:** **Dr N Houreld**

The Faculty Academic Ethics Committee has scrutinised your research proposal and confirm that it complies with the approved ethical standards of the Faculty of Health Sciences; University of Johannesburg.

The AEC would like to extend their best wishes to you with your postgraduate studies.

Yours sincerely,

Marie Poggenpoel
Prof M Poggenpoel

Chair: Faculty of Health Sciences AEC

APPENDIX B

CERTIFICATE OF ANALYSIS

CERTIFICATE OF ANALYSIS

……………………………………………………………………………………......

ATCC® Number: **HTB-22™**

Lot Number: **60731981**

Name: **MCF7**

Description: **Breast Adenocarcinoma**

Species: **Human (Homo sapiens)**

Volume/Ampule: **1 mL**

Date Frozen: **07/09/2012**

Recovery: **A T-25 setup at a dilution of 1:10 reaches approximately 40% confluence in 1 day.**

    A T-75 setup at a dilution of 1:15 reaches approximately 20% to 30% confluence in 2 days.

Product Format: **Cells cryopreserved in the appropriate cryopreservation medium**

Expiration Date: **Not applicable**

Storage Conditions: **Vapor phase of liquid nitrogen**

Test	Specification	Result
Ampule passage number	Report results	147
Population douling level (PDL)	Report results	Not applicable
Total cells/mL	Report results	5.6×10^6 total cells/mL
Post-freeze viability	≥50.0%	93.5%
Growth properties	Mixed-adherent and/or suspension	Mixed-adherent and suspension
Morphology	Epithelial-like and/or rounded*	Epithelial-like and rounded
Test for mycoplasma contamination Hoechst DNA stain (indirect) Agar culture (direct)	None detected None detected	None detected None detected
Species determination:COI assay (interspecies)	Human	Human
Species determination:STR analysis (intraspecies)	**Human (unique DNA)** D5S818:11,12 D13S317:11 D7S820:8,9 D16S539:11,12 vWA:14,15 TH01:6 Amelogenin:X TPOX:9,12 CSF1PO:10	**Human (Unique DNA)** D5S818:11,12 D13S317:11 D7S820:8,9 D16S539:11,12 vWA:14,15 TH01:6 Amelogenin:X TPOX:9,12 CSF1PO:10

……………………………………………………………………………………………....

ATCC (American Type Culture Collection)   800-638-6597 or 703-365-2700
P.O. Box 1549   Fax: 703-365-2750
Manassas, VA 20108 USA   E-mail: tech@atcc.org
www.atcc.org   or contact your local distributor

APPENDIX C

LASER CALCULATIONS

Calculation average laser irradiation times for the diode lasers

• The output power of the 680 nm diode laser was 52 mW and the output power of the 532 nm diode laser was 642 mW. From these output power values the power densities (W/cm^2) were determined and used with different fluences (5, 10 and 15 J/cm^2) to determine the duration of irradiation.

• The following formular was used to calculate all laser irradiation times:

$$\frac{mW \times 4}{\pi(d)^2} = mW/cm^2$$

$$\frac{mW/cm^2}{1\ 000} = W/cm^2$$

$$\frac{Energy\ fluence\ (J/cm^2)}{Work\ (W/cm^2)} = Time\ (s)$$

$$\frac{Time\ (s)}{60} = Time\ (X\ min)$$

$$X\ min \times 60 = Y$$

$$Time\ (s) - Y = Seconds\ to\ add\ to\ X\ min$$

APPENDIX D

ITEM NAMES, CATALOGUE NUMBERS AND COMPANY

Items	Catalogue Number	Company
AE buffer	19077	Qiagen
Amphotericin-β	P11-001	PAA Laboratories GmbH
AnnnexinV-FITC/PI apoptosis detection kit for apoptosis and necrosis (for flow cytometry):	A2214	Sigma Aldrich
alamarBlue®	DAL1100	Sigma Aldrich
Biofreezing medium	F2270	Biochrom
CellTiter-Glo® Luminescent Cell Viability kit	G7570	Promega
Centrifuge tube, 50 ml, PP flat top, sterile, bulk	CR430829	Corning Products
Clear nail varnish	NY11553	Sally Hansen®DIV. DIST
Cryogenic vial, Int-thread, 2 ml, round	CR430489	Corning Products
Culture dishes	430165	Adcock Ingram
Coverslips	CG88	Lasec
Cyto Tox96® non-radiactive cytotoxicity	G1780	Promega
4'6-diamidine-2-phenylindole (DAPI)	AP402-0010	Sigma Aldrich
1 ml Disposable pipette	BD357522	Beckson Dickinson
2 ml Disposable pipette	BD357507	Beckson Dickinson
5 ml Disposable pipette	BD357543	Beckson Dickinson
10 ml Disposable pipette	BD357551	Beckson Dickinson
25 ml Disposable pipette	BD357525	Beckson Dickinson
Dulbecco's Modified Eagle Medium	INV41966-029	Gibco Invitrogen Corporation
ELISA cell death detection kit	11774425001	Roche
Eppendorf®, Microtubes	Z666521	Sigma Aldrich
Eppendorf®, Microtubes	Z666505	Sigma Aldrich
Eppendorf®, Microtubes	Z666515	Sigma Aldrich
Ethanol absolute	32221	Sigma Aldrich
Falcon (5ml) Polystyrene round bottom tube	BD352054	Beckson Dickinson
Foetal bovine serum	A15-101	PAA Laboratories GmbH
37% Formaldehyde solution	F8775	Sigma Aldrich

Glass slides	MG42	Lasec
Hanks balanced salt solution	INV14170088	Gibco Invitrogen Corporation
Heavy Tin foil	6001007162603	Pick n' Pay
Hoechst 33258	H6024	Sigma Aldrich
Human malignant breast cancer cell line MCF-7	ATCC: HTB 22	Sigma Aldrich
Latex Gloves, medium, powder free	EV40511	Scientific Group
Microscope slides, frosted one side	CLS294875	Corning Products
Penicillin-streptomysin	P11-010	PAA Laboratories GmbH
Phosphate buffered saline	P3744	Sigma Aldrich
Propyl gallate, Fluka	02370	Sigma Aldrich
Quant-IT^{TM} RNA assay	Q32852	Gibco Invitrogen Corporation
QuantiTect Reverse transcription kit	205311	Qiagen
RNeasy kit	74104	Qiagen
RT^2 profiler PCR array human cell death	330231-A-12 PAHS-212A	SABiosciences
RT2 qPCR SYBR Gree/ROX	330522	SABiosciences
Tissue culture dish 3.3 cm^2 diameter	BD/353001	Beckson Dickson
Tissue culture flask 25 cm^2, angled neck, vent, sterile	CR/423052	Corning Products
Tissue culture flask 75 cm^2, canted neck, anti-tip, vent, sterile	CR/430641	Corning Products
Tissue culture flask 175 cm^2, canted neck, vent, sterile	CR/431080	Corning Products
Triton X-100	T9284	Sigma Aldrich
Trypan Blue powder	T6146	Sigma Aldrich
TryplExpress	INV12605028	Gibco Invitrogen Corporation
Universal fit pipette tips,1-200 µl, Natural, Bulk	CR4798	Corning Products
Universal fit pipette tips,100-1000 µl,Bulk	CR4868	Corning Products
ZnPcS$_{mix}$ powder, molar mass:883g/mol		Synthesised and donated by Prof Tebello Nyokong

APPENDIX E

PREPARATION OF SOLUTIONS, MEDIA, AND CHEMICALS

MCF-7 Cell culture		
Complete DMEM for cell growth with 10% FBS	DMEM	44.5 ml
	FBS	5 ml
	Penicillin-streptomycin	0.25 ml
	Amphotericin	0.25 ml
Complete DMEM for cell growth with 20% FBS	DMEM	39.5 ml
	FBS	10 ml
	Penicillin-streptomycin	0.25 ml
	Amphotericin	0.25 ml
Photosensitisers		
0.0005 M ZnPcS$_{mix}$ (stock)	ZnPcS$_{mix}$ powder	0.0005 g
	0.01 M PBS	1.25 ml
0.0005 M Hypericin (stock)	Hypericin powder	1 mg
	DMSO	4 ml
Sterilisation		
70% Ethanol	Absolute ethanol	70 ml
	Autoclaved distilled water	30 ml
Experiments		
1 µg/ml Actinomycin D	Powdered Actinomycin D	1 mg
	DMSO	0.8 ml
1x Annexin V-FITC/PI	10x binding buffer	1.7 ml
	Autoclaved distilled water	17 ml
	Powdered Propidium Iodide	250 mg
	1x binding buffer	1 ml
ATP Cell Titre-Glo reagent	ATP Cell Titre-Glo buffer	1 ml
	ATP Cell Titre-Glo substrate	0.007 mg
0.01 M PBS	Phosphate buffered dry saline powder	1 packet

	Autoclaved distilled water	1 l
0.1 mg DAPI	5 mg/ml DAPI (stock)	0.2 ml
	Autoclaved distilled water	9.8 ml
3.5% Formalin solution	37% Formaldehyde solution	9.5 ml
	Autoclaved distilled water	90.5 ml
10 mg/ml Hoechst stock	Powdered Hoechst	0.001 g
	Autoclaved distilled water	1 ml
LDH reconstitute substrate	LDH assay buffer	1.2 ml
	LDH substrate mix	0.012 g
0.1 M Propyl gallate in solution with glycerol and PBS	Powdered Propyl gallate	0.212 g
	Concentrated glycerol	9 ml
	0.01 M PBS	1 ml
0.5% Triton X-100	Triton X-100	0.5 ml
	Autoclaved distilled water	99.5 ml
0.4% Trypan blue	Powdered Trypan blue	0.4 g
	HBSS	100 ml

APPENDIX F

CALCULATIONS AND PURITY RATIO

Calculation of cell viability

- For cell viability assays the percentage of viable cells was determined after using the Trypan blue exclusion assay.

- Once 100 µl of cellular suspensions were stained with 0.4% Trypan blue, and transferred to the hemocytometer slide which was placed under a light microscope they were counted using the 10 x objective .

- The number of viable cells which remained unstained and so were clear in colour were noted and the number of non viable cells which stained blue was noted.

- All ten squares or chambers of the hemocytometer were counted.

- An average count of viable cells which per square was determined by adding up the total number of viable cells per all the squares counted on the hemocytometer and dividing this total number by 10, the total number of square counted on the hemocytometer.

- An average count of non viable cells per square was determined by up the total number of non viable cells per the entire square counted on the hemocytometer and dividing this total number by 10 (the total number of squares counted on the hemocytometer.

- The average number of total cells per square was determined by adding the average count of viable cells per square to the average count of non viable cells per square.

- The percentage of viable cells pen an experimental or control group calculated using the following formula:

% cell viability = (average count of viable cells per square) x 100

(average number of total cells per square)

Calculation of cell seeding for culturing of cell in flasks

- The number of viable cells obtained during cell viability calculation (C1) was multiplied by the total resuspension volume of cell media.

- Once the total number of viable cells contained within the total resuspension volume of cell media was determined, the seeding ratio of cells per a cm^2 was divided by this number, in order to obtain the volume of cells required to cover a cm^2 surface area of the flask.

- This number was then multiplied by the total surface area of the actual culture flask and the volume of the cells from the cell suspension that had to be added to the culture flask in order to obtain the correct seeding ratio of cells would be acquired.

- Example calculation: if the average count of viable cells per a square after performing a Trypan blue was 180, and the cell pellet was resuspended in 5 ml of complete culture media and you wanted to produce a 75 cm^2 cell culture flask with a seeding ratio of $5X10^5$ cells/cm^2 the following would perform calculation:

- Viable cells = (180 viable cell / square) (10) (10^4)/ml

-                     = 1.8×10^7 cells / ml

- 1.8×10^7 cells x 5 ml = 9×10^7 cells / 5 ml

- (5×10^5 cells /cm^2) / (9×10^7 cells / 5ml) = 0.005 ml/cm^2

- (0.028 ml/cm^2) (75 cm^2) =0.375 ml

- Therefore from the 5 ml cell suspension you would remove 0.375 ml and pipette it into a 75 cm^2 cell flask containing complete cell culture medium in order to seed the flask at a ratio of 5×10^5 cells/cm^2

Calculation of cell seeding for cryopreservation

- The number of viable cells obtained during cell viability calculation (C1) and was divided by the required cryopreservation seeding ratio of cells (4×10^6) in order to obtain the volume of freezing media to be added.

- After centrifugation, the determined volume of freezing media was added to resuspend the cells and then 2 ml was allocated to each cryovial, in order to acquire the correct seeding ratio.

Example calculation: if the average count of visible cells per a square after performing Trypan blue staining was 160, and the cell pellet was suspended in 5 ml of HBSS and you wanted to cryopreserve cells with a seeding ratio of 4×10^6 cells/ml.

Calculation:

- Viable cells / ml = (160 viable cells/ square)(10) (10^4)/ml
- $=1.6 \times 10^7$ cells /ml
- 1.6×10^7 cells / ml x 5 ml $=8 \times 10^7$ cells / 5 ml
- $(8 \times 10^7$ cells) / $(4 \times 10^6$ cells) = 5 ml+ 15 ml cryopreservative medium= 20 ml cryovials
- 20 ml / (2 ml of cell suspension per vial) = 10 cryovials

Calculation for seeding of cell culture plates

- To calculate the cell seeding ratio into a culture plate, the number of viable cells (C1) per ml, was multiplied by the total suspension volume cell media.
- Once the total number of viable cells contained within the total suspension volume of the cell media was determined, this number was divided by the required culture plate seeding ratio of cells, in order to obtain the number of cell culture plates the cell suspension could produce.
- The total suspension volume of cell media was then divided by the total of culture plate the cellular suspension could produce, obtaining the volume of cellular suspension to be added to each culture plate in order to acquire the correct seeding ratio.
- The volume of cellular suspension to added to each culture plate was then subtracted from the volume of complete cell culture medium to be contained within the culture plate in order to obtain the correct

volume of complete cell culture medium to be added to each culture plate, before adding the calculated volume of cell suspension so each culture plate contained the exact same volume of culture media.

Example calculation: if the average count of viable cell per cells per square after performing a Trypan blue was 80, and the cell pellet was resuspended in 2 ml of complete culture media and you wanted to calculate how many 3.3 cm^3 in diameter culture plates containing 3 ml of complete culture medium could be produced with a seeding ratio of 5 x 10^5 cells / 3.3 cm^3, then would perform the following calculation:

- Viable cells / ml = (80 viable cells / square)(10)(10^4)/ml
  $$=8 \times 10^7 \text{ cells / ml}$$
- 8 x 10^7 cells /ml x 2 ml = 1.6 x 10^8 cells / 2 ml
- (1.6 x 10^8 cells / 2ml) / (5 x 10^5 cells / 3.3 cm^2) = 320 plate
- (2 ml)/(320 culture plates)= 0.00625 ml of cell resuspension per culture plate
- 3 ml volume of complete culture medium and 6.25 µl of cell resuspension per culture plate to be added.
- Therefore from 2 ml cellular resuspension you would remove 6.25 µl and pipette it into a 3.3 cm diameter culture plate containing 2.99375 ml of complete cell culture medium, in order to obtain a culture plate which contains a total volume of 3 ml of complete culture medium and seeding ratio of 5 x 10^5 cells / 3.3 cm diameter culture plate.

Purity of Nucleic Acids

Absorbance ratios of samples used for gene expression analysis.

	$A_{260/280}$ ratio	
	RNA	**cDNA**
	1.86	1.84
Untreated control	1.88	1.97
samples	1.89	1.85
	1.92	1.86
	1.83	1.87
ZnPcS$_{mix}$ treated	1.94	1.83
samples	1.86	1.93
	1.89	1.86
	1.91	1.95
PDT treated	1.89	1.97
samples	1.84	1.89
	1.95	1.82

UNIVERSITY
OF
JOHANNESBURG

APPENDIX G

RT-PCR RESULTS

Gene expression profiling (p-values)

Table G1: The p-values of genes analysed during the RT-PCR array.

Position	Symbols	p-value (compared to control group)	
		ZnPcS$_{mix}$ treated	PDT treated
A01	ABL1	0.234	0.245
A02	AKT1	0.753	0.121
A03	APAF1	0.345	0.989
A04	APP	0.236	0.353
A05	ATG12	0.314	0.624
A06	ATG16L1	0.414	0.279
A07	ATG3	0.824	0.286
A08	ATG5	0.126	0.375
A09	ATG7	0.209	0.236
A10	ATP6V1G2	0.976	0.365
A11	BAX	0.234	**0.035**
A12	BCL2	0.195	**0.044**
B01	BCL2A1	0.175	0.979
B02	BCL2L1	0.120	0.242
B03	BCL2L11	0.136	0.173
B04	BECN1	0.946	0.243
B05	BIRC2	0.872	0.544
B06	BIRC3	0.087	0.376
B07	BMF	0.264	0.252
B08	C1orf159	0.431	0.363
B09	CASP1	0.174	0.107
B10	CASP2	0.137	**0.006**
B11	CASP3	0.190	0.127
B12	CASP6	0.236	0.121
C01	CASP7	0.276	0.298
C02	CASP9	0.243	0.410
C03	CCDC103	0.631	0.623
C04	CD40	0.364	0.576
C05	CD40LG	0.854	0.246
C06	CFLAR	0.738	0.119
C07	COMMD4	0.236	0.126
C08	CTSB	0.576	0.414
C09	CTSS	0.482	0.570
C10	CYLD	0.234	0.141
C11	DEFB1	0.171	0.325
C12	DENND4A	0.223	0.622
D01	DFFA	0.246	0.241
D02	DPYSL4	0.421	0.841
D03	EIF5B	0.186	0.318
D04	ESR1	0.733	0.407
D05	FAS	0.242	0.398
D06	FASLG	0.176	0.095
D07	FOXI1	0.794	0.154

D08	GAA	0.205	0.227
D09	GADD45A	0.321	0.976
D10	GALNT5	0.964	0.264
D11	GRB2	0.422	0.694
D12	HSPBAP1	0.964	0.434
E01	HTT	0.990	0.552
E02	IFNG	0.139	0.113
E03	IGF1	0.167	0.084
E04	IGF1R	0.763	0.337
E05	INS	0.162	0.104
E06	IRGM	0.168	0.112
E07	JPH3	0.551	0.637
E08	KCNIP1	0.171	0.097
E09	MAG	0.266	0.627
E10	MAP1LC3A	0.283	0.483
E11	MAPK8	0.942	0.425
E12	MCL1	0.255	0.459
F01	NFKB1	0.365	0.445
F02	NOL3	0.209	0.350
F03	OR10J3	0.336	0.106
F04	PARP1	0.214	0.142
F05	PARP2	0.386	0.361
F06	PIK3C3	0.445	0.484
F07	PVR	0.472	0.501
F08	RAB25	0.375	0.168
F09	RPS6KB1	0.156	0.172
F10	S100A7A	0.173	0.097
F11	SNCA	0.242	0.114
F12	SPATA2	0.284	0.324
G01	SQSTM1	0.525	0.322
G02	SYCP2	0.636	0.614
G03	TMEM57	0.646	0.531
G04	TNF	0.523	0.642
G05	TNFRSF10A	0.165	0.341
G06	TNFRSF11B	0.302	0.131
G07	TNFRSF1A	0.532	0.149
G08	TP53	0.123	0.324
G09	TRAF2	0.456	0.476
G10	TXNL4B	0.519	0.151
G11	ULK1	0.943	**0.038**
G12	XIAP	0.312	0.104